RIGA TECHNICAL UNIVERSITY

J. Kandis

New Method for Quality Inspection of Extrusion Welding

PhD Thesis

Riga 2013

RIGA TECHNICAL UNIVERSITY

The Faculty of Transport and Mechanical Engineering

Institute of Mechanical Engineering Technologies

Janis KANDIS

PhD candidate at programme "Apparatus Engineering"

NEW METHOD FOR QUALITY INSPECTION OF EXTRUSION WELDING

PhD Thesis

Supervisor of research:

Dr. sc. ing., Assistant Professor

N.MOZGA

Riga 2013

ANOTĀCIJA

Promocijas darbā „Jauna metode ekstrūdēto šuvju kvalitātes pārbaudei” izstrādāta jauna alumīnija profilu kvalitātes pārbaudes metode ekstrūdēto šūvju pārbaudei un defektu identificēšanai. Jaunā metode ļauj paaugstināt pārbaudes produktivitāti un no 2012. gada tā ir ieviesta ražošanā. Stiepes un spiedes metodes vietā tiek piedāvāta jauna alumīnija profilu kvalitātes pārbaudes metode. Ar eksperimentiem un FEM, un FEA ir analizēts metāla bīdes process. Eksperimentāli izstrādāta praktiski pielietojama diagramma "Ekstrūzijas formas ģeometrijas robežu diagramma (ESWLD)", pēc kuras ir iespējams prognozēt pie kādām ekstrūzijas formas ģeometrijām ekstrūzijas procesā metināšanas kamerā ir iespējams izvairīties no gāzes kameras klātbūtnes.

Darbs satur 109 lpp. teksta, 4 nodaļas, secinājumus un 66 izmantoto informācijas avotu sarakstu, 3 pielikumus, 53 attēlus.

ANNOTATION

In the Thesis work "New method for quality inspection of extrusion welding" has developed a new aluminum profile extrusion quality inspection method for extrusion welds tests and defect identification. The New method allows to increase productivity and it has been launched in production since 2012. Instead of tensile and compressive methods offers a new aluminum profile quality inspection method. With experiments and FEA and FEM was analyzed the metal shearing process. Experimentally was developed applicable diagramm "Extrusion seam weld limit diagram (ESWLD)" to predict what kind of extrusion form dimension at extrusion process in extrusion welding chamber avoids the presence of gas chambers.

The Thesis work includes 109 pages of text, 4 chapters, conclusions and 66 sources of information, 3 appendixes and 53 figures.

TABLE OF CONTENTS

INTRODUCTION

Topicality of Subject

Nowadays, in order to remain competitive in the field of production, metalworking companies are expected to offer the lowest price possible, maintaining flawless quality. The low price level and high quality standard can be achieved only by cutting the labor cost, making production technologies more efficient and establishing new quality testing technologies.

Aluminum has become one of the most progressive metals of the present and future. It is light, solid, not subject to corrosion, easy to process and shape and environmentally friendly, as well as it is recyclable. Since aluminum is widely used in such fields as auto industry, construction of buildings, air transport production, then elimination of the identified casting defects of aluminum has become a requirement of great importance. Such quality tests determine the course and safety of further utilization of profiles.

The currently applied testing technologies for identification of defects in the extrusion welds of aluminum are expensive, time consuming and what is more – they are inaccurate [49, 53], which results in the loss of time and resources of a company. Therefore it is necessary to develop a more accurate method to replace the current ones and provide more accurate information on the quality of welds of the extruded profiles.

The topicality of the research determines a necessity to develop a quality testing method for inspection of the quality of the extruded welds directly focused on testing the extrusion welding instead of the overall test of the profile, therefore the subject is topical.

Objective and Tasks of Thesis

The objective of the promotion thesis is to develop an accurate and practically usable method for inspection of the extrusion welding of aluminum and identification of defects.

The following tasks were set to accomplish the objective:

1. Analysis and case study of the current quality inspection methods of the extrusion welding;
2. To perform shearing inspection of the aluminum specimen, using the mechanical press, force and stroke measurement indicators;

3. To perform the analysis of development of defects in the extrusion welded joints depending on the geometrical values of the forms;

Methods of Research

In order to accomplish the set objectives and fulfill the given tasks, the following research methods were used during the course of development of the promotion thesis: comparative, analytical and graphical methods. In order to carry out the experimental part, the mechanical presses with capacities of 60 and 2 tons and the extrusion press with a capacity of 180 tons were used. In order to read the experiment data, a force and speed reading indicator was used. The software BLACK CAT® was used for data summarization and visualization. The graphical software DEFORM® 2D and DEFORM® 3D were used for the FEM (Finite element method) and FE-analysis (finite element analysis). Diagrams and figures were used to provide clearness of the research results.

Scientific Novelty

The scientific novelty of the promotion thesis is as follows:

1. A new method for quality inspection of extrusion welding developed to identify defects of the welded joints in the extrusion process;
2. An *extrusion seam weld limit diagram* (ESWLD) was developed to determine the minimum parameters of geometry of the extrusion die's welding chamber.

Main Research Results

The main research results of the promotion thesis are as follows:

It was established that:

1. The current quality inspection methods of extrusion welding do not identify defects of the welded joints;
2. After shearing 1/5 of an aluminum specimen, a crack develops in the specimen. After shearing 3/5 of the aluminum specimen, the effect of the Plateau is observed;
3. The quality of extrusion welded joints depends on the geometry of extrusion forms;

4. A new method for inspection of quality of the welded joints in the extrusion process is developed.

All above mentioned results are a new contribution to the machine science.

Practical Application

The researches carried out in the promotion thesis "New Method for Quality Inspection of Extrusion Welding", compared to the current testing methods, permit focusing the inspection on the welded joints in the extrusion process and provide recommendations for improvement of the extrusion technologies. The method developed is universal.

The developed method permits increasing industrial inspection productivity and since 2012 it is launched in production [42] (see Appendix 2 and Appendix 3).

The developed diagram for *extrusion seam weld limit diagram* (ESWLD) provides recommendations to the manufacturers of extrusion dies – to follow the geometrical parameters of extrusion dies.

In this thesis the author presents

1. The quality inspection method of the welded joints in the extrusion process;
2. The practical application of the new method for quality inspection of extrusion welding;
3. The practical application of the geometrical diagram for *extrusion seam weld limit diagram* (ESWLD).

Approbation of Thesis

The main promotion thesis results were presented in the subsequent conferences and seminars with a high level of reputation, receiving approving feedback from the teaching staff of other universities and representatives of the industry:

1. J. Kandis, H.Valberg and Wu Wenbin; "Use of Axisymmetric Shearing as Technological Test Method to gather Flow Stress Data for Metals", AMPT Paris, Oct., 2010;

2. J. Kandis, Wu Wenbin and H. Valberg; “The Mechanics of the Shearing Process studied by FEM-Analysis with Experiments”, AMPT Paris, Oct., 2010;
3. J. Kandis, H. Valberg and Wu Wenbin; “On the Mechanics of the Shearing Process in Bar Shearing”, ESAFORM Belfast, April, 2011;
4. J. Kandis, H. Valberg and Wu Wenbin; “On the Deformation Mechanism in Shearing with concurrent Crack Growth over the Cut Section”, ESAFORM Belfast, April, 2011;
5. J. Kandis, H. Valberg; „Metal flow in two-hole extrusion of Al-alloys studied by FEA with experiments”, ESAFORM Germany, March, 2012
6. Henry Valberg, Tony Melkild and Janis Kandis: “Determining The Weld Quality In Extrusion Welding”, Italy, 2011;

Publications

There are six scientific articles published on the conducted researches and results and one application for patenting the method submitted:

1. J. Kandis, H.Valberg and W. Wu; „Use of Axisymmetric Shearing as Technological Test Method to gather Flow Stress Data for Metals”, Advances in Materials and Processing Technologies, Paris, France, Oct., 2010, pp.352.- 356.;
2. J.Kandis, W. Wu and H. Valberg; “The Mechanics of the Shearing Process studied by FEM-Analysis with Experiments”, Advances in Materials and Processing Technologies, Paris, France, Oct., 2010, pp.108.- 112.;
3. J.Kandis, H. Valberg and W. Wu; „On the Mechanics of the Shearing Process in Bar Shearing”, Submitted to: European Scientific Association for Material Forming, Belfast, United Kingdom, April, 2011, pp.615.- 620.;
4. J.Kandis, H. Valberg and W. Wu; „On the Deformation Mechanism in Shearing with concurrent Crack Growth over the Cut Section”, European Scientific Association for Material Forming, Belfast, United Kingdom, April, 2011, pp.615.– 620.;
5. J. Kandis, H. Valberg, T. Melkild; „Determining the Weld Quality in Extrusion Welding” // International Conference on Extrusion and Benchmark, Bologna, Italy, 2011.pp.461.– 466.;

6. J. Kandis, H. Valberg; „Metal flow in two-hole extrusion of Al-alloys studied by FEA with experiments", European Scientific Association for Material Forming, Erlangen, April, Germany 2012.pp.493.- 498.

1. BASIC CONCEPT OF PROBLEM

1.1. Extrusion

Extrusion (*extrusion – pushing out* from Latin) is formation of a material, pushing it through the extrusion die in order to obtain constructions of a certain profile. It is shown in Figure 1.1 that the raw material always is in the shape of a bar – a cylindrical aluminum block, which is heated in the induction cooker up to the temperature of 450–500 °C (depending on the aluminum series number). The heated bar is pushed through the extrusion die with a large force (depending on the temperature and dimensions of the specimen), giving a form to the profile.

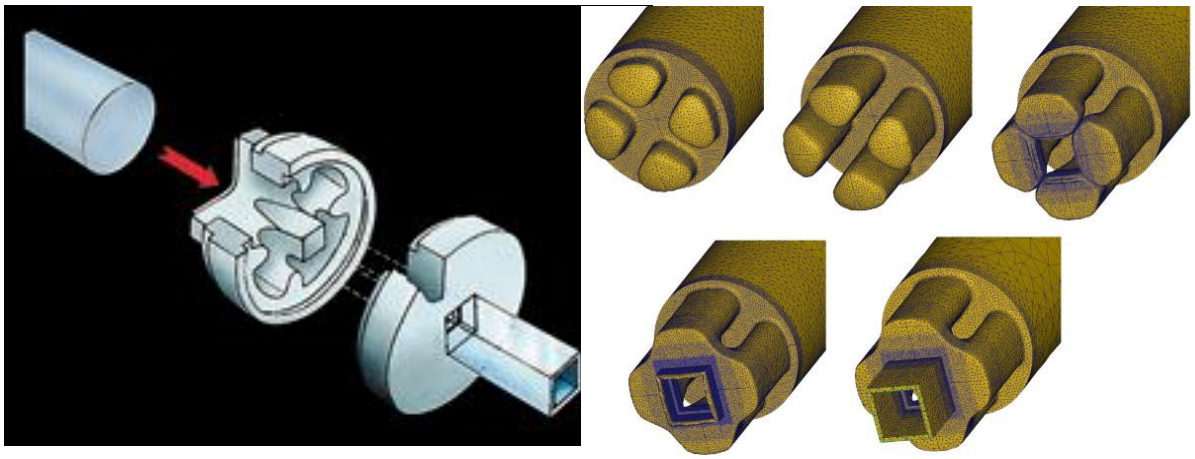

(a) (b)

FIGURE 1.1. Layouts of extrusion dies (a) and the material flow of billets in the extrusion die (b)

The length of profiles is usually from 25 to 45 meters – depending on the form and needs. As soon as the profile has left the extrusion die, it is cooled with air or water. In order to avoid formation of stress and to obtain a completely straight product, the profile is stretched prior to testing all important dimensions and quality of the surface.

If the initial parameters of the extrusion welding process are not set correctly, for example, a stable, constant temperature is not maintained, geometry of the extrusion die is not correct, the extrusion die is not cleaned from the accumulated deposits from the previous extrusion process in a quality way, the extrusion die is damaged, there is an insufficient

quantity of the oiling substance, etc., then some individual parts of the extruded profile or the whole profile can have an insufficient quality of the extrusion welds.

In order to examine the processes taking place during the extrusion welding, there have been numerous researches carried out over the years. In 2002 a paper [52] was published, where the most important know-how on the extrusion welding throughout the 20th century was summarized. The early researches were mainly conducted by the means of experiments, nevertheless they facilitated to good understanding of the basic processes of extrusion welding, paying attention also to the extrusion welding, when the distribution of material flows takes place with the assistance of a web in the extrusion dies. Technologies for testing and inspecting joints are out-of-date, very expensive, time consuming and inaccurate.

During the 21st century, it was possible to study the metal flow in the FEM simulations [66, 60, 61, 63, 59, 58] with powerful and fast computers, as well as, using the powerful FEA programmes. Nowadays, within the framework of extrusion welding research, the FEA pays the main attention to experimenting and studying the variable conditions in the extrusion welding chamber, when distribution of the metal flow with the assistance of the web takes place [7].

The extrusion welding process it is important to apply the correct conditions of the metal flow in the extrusion die in order to obtain the necessary pressure of the metal flow in the welding chamber, which would provide an adequate welding quality of joints. The most important conditions are sufficient heating of the billet's material, extrusion welding velocity and geometry of the extrusion dies. During the 21st century the attention was mainly focused on studies of the first two conditions.

1.2. Testing methods of welded joints in the extrusion process

The most common testing method to assess the quality of extrusion welding is a tensile test established by the European standard EN ISO 6892-1:2010 [23]. Specimens for the test are made according to the European standard EN ISO 2740:2009 [22]. Test specimens oriented in the direction orthogonal to the weld are prepared, and then stretched to fracture.

If failure occurs in the weld, the strength of the weld is evaluated from the yield stress or the tensile strength of the material as measured in the test, while ductility is evaluated from either elongation, or contraction of area of the test specimen at fracture. It is generally agreed upon that the ductility of the weld is a better measure of quality than strength, as welds with

quite serious defects might have good strength. Defective welds therefore can be sorted out and scrapped based on ductility values if the specimen fractures in the weld.

Having examined several profiles of the extruded aluminum, we have come to conclusion that the ductility of deformation (change of the specimen's dimensions) is a better quality indicator than the tensile test, because during the course of experiment it was observed that due to a repeated crystallization of the specimen's metal, the material has a different solidity at different sections. Thus the specimen's material at different sections can have a less solidity than the joints originated during the extrusion process with the solidity of defects. In that way the tensile diagram does not provide information on the quality of joints originated at the time of extrusion welding. The low-grade joints can be better identified based on the deformation degree measurements. The deformation degree is determined according to the changes in the specimen's dimensions.

Deformation of the material in point of fact can be flexible, which disappears when the load is removed and the parts return to the initial state. The plastic deformation that remains, when the load is removed, starts when the impact of force is increased. This deformation – change of dimensions of the material are characterized by the deformation degree:

$$\varepsilon = \frac{\Delta l}{l} \cdot 100\,, \qquad (1.1.)$$

where ε – deformation ductility (%);

Δl – dimension of a specimen after tearing (mm);

l – dimension of a specimen before tearing (mm).

In order to determine the quality of a joint obtained as a result of extrusion welding, apart from the tensile test there are other static testing methods used, such as bending, torsion and other micro cracks inspection tests (micro analysis, study of the material structure, etc.).

Other static test methods than tensile testing has been used to determine weld quality in extrusion welding. Such methods are the bending test, the flattening test and various fracture mechanical tests. The quality of industrial extrusion welds is also commonly tested by expansion tests; a mandrel is then pressed into the open end of a hollow profile, or the profile is expanded hydraulically. If the profile expands sufficiently before it fractures, this ensures acceptable ductility in the material and confirms that the profile does not contain

serious defects. Expansion tests can be difficult to apply in some non-circular hollows, and in these cases flattening, or etching tests may be used instead.

For critical applications of light metals profiles with extrusion welds one can use fracture mechanics tests on samples taken from the profiles. In such tests a pre-crack is forced to propagate along the weld plane. Extrusion welds that behave satisfactorily in a tensile test may in a fracture mechanics test have reduced toughness compared to that of the parent metal away from the weld. In this case the welds usually have higher content of inclusions in the extrusion weld than outside it. The weld will thus represent a favorable plane for crack propagation compared to the locations away from the weld.

1.3. Defination of problem

If a crack is observed outside the area of a joint, it is considered that the quality of the extrusion welds is better than the quality of metal. But is it always true? Unfortunately, it is not always so. Figure 1.1 (a) shows a layout of an aluminum profile welded in the extrusion process, which is obtained from the aluminum profile with a joint in the middle of it, torn in the tension device. As it can be seen in Figure 1.2 (b) and (c), initially there are some micro cracks (two un-welded stripes with no metallic bond that extended along the length of the profile) observed in the area of the welds, which are indicative of a low-grade weld. The micro cracks have originated from an insufficient pressure in the weld chamber. It can be seen that the specimen breaks outside the low-grade extrusion welding area, despite the fact that there is a clearly visible defect in the joint. This example shows that the specimen with an extrusion joint can demonstrate a good result (i.e. the specimen does not break in the joint area) in the tensile test, even if the quality of the joint is not sufficient.

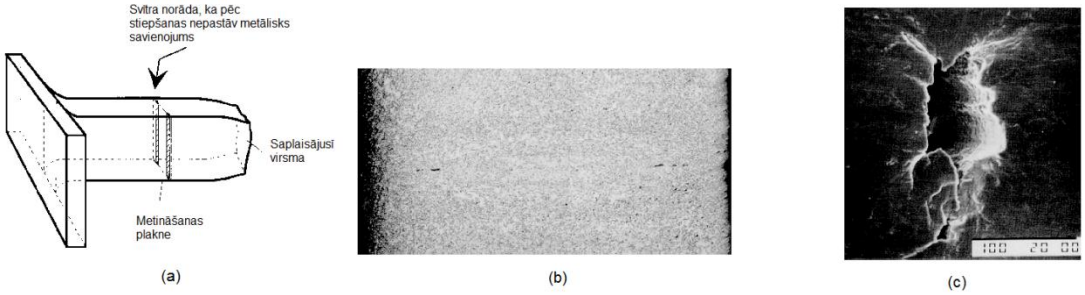

FIGURE 1.2. Specimen deformed in the tension device; (a) Specimen torn in two as a result of the tensile test; (b) Extrusion welded joint defect, and (c) Micro cracks in the joint area in magnification

Such a behavior of the specimen can be justified that as often as not the material is not of a similar solidity at all sections. During an extrusion process the billet and extrusion die are heated from outside up to the temperature of 500 degrees above zero, as a result there can be some temperature differences between the central part and outside, which harden differently during the process of precipitation hardening. As a result in the case seen in Figure 1.2, the material is softer away from the location of a weld then the extruded joints. When the tensile test is performed, the softest area of the material starts deforming faster than the solid one or the extrusion welded area. The stress of the material in the incompletely welded section of the joint is not sufficient to identify the low-grade extrusion welds. When pulling is continued, the deformation localizes and grows in strength only in the already deformed section despite the fact that the material has significant faults in the adjacent extrusion welds area. As a result the low-grade extrusion weld is not identified.

Also this behavior is easily explained if the material away from the weld where the neck appears is softer than that in the weld zone itself. Upon stretching necking would then start in the softer region instead of in the hard weld zone. The degree of plasticization in the section of the specimen containing the defects would therefore not become so high that it would demonstrate the material weakness in reality present in this location. On continued stretching deformation would therefore be localized and would only take place in the neck, in spite of the presence of a serious material defect in the cross-section nearby.

In order to eliminate the shortages established in this chapter, an inspection method of the extrusion welded joints was developed, focusing the quality inspection directly on the locations of extrusion welds. The new testing method is based on the deformation measurements in the weld area and the result is described as a degree of deformation.

1.4. Conclusions

Considering the fact that there is a large probability that a break will originate outside the extrusion welding area, when the tensile tests of the aluminum specimen are performed, and frequently the quality of the welds joint area is better than the quality of metal, and that the material is heated not only from outside and a repeated process of precipitation hardening develops partly during the process, there is a need for more accurate tests to inspect the extruded welds.

In order to develop a simplified and accurate testing method focused on the extrusion welds, initially it is necessary to perform researches on deformations and behavior of the material, breaking them.

Being aware of the impact of temperature [7, 66] and speed [52, 66] on the quality of formation of welds, perform researches on the impact of geometry of the extrusion die on formation of the extrusion welding joints in the course of the thesis.

2. EXPERIMENTAL STUDY AND FEM-MODELLING OF SHEARING PROCESS

2.1. Introduction

In shearing a piece of metal is cut away from a sheet, plate or a bar of metal. In soft metals most of the cut is formed by a shearing mechanism before (eventually) the last part of the cut surface is created by fracturing. During the shearing process localised shear deformation may take place in a thin layer inside the metal between the applied shearing edges [28, 57].

It is easy to measure the load-stroke curve for a metal being cut by shearing. The load rises steeply in the beginning of the process, then flattens out and reaches a peak value. After the peak the loads drops down as shearing progresses.

The shearing process has been considered used as a technological test [29] to measure mechanical properties corresponding to those commonly measured in tensile testing, i.e. yield stress and ultimate tensile strength. This is relevant when there is too little material available for producing a tensile test specimen.

Attempts have been made to determine the strain hardening exponent [29, 19] from shearing tests conducted on metals, and also the strength coefficient [19]. In [19] isothermal FEA was used to investigate the possibility of using shearing for the purpose of determining the strain hardening exponent (n) and the strength coefficient (K) of metals. It was mapped how variation in n and K was predicted to influence the simulated load-stroke curve for power-law materials. The investigation showed that the n-value correlated well to the punch displacement value of the peak in the load-stroke curve. In addition the strength coefficient correlated to the peak value of the load. In this article emphasis is on the use of the shearing process to obtain flow stress data for soft Al-alloys when thermal effects are included.

Shearing, also called blanking, is a partitioning process where a piece is cut away from a sheet, plate or eventually a bar of metal. The part cut out in the process and the remains of the material should have geometrical shape of sufficient accuracy for the intended application. Most commonly the requirement is that the parts should be flat and the sheared edges should be straight, smooth and orthogonal to the surface of the parts. Because of this requirement a modified process called fine blanking has been developed in addition to conventional blanking. While in conventional shearing there is some plastic deformation subjected to the

cut parts so a perfect cut shape is not achieved, better shape is obtained in fine blanking by use of counter-pressure dies applied in addition to the shearing punch and the shearing die.

The formation mechanism of the cut edge depends on whether the metal to be cut is soft or hard. While in sufficiently soft metals most of the cut surface is formed by shearing, in hard materials a greater portion of this surface is created by the metal undergoing fracture. Before the fracture is created across the section there is localised shear taking place in a layer inside the metal in the region between the upper and the lower shearing edge. In this article emphasis is on the mechanics of shearing taking place in this layer in soft aluminium alloys where the fractured part of the cut edge is either absent or represents a minor part of the cut cross-section.

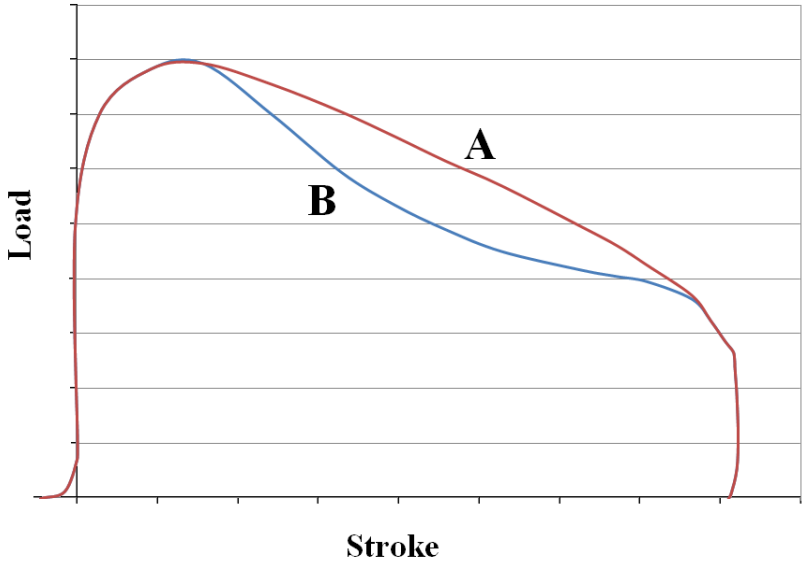

FIGURE 2.1. Principal sketch showing typical appearances of load-stroke curves in shearing.

A number of investigations into the mechanics in the deformation zone in shearing have been reported in the technical literature. Experimental work in which shearing was investigated by measurement of the load-stroke curve are for instance available in [12, 13, 46, 33, 20]. The experiments were either performed in tensile test machines run in compression or in mechanical presses.

The measured load-stroke curve obtained for Al seems to have different appearance dependent on the test machine applied in the shearing process, see Fig.2.1. The load rises steeply in the beginning of the process then it flattens out after a while. As shearing continues it starts to decrease so that there is a distinct peak value of load. Behind the peak the declining

part of the graph is approximately flat or it curves upward (A) or downward (B). Upward curvature is obtained when shearing is conducted in a tensile test machine [12, 13] and downward curvature when the process is set up in a mechanical press[46, 33, 20].

Bar shearing is a commonly applied cutting process in which a long bar is partitioned in shorter pieces by a shearing operation. It involves shearing by use of an upper die edge and a corresponding lower counter-edge in between which the material of the bar is subjected to shear until the bar is cut apart over the plane extending between the two edges. The process was early subjected to experimental analysis [10] and this work lead to a good understanding of the mechanics of the process, and what are good process conditions. Optimum conditions are those that provide a good cut in terms of a plane cut surface, and cut-away pieces of the bar with good shape.

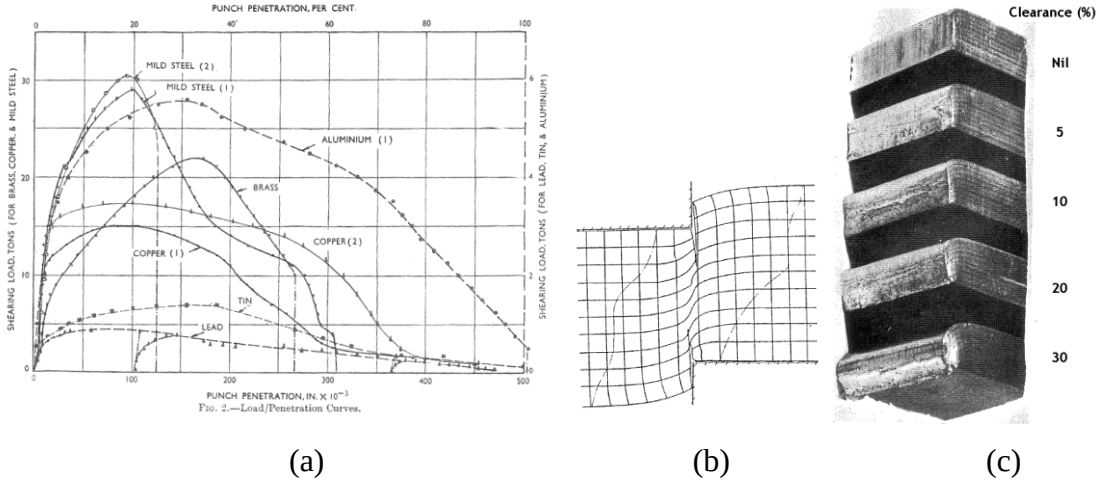

FIG. 2.—Load/Penetration Curves.

FIGURE 2.2. Results from experimental investigation on bar shearing (a) Load-stroke curves, (b) Grid pattern deformations and cracking (Mild steel, nil clearance, 25% penetration) (c) Effect of clearance on quality of cut aluminum bars.

(a) (b) (c)

FIGURE 2.3. Tooling designed and applied for small sized bar shearing experiments: (a) Punch with slot to insert specimen into, (b) Bar specimen (Al) and lower ring-shaped cutting die, (c) Configuration of dies and specimen at beginning of shearing.

Some figures from this early work are shown in Fig.2.2. As Fig.2.2 (a) depicts load-stroke curves were recorded during cutting of bars for different metals. Moreover, as Fig.2.2 (b) shows by an example, grid patterns were applied for the analysis of the deformations occurring in the shear zone. Finally, Fig.2.2 (c) shows that a cut of good quality was obtained when the clearance between the upper and the lower shearing die was made small. When larger clearances were applied rather large additional plastic deformations occurred in the bars away from the cutting plane. This resulted in cut pieces with bad shape.

Use of internal grid patterns inside workpieces subjected to shaping has been applied intensively throughout the years to map the actual deformations present in metal forming operations. Such techniques are commonly referred to as visio-plastic techniques. Often they are based on use of split specimens with grid patterns inscribed on one the split surfaces. Such studies on shearing processes are available in the literature [44, 31], see Fig.2.2 (b).

A special variant of this technique is based on creating the pattern by means of stripes of contrast materials inside the workpiece subjected to forming. It has been applied extensively at NTNU [50] to map the deformations occurring in various metal forming applications. The technique has certain advantages in relation to use of scratched patterns, one being that it is not necessary to use a split specimen. Another advantage is that while

scratched patterns tend to erase and become invisible at large plastic deformations, this is not the case when the internal stripe pattern is used.

Even though a large number of scientific investigations have been conducted on the process of shearing (also named blanking) the situation is still one where the mechanisms of deformation in the process are not yet fully understood. Some early experimental investigations [11, 45, 32] performed in the period 1950-70 revealed that in shearing of bars or blanks using sharp-edged dies, the mechanism of cutting was one where crack initiation can take place at each of the two approaching die edges rather early during shearing, so after the cracks have appeared the mechanism of partitioning will include crack growth across the thickness of the plate, instead of pure shearing over the full section. In some cases initiation and growth of the crack from the top edge of the die could be suppressed, then cracking would only occur from the bottom edge, see Fig.2.4.

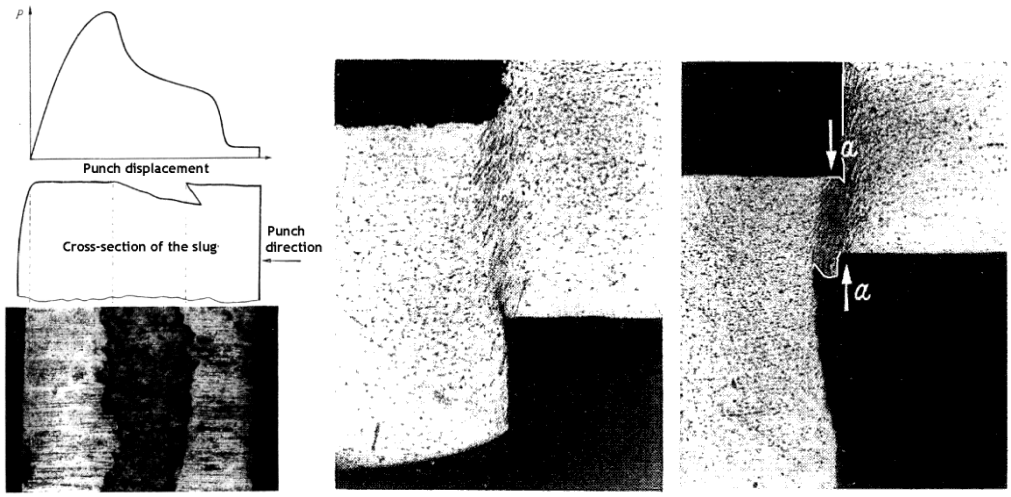

(a) (b)

FIGURE 2.4. Shearing by crack growth from the cutting edges; (a) Load-stroke curve and appearance of sheared surfaces, (c) Cross-section through partially cut specimen at different stages of shearing.

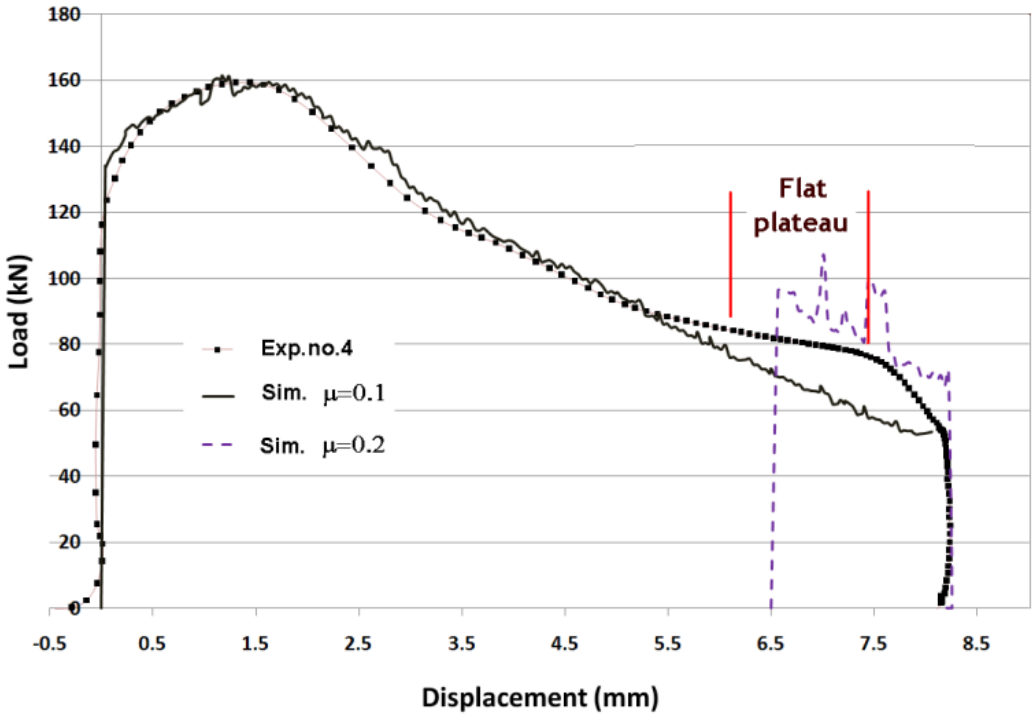

FIGURE 2.5. Load-stroke curve in shearing from experiment and previous FEM-simulations.

A special characteristic commonly observed in experimental investigations of shearing is that the measured load-stroke curve has approximately a flat plateau toward its tail end, see Fig.2.4 (b). In an earlier investigation [25] we tried to FE-model the shearing process to study the conditions in the shear zone. When we modeled the process we assumed partitioning to take place by shearing only, i.e. without crack formation and crack growth. The model then predicted that the shear zone established over the thickness of the blank, extending from the top edge to the bottom counter-edge, would remain in the same location throughout the cutting operation. Moreover, prediction was that shearing would become more intense as cutting proceeded, so actually there would be strong shear localization in the shear zone.

Efforts aiming at getting the FE-model to reproduce the flat plateau near the end of the load-stroke curve were not successful at that occasion. The flat plateau did not occur in simulation unless we either assumed a strong thermal softening in the material, or a significant friction increase between dies and workpiece material towards the end of the stroke. When the flat plateau appeared both effects were exaggerated beyond what is realistic.

Successful work has been reported [5] in the literature where the shearing process has been FE-modeled with concurrent cracking over the thickness of the workpiece. But in our

work presented here we have chosen to use a different approach; crack initiation and growth is mimicked in the FE-model by use of a wedge-shaped die that penetrates into the sheared-off edge of the blank. The advantage of this concept is that it allows creation and propagation of the crack with full degree of freedom.

2.2. Experimental study and FEM-modelling of axisymmetric shearing

Shearing experiments and FEM-modeling work were performed to study the nature of the shearing process. The experimental work has been described fully elsewhere, see [28]. A shearing experiment in which a 10.4mm thick plate specimen was cut by partial shearing in a mechanical press is considered in more detail here.

The experiment was tried reproduced by FEM-simulation using the DEFORM-2D FEM-program. A vertical section through the model before start of simulation is shown in Fig.2.6. The model (non-isothermal) corresponds well to the experiment as regards geometrical conditions of specimen and tooling, and the experimental shearing velocity profile was used in the model. To model the shear zone in the specimen accurately a dense FEM-mesh was created locally in the material layer of the plate situated between the shearing edges, see Fig.2.6.

The specimen was modeled as rigid-plastic and the Coulomb coefficient of friction between tooling and plate was assumed to be 0.1. Material models, i.e. flow-curves from the DEFORM-2D data base were first used, but did not give a load response that agreed well with the experiment. An inverse modeling approach was then used to find flow stress data that gives the right simulated punch force.

Starting point were flow stress data in the database for alloy Al99.7, see Fig.2.7 (a). With higher alloy content in our used material than in Al99.7 the flow curve at each temperature had to be increased to obtain the load response measured in the experiment. For temperatures of 20, 40, 50 and 60ºC, respectively, the flow stress values were increased by multiplying the flow stress values of Al99.7 by factors; 2.1, 1.9, 1.2 and 1.1 for each temperature level. Resulting flow stress data obtained this way are shown in Fig.2.7 (b).

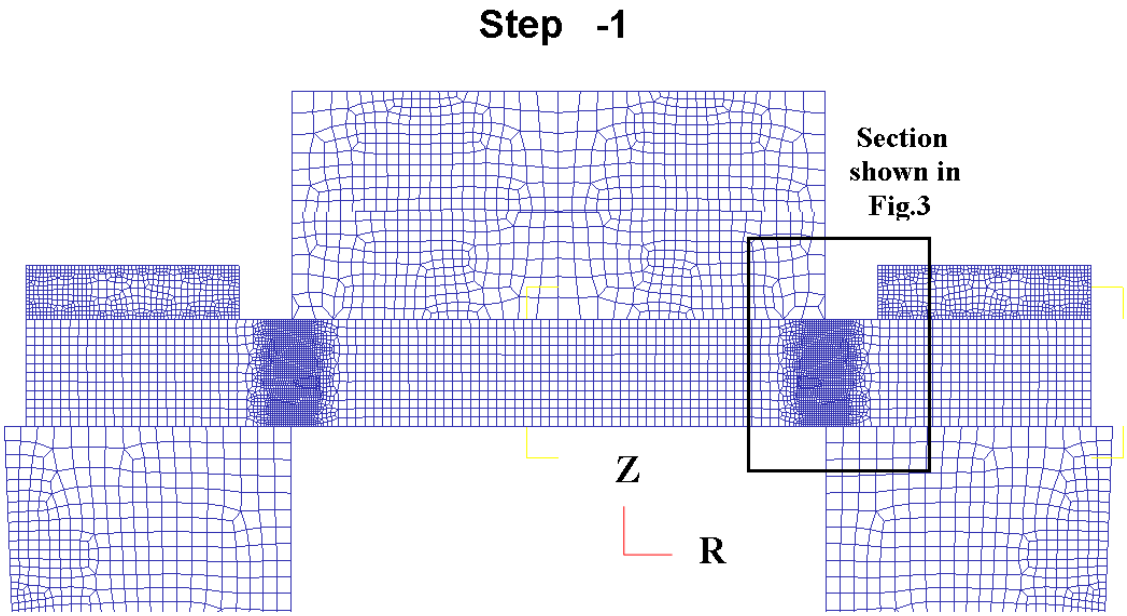

FIGURE 2.6. Mirrored version of FEM-model of shearing of the thick specimen.

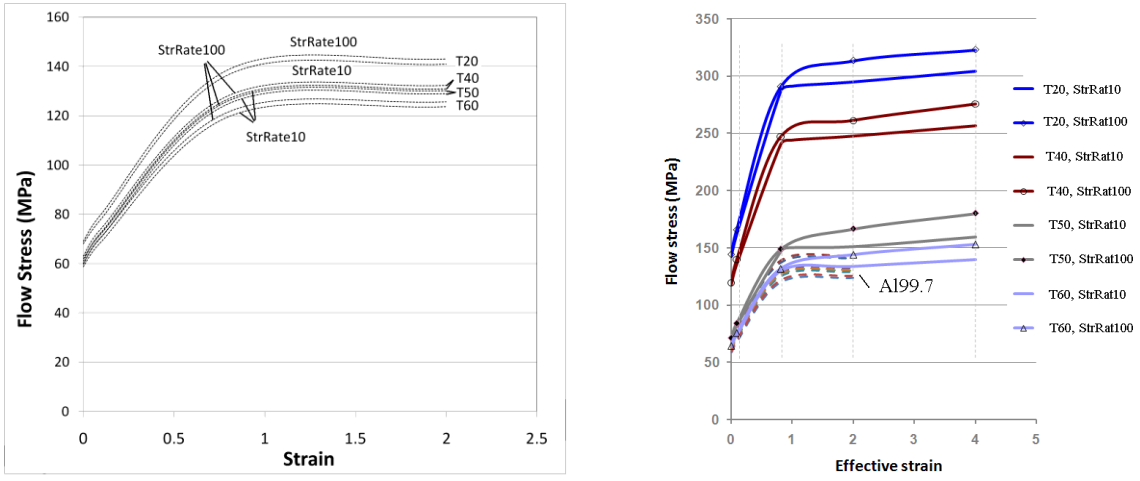

(a) (b)

FIGURE 2.7. Flow stress data (a) Al99.7 from Deform database and (b) Modified flow stress data that reproduces the experimental load-stroke curve.

In addition a modified FEM-model was also made in which the punch velocity was set constant throughout the stroke, while in the experiment it decreased in a sinusoidal manner. In the modified model the plate was given the same but opposite directed movement as the punch. A horizontal midline laid through the plate will in this modified model remain in the

horizontal midplane of the shear zone. Finding the distribution of a state variable along this line is then easy in the modified model.

2.3. Results

With the FEM-model one can easily obtain a lot of information regarding predicted deformation in the process, as shown in the forthcoming sections.

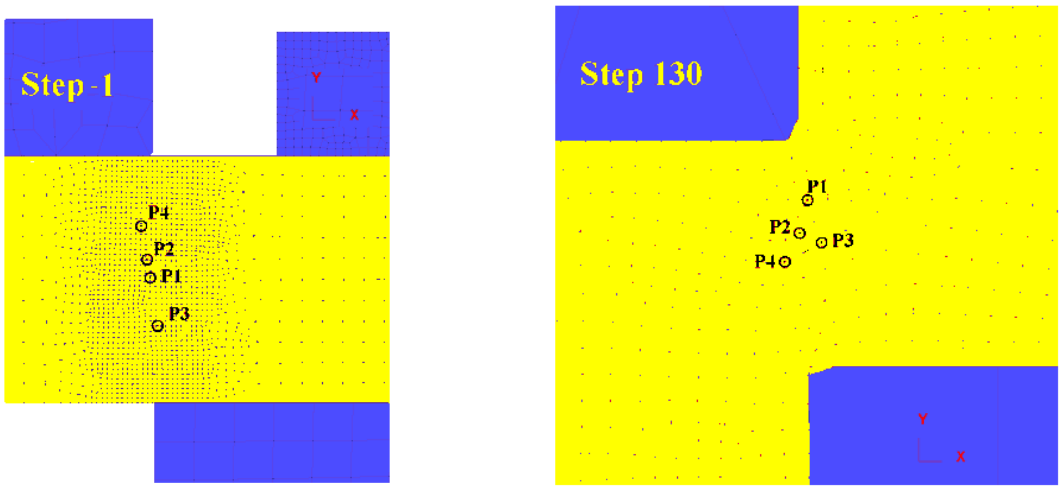

(a) (b)

FIGURE 2.8. (a) Points used in point tracking and (b) Position of points after shearing.

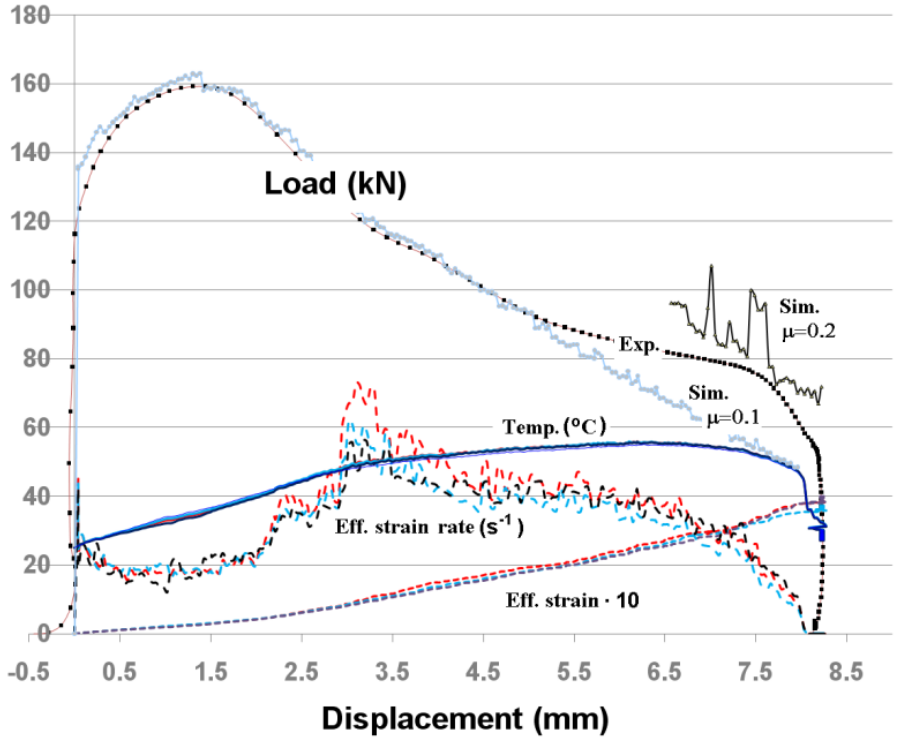

FIGURE 2.9.Load stroke curve from simulation and experiment.
Temperature/strain/strain rate conditions in shear zone from point tracking.

With flow stress data acquired by inverse modeling the resulting load-stroke curve was well reproduced in the simulation of the thick specimen shearing experiment, see Fig.2.9. Exception is the tail end of the curve being higher in the experiment than in the simulation. Increased friction between tooling and workpiece towards end of the stroke will increase the load and may explain this high level of load at the end of the curve.

It is interesting to know how the thermo-mechanical conditions in the shear zone are predicted by the FEM-model, like temperature, effective strain and effective strain rate in the shearing operation. The point tracking option in DEFORM-2D was therefore used to determine these conditions. Four points remaining in the shear zone during shearing are shown in Fig.2.8. Simulated data for three of these points were plotted into the diagram showing the load-stroke curve, see Fig.2.9. The prediction is that the shear zone temperature will increase from RT up to ~56°C in the first 2/3^{rds} of the shearing operation where after it remains approximately constant. The effective strain rate is ~20s^{-1} in the first 1/3rd of the stroke and is then approximately doubled and remains rather constant until it drops down to zero at the end of the shearing operation. The effective strain value of the shear zone increases approximately linearly throughout the stroke and reaches ~3.8 at the end of shearing.

In [28] it was shown how the distribution of different state variables (such as for example the total velocity) for material particles located on the horizontal midline across the shear zone can be obtained by the FEM-model. Fig. 2.10 shows similar results for temperature, effective strain and effective shear strain (τ_{RZ}). As Fig.2.10 depicts these parameters have a maxima in the middle of the shear zone. This is to be expected but simulation also predicts the numerical value of the maximum point.

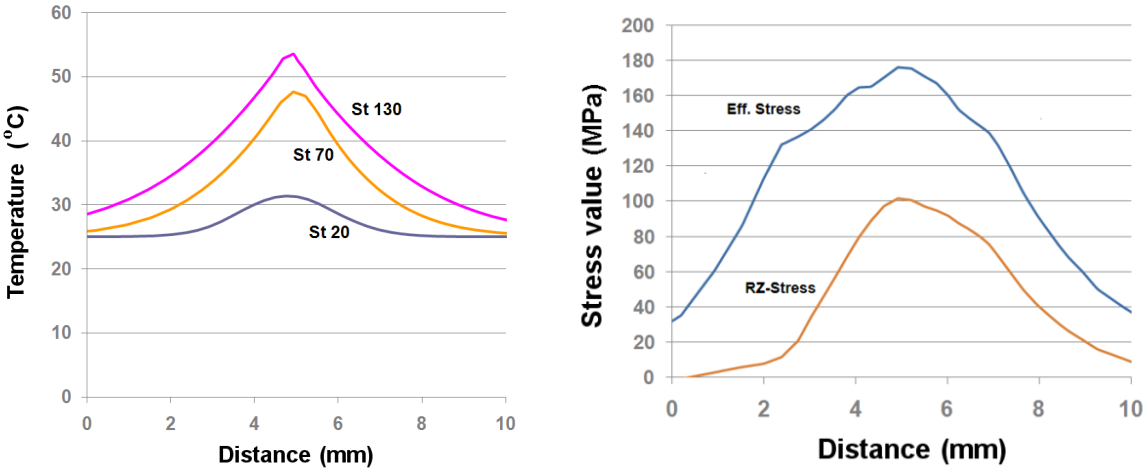

(a) (b)

FIGURE 2.10. FEA-predicted distribution over shear zone of (a) temperature and (b) effective and shear stress.

The effective stress in the shear zone can be determined in different ways. One is from FEA by point tracking and the other by deriving it from the shear stress calculated from the shearing force obtained in the experiment. Assuming pure shear in the middle of the shear zone the effective stress should then equal the shear stress multiplied by a factor of $\sqrt{3} \approx 1.73$. The two upper curves in Fig.2.9 show that there was good agreement between the values of effective stress determined these two ways for the frictionless case.

Another effect depicted in Fig.2.11 is that the FEA-predicted effective stress (i.e. the flow stress) in the shear zone increases during the first part of the stroke and then start to drop down at ~2mm punch stroke length. This is due to the fact that in our material model we specified the flow stress of the plate material to drop by ~50% upon heating it from RT to 56°C, which is too much thermal softening to be realistic for an Al-alloy.

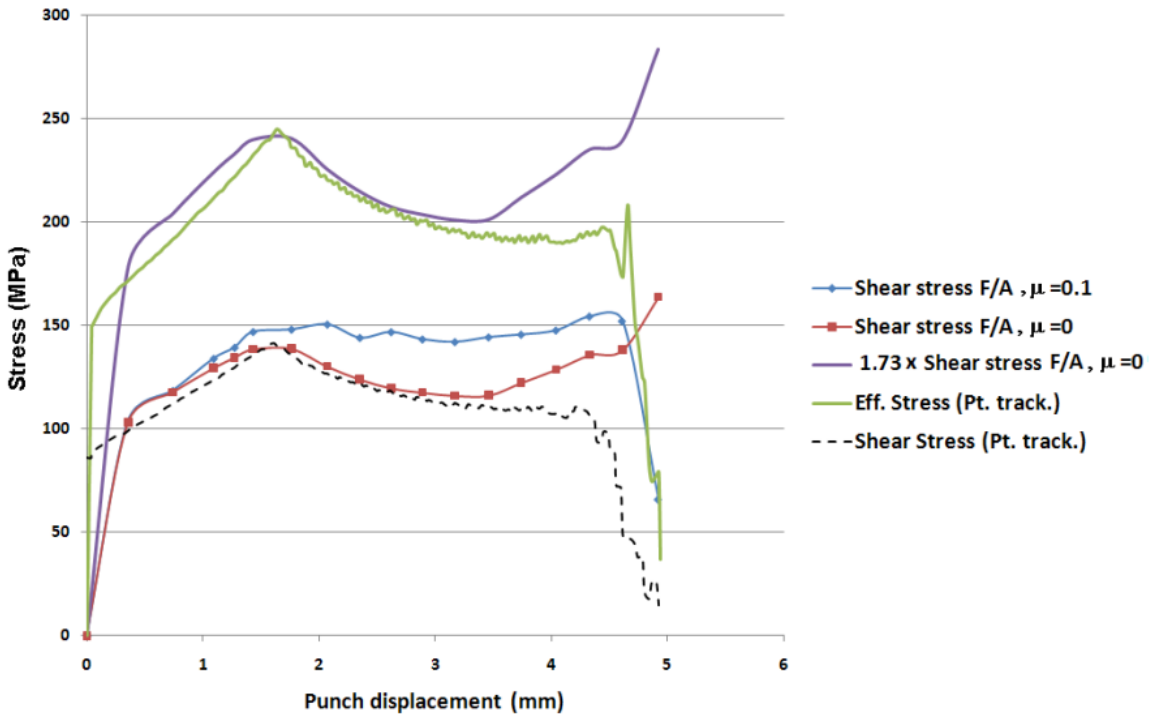

FIGURE 2.11. Shear flow stress and effective stress of shear zone from simulation.

2.4. Experimental work of axisymmetric shearing

Axisymmetric experiments were performed in a mechanical press where four flat specimens of three different thicknesses were partially sheared with zero clearance between punch and shearing die. The initial thicknesses were 3.7 (Exp.no.1 and no.2), 5.6 (Exp.no.3) and 10.4mm (Exp.no.4) for the specimens used. The partial shearing depths of the specimens were 1.9, 3.5 and 8.3 mm. The punch and the die had sharp edges.

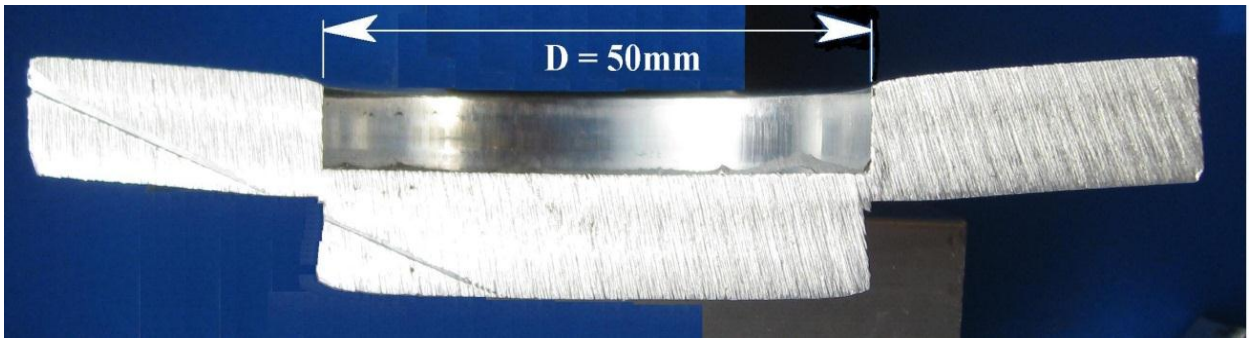

FIGURE 2.12. Section through the partially cut thick specimen.

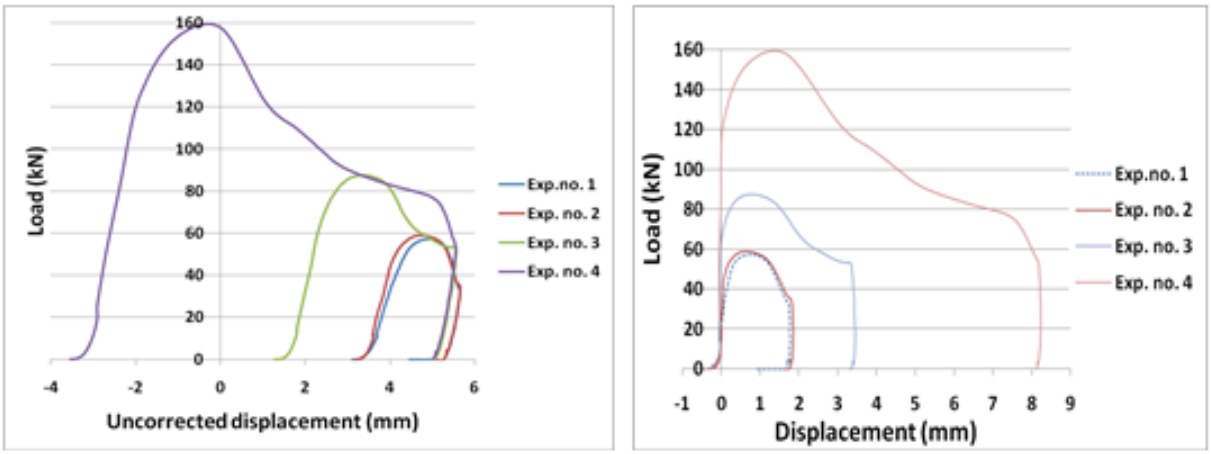

(a) (b)

FIGURE 2.13. Load-stroke data from shearing experiments; (a) before and (b) after adjustment of the zero displacement and correction for elastic deflections.

A photo of the cross-section cut through the thickest specimen is shown in Fig.2.12. Experimental shearing load on the punch was measured vs. the punch displacement. The recorded data are shown as graphs in Fig.2.13. As this figure shows the declining part of the curve behind the peak curved downwards; i.e. a B-type (see Fig.2.1) of load-stroke curve was obtained. Since shearing was done as partial shearing in a mechanical press the velocity varied throughout the stroke, being high in the beginning, then dropping down in a sinusoidal manner until it reached zero at the end of the partial cutting operation. For the thick specimen the velocity in the beginning was 85mms^{-1}.

2.5. FEM-model of the axisymmetric shearing process

A non-isothermal FEM-model was made to mimic the thick specimen shearing experiment using the software DEFORM-2D. Only a short description of the FEM-model is given here, for a full description see [27]. The model corresponded closely to Exp.no.4 with respect to geometrical and shearing conditions, as the real shearing speed was used in the model. A fine FEM-mesh was used in the workpiece material in the layer between the shearing edges to model the shearing process accurately.

The specimen was defined rigid-plastic with Coulomb friction (μ=0.1). A special procedure was used to obtain flow stress data that gave the right simulated punch force. Starting point was the flow stress data given for the alloy Al99.7 in the DEFORM-2D data base. For different temperature levels in the range 20-60 ºC the flow stress values of this alloy was increased by factors in the range 2.2 to 1.1, see [27]. Besides the flow stress was extrapolated up to an effective strain value of 4.

A modified version of the FEM-model was also made, in which the downward punch velocity was set constant and equal to 10mms^{-1}, while the outer shearing tool moved upwards with 10mms^{-1} velocity.

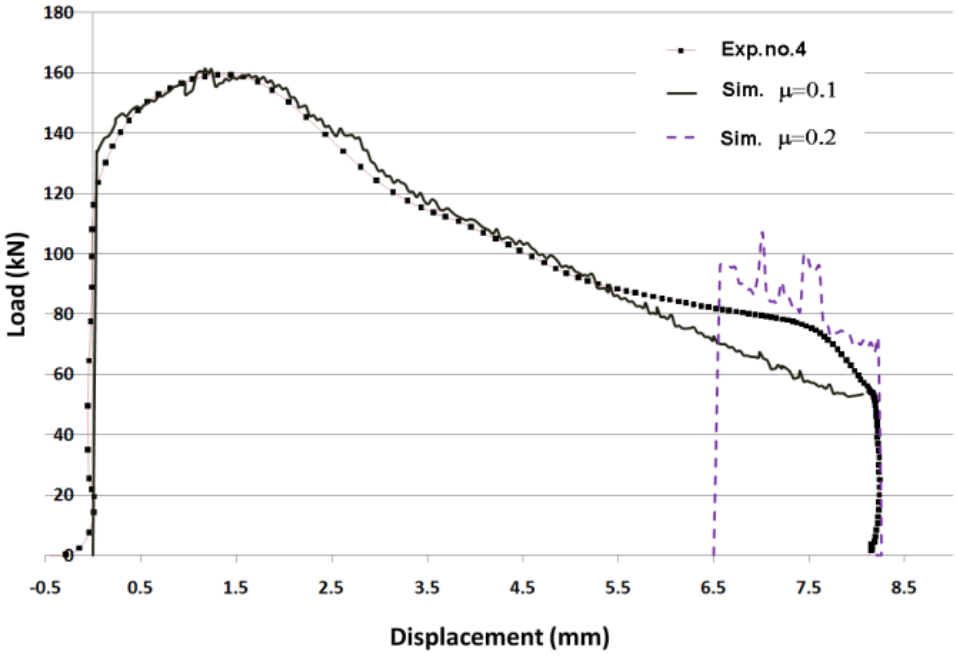

FIGURE 2.14. Comparison between load-stroke curve obtained in experiment and FEA.

2.6. Results of the FEA

When a FEM-model of a forming process has been made it is fast to obtain a lot of information about the predicted mechanics of the process. Results from the thick specimen shearing model will now be shown and discussed.

Fig.2.14 shows an overlay plot of the load-stroke curve as obtained in the experiment and the corresponding FEM-simulation curve. As the figure depicts; with use of the modified flow stress data the experimental punch load response is predicted accurately by the model.

The modified model with constant $10mms^{-1}$ downward punch velocity and $10mms^{-1}$ upward velocity of the shearing die was also used for analysis. It corresponds to shearing with a stationary die and the punch moving downward with $20mms^{-1}$ velocity. The advantage with this model is from a post-processing view because upon shearing the horizontal midline between the two shearing edges remains stationary.

Post-processing was done with the modified model to find predicted shearing conditions along a midline laid through the shear zone of the process, see Fig.2.15 (a). For results from the analysis see Fig.2.15, Fig.2.16 and Fig.2.17. Fig.2.15 shows the predicted velocity distributions in a longitudinal section across the layer between the shearing edges. Fig.2.16 (a) visualizes the total velocity distribution across the shear zone by graphs representing different partial stages of shearing. Fig.2.16 (b) shows the derivative of the velocity distributions in Fig.2.16 (a).

The figures depict that early during shearing there is predicted a velocity gradient in a rather thick layer across the shear zone. As shearing progresses the layer with velocity gradient narrows down and shearing localizes in a thinner layer than before. The degree of shear localization can be quantified by the peak value of the velocity derivative vs. simulation step, see Fig.2.17. This parameter expresses the intensity of shearing in the layer. Fig.2.17 shows that this value is predicted to be low in the beginning. When shearing reaches a certain stage, i.e. simulation step 50 where 30% of a full cut has been obtained, however, this parameter start to increase. From now and onwards this parameter increases steadily until the full section has been sheared off.

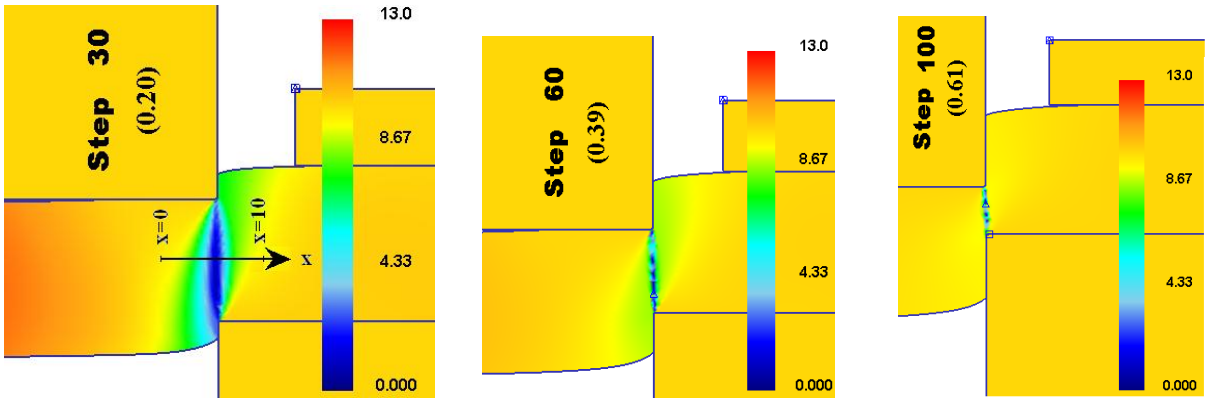

(a) (b) (c)

FIGURE 2.15. Velocity distribution in the shear zone at different stages of shearing. Numbers in parenthesis in this and following figures denote fraction of a full cut.

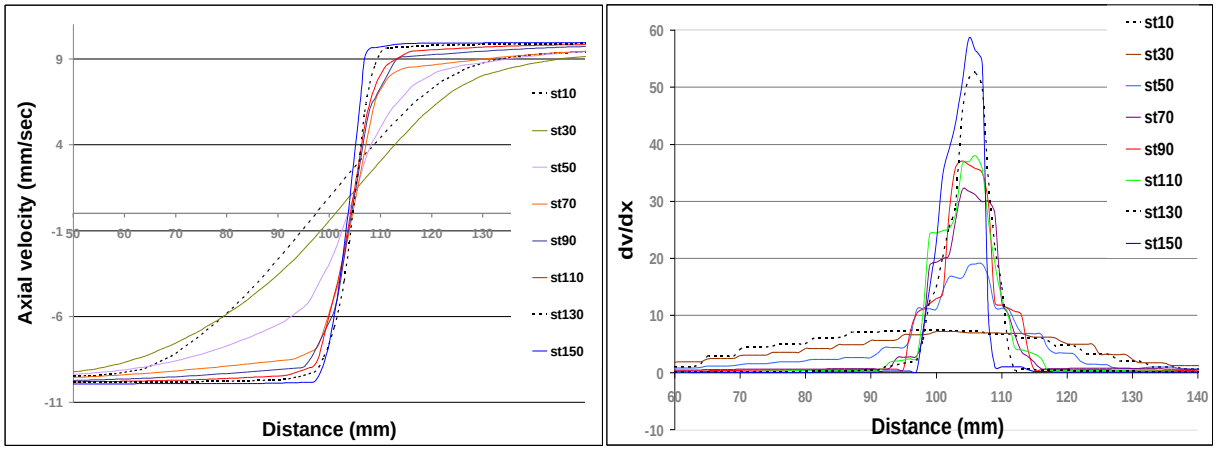

(a) (b)

FIGURE 2.16. Distribution across midline of shear zone of (a) Total velocity and (b) Derivative of velocity.

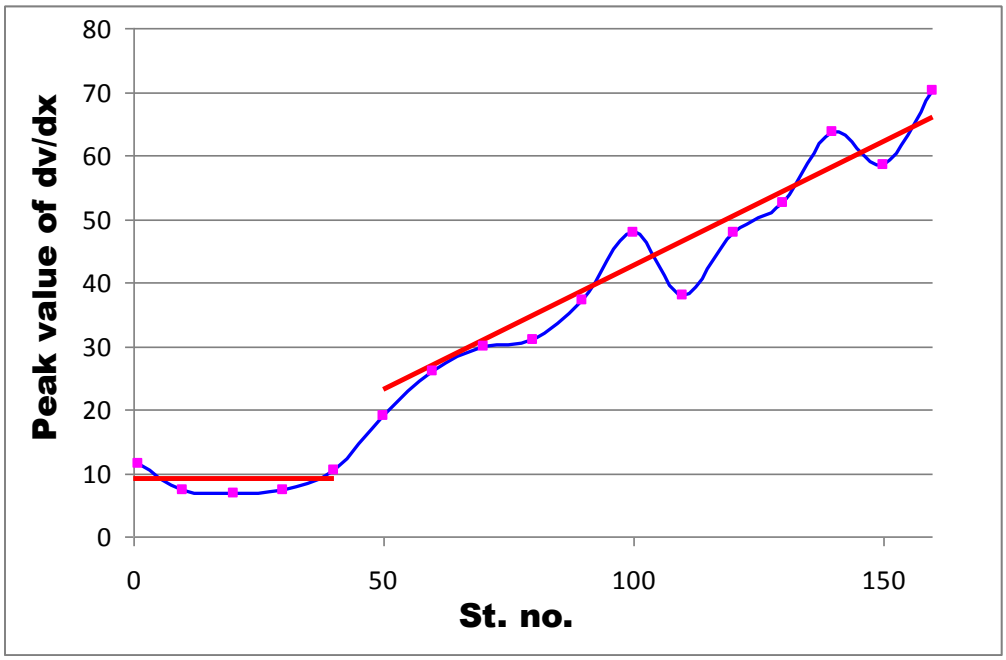

FIGURE 2.17. Maximum value of dv/dx in shear zone vs. simulation step no.

2.7. Experimental study of bar sheraing

In order to be able to perform bar shearing experiments with good control of the shearing parameters the equipment shown in Fig.2.3 was designed and manufactured. The upper shearing punch is shown in Fig.2.3 (a). It was designed with a deep slot into which the bar specimen is inserted before start of shearing. The slot width was 12mm to allow cutting of bars of the same width and different heights (height was12.2mm in the experiments). The punch had round shape with a diameter of 50mm. The lower shearing die and the bar specimens used are shown in Fig.2.3 (b). The experimental setup at start of shearing is shown in Fig.2.3(c). As this figure shows the punch was positioned with its front end extension inside the hole of the lower die ring. As the hole of the die ring had the same diameter as the punch this secured cutting characterized by accurate nil clearance. Both the upper and the lower shearing edges were made sharp without any intentional radius of curvature.

Two experiments are reported here. They were run in a tensile testing machine at low constant shearing speed of 0.03mms^{-1}. The appearance of the specimens after end of the experiments is shown in Fig.2.18. In Exp.no.1 the shearing operation were run until the specimen was cut into three parts, see Fig.2.18 (a). After the first experiment had been conducted one knew when fracture would be expected, so in the second experiment, Exp.no.2,

the shearing operation was stopped before the specimen fractured, i.e. only partially shearing was conducted as the specimen still remained in one piece.

The experiments were performed without any support to the free ends of the bars outside the slot. This caused the free ends to tilt upwards during the shearing operation (up to an angle of ϕ=8°) and the ends were compressed locally against the lower die ring and obtained a depression from the die ring with approximately triangular shape, see Fig.2.18(b).

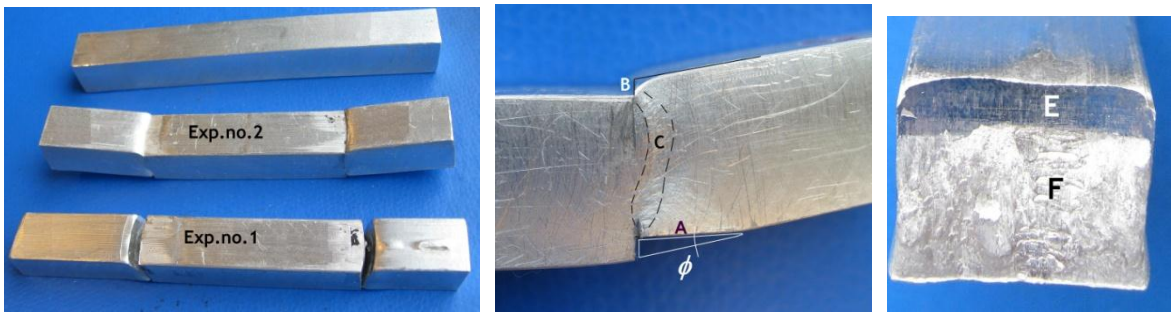

(a) (b) (c)

FIGURE 2.18. Appearance of specimens after the shearing operation: (a) Specimens viewed from the top/ side, (b) Magnified view of side of specimen near the shear zone and (c) View of cut surface of specimen in Exp.2 where a full cut was obtained.

Because of the tilting the free ends of the bar was lifted up from the lower shearing die and the contact zone between the bar and the lower die ring became only the small area (A) near to the ring hole, see Fig.2.18 (b).

However, the sheared-off mid-piece of the bar had rather perfect shape with only a small roll-over depth (B), see Fig.2.18 (b). At the side face of the bars the surface (C) was roughened up because of the shearing action so a pattern of grooves became visible here, mainly present on the surface of the cut-away ends of the specimen. The material of the bar was an AA6005 alloy which had been stored at RT for some weeks after hot extrusion so it had been somewhat naturally aged. This means that the material was in a rather hard condition.

The bars were taken from an extruded strip profile which during the extrusion process had been provided with internal contrast stripes. The contrast material used was an Al-alloy with a low content of Cu. The pattern was placed locally at the mid-width of the strip as longitudinal stripes extending along the length of the strip.

The partially sheared bar in Exp.no.2 was cut along the plane that contained the internal stripe pattern. Then the pattern was revealed by grinding and etching of the section as it occurred in deformed state at end of the shearing operation. Photographs of this section with the deformed grid pattern are shown in Fig.2.19. In Fig.2.19 (b) a black line has been drawn across the bar section indicating the ideal cutting plane stretching between the two shearing edges at the instant when cutting was interrupted. From the photograph it is seen that in connection with the contrast material stripes inside the specimen there is localized shear deformation (see arrows) in the material.

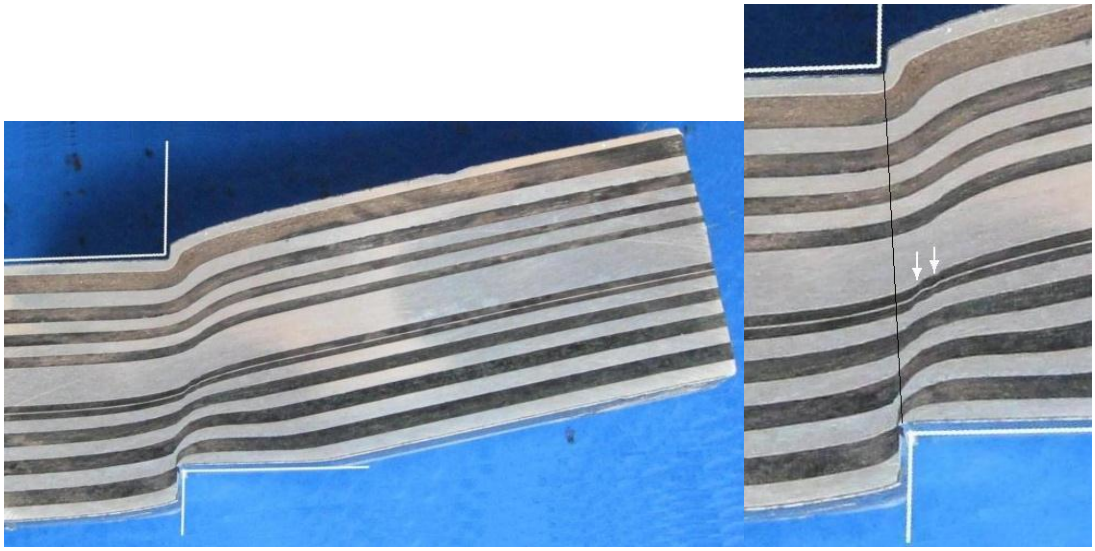

(a) (b)

FIGURE 2.19. Deformed internal stripe pattern in Exp.no.2: (a) Longitudinal section through piece cut from sample, (b) Detail showing material in the shear gap at bigger magnification.

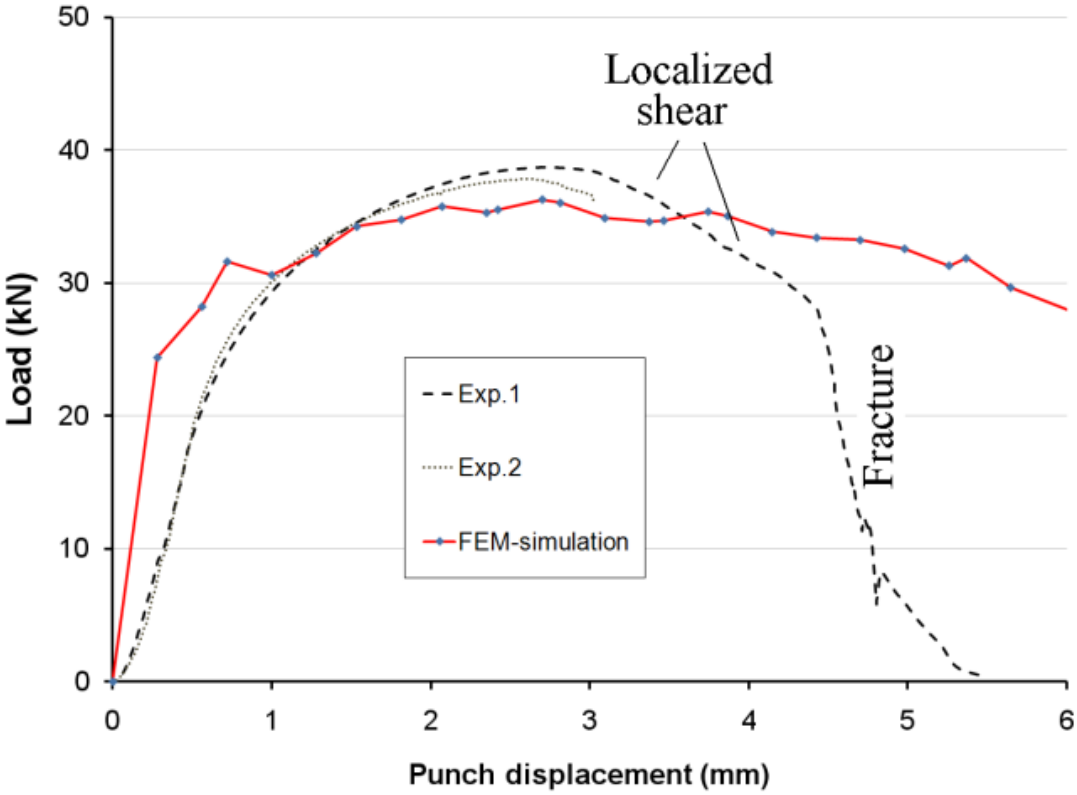

FIGURE 2.20. Comparison between experimental and FEM-simulated load-stroke curves.

The load-stroke curves in the shearing experiments were measured. They are shown in Fig.2.20 for the two experiments together with the load-stroke curve obtained in our FE-model (see next paragraph). As we can see from this figure the load rises steeply up in the beginning of the shearing process, reaches a peak value before it starts to drop down.

In Exp.no.2 the shearing operation was interrupted before there was any fracture or visible crack in the specimen. As Fig.2.20 depicts the shearing process in this experiment was stopped right after the peak value of the punch load had been reached. On the other hand, in Exp.no.1 shearing was conducted fully until the specimen had been cut into pieces. The instant of fracturing of the bar can be identified from this curve since it causes a rapid drop in punch load. From the observations mentioned above that localized shearing starts adjacent to the internal grid pattern inside the bar (see arrows in Fig.2.19 (b)), it is thought that the decrease in the curve just behind the peak is induced by beginning break-down of the material in the shearing gap due to shear localization.

2.8. FEM-simulation of bar shearing

The bar shearing process we used in the experiments was FE-modeled using the software Deform 3D. The FE-model in the initial state of the process is shown in Fig.2.21(a). For reasons of symmetry we reduced the model to 1/4th of the full process, but in Fig.2.21(a) the mirroring option of the software has been used to mirror the bar specimen so it is shown with its full geometry, while only 1/4th of the tooling are shown. The workpiece was assumed rigid-plastic in the model, and thermal effects were included.

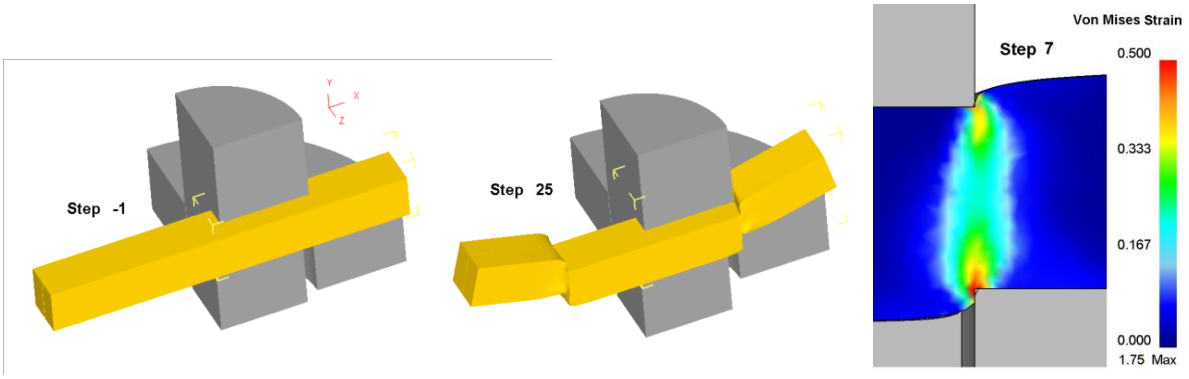

(a) (b) (c)

FIGURE 2.21. FE-model showing: (a) Initial state, (b) Partial stage of shearing and (c) Predicted strain distribution in the shear zone of the bar at the stage corresponding to the end stage in Exp.2.

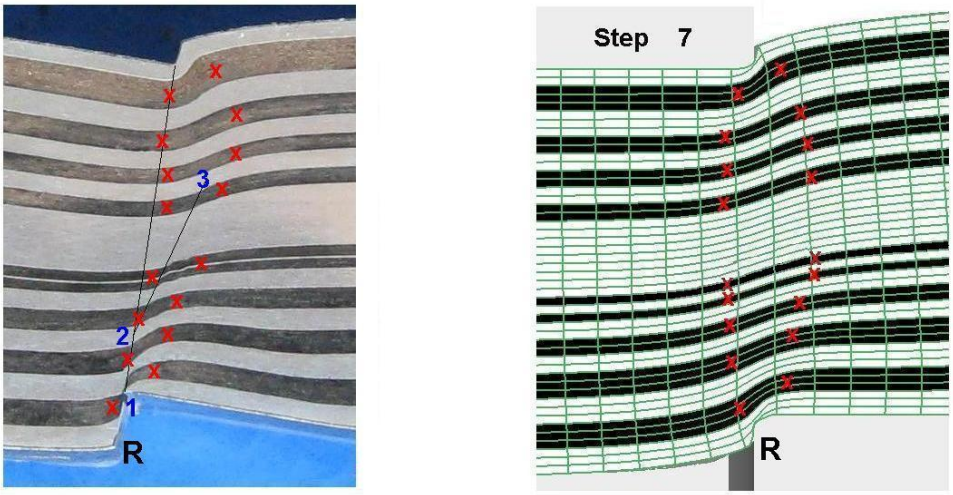

(a) (b)

FIGURE 2.22. Comparison of a) the experimental grid pattern at the end stage of Exp.1 and (b) the corresponding simulated pattern.

Friction was modeled as Tresca friction with the friction factor set equal to 0.6. Since there were uncertainties regarding what material model should be used we tried various models. Rather good agreement was obtained between the simulated and the measured load-stroke curve when we applied a Voce type of material model in terms of $\sigma = A - Bexp(-C\varepsilon)$ with A=200*M Pa*, *B=115* and *C=7.5*.

A dense pattern of fine mesh elements was used in the shear zone where there are strong deformation gradients, and a rougher mesh in the rest of the workpiece. The punch velocity was set equal that in the experiment.

2.9. Simulation result

Load-stroke curves from the simulation work are shown in Fig.2.20 with an overlay plot of experimental curves. As seen from the figure the curves are steeper in simulation than in the experiment because the latter were not corrected for the elastic deflections in the tooling. The peak points of the curves occur at approximately the same punch displacement value both in the simulation and in the experiments, but the load is slightly less in simulation than in the experiment.

In Fig.2.21 (c) is shown the predicted effective strain distribution in the shear zone of the bar at the stage of shearing when Exp.no.2 was interrupted. As this figure shows the largest strains occur near to the lower shearing edge, and have reached as high as ~0.5 here. The region that has been strained in the cross-section has approximately shape as a fir cone oriented at an angle to the vertical axis. As expected there are higher strains in the shear zone near the edges than in the middle of the bar where the shear zone is wider.

In the simulation model a grid pattern was introduced into the longitudinal mid-section of the bar before start of shearing corresponding to the experimental pattern used in exp. no.2. The deformed simulated pattern is shown in Fig.2.22 (b). To ease comparison the pattern from the experiment has been shown again in Fig.2.22 (a). As seen there is quite good agreement between the two patterns with some exceptions. In the experiment the deformation is characterized by more localized shear than in the simulation, as there is a band of localized shear that extends along the thin black lines drawn onto the photograph, between the points numbered from 1 to 2, and then onwards in the new direction to pt. 3. Red crosses were added on top of the contrast stripes in the deformed grid patterns to identify the point where each line shifts orientation from running approximately horizontally along the specimen outside the shear zone, while developing S-shape inside the shear zone. When this is done, see Fig.2.22, it can be seen that the shear zone in the experiment differ from that in the simulation, especially in the lower region where in the experiment the deformations tend to localize.

Another difference is that the rounding (R) of the bottom edge of the bar under the punch head is significantly less in the experiment than in simulation, see Fig.2.22.

2.10. Experimental work including experimental results axisymmetric shearing

At an earlier occasion [25, 26] we performed a series of axisymmetric shearing experiments where small blanks were partially cut across in a mechanical press. The material of the blank was a soft Al-alloy, and different thicknesses of the material were cut. The experiments have been described at an earlier occasion, for details see the earlier article [26]. When we tried to FE-model the thick specimen shearing experiment (t=10.4mm) without including cracking we did not have success. Thus we realized that we had to examine with more scrutiny the partially cut-off sample obtained in that experiment. In Fig.2.23 is shown photographs of this cut sample from different angular views.

A number of characteristic details (agrees with observations reported in the literature) are seen in this figure. First of all, see Fig.2.23 (a, b), the partially sheared off circumferential surface of the slug has a thin stripe-like area (A) with a burnished, shiny appearance at its bottom side. This stripe was created by shearing in the very beginning of the cut. Above there is a broader area with high surface roughness and dull appearance (B). It was created by fracture and crack growth in the shear zone. At the top of the slug one can see the crack (C) which has propagated across the thickness of the specimen. During its growth it has created the fractured surface (B). From the oblique orientation of this surface (angle α in relation to punch movement direction), see Fig.2.23 (a), it is evident that the crack has grown inwards into the material now contained in the slug.

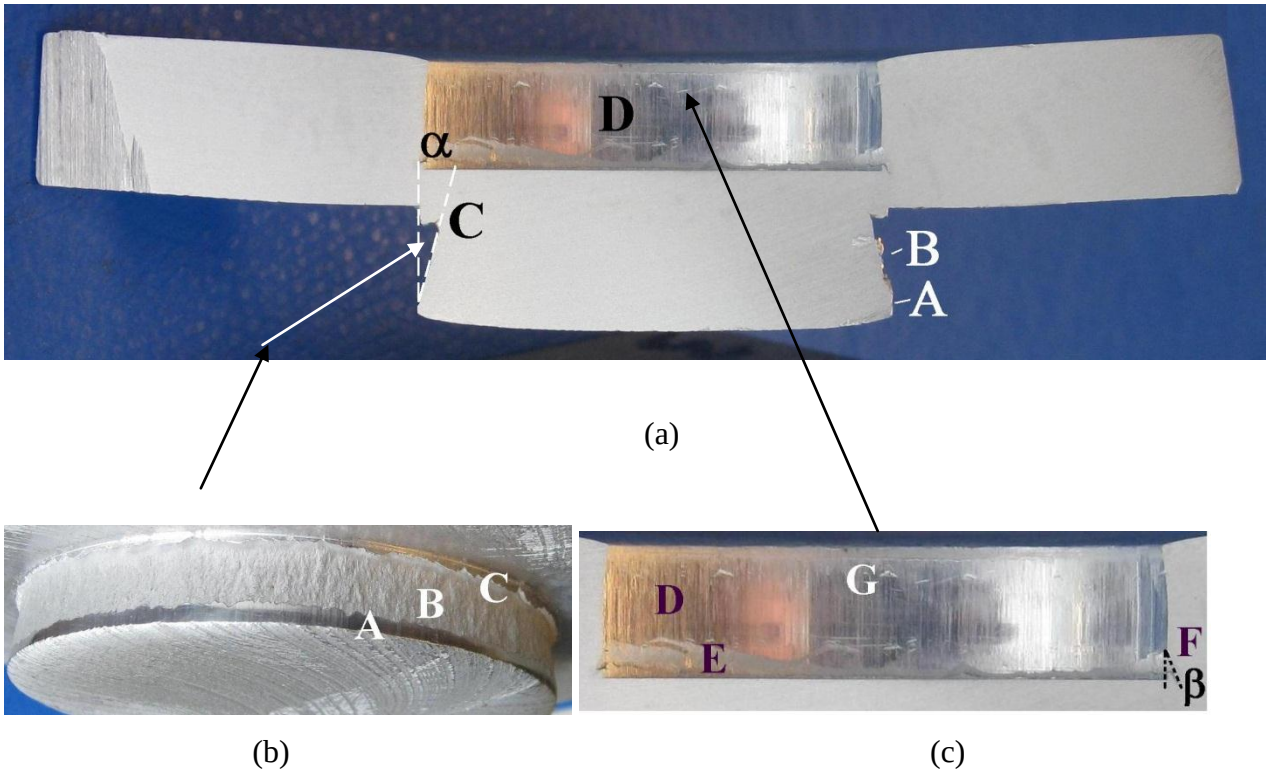

(a)

(b)

(c)

FIGURE 2.23. Photographs of partially sheared thick specimen; (a) Section through specimen, (a) Close up view of sheared surface of blank and (c) Close up view of sheared surface of slug.

In Fig.2.23 (c) is shown the cut-off surface of the blank. It is totally different from that of the slug (Fig.2.23 (b)). It has a burnished, shiny appearance and has been created by a shearing mechanism over the upper cutting edge. Near to the top of this surface there are

some small local arrowhead cracks with white color (G). At the bottom side of this surface cracking appears in a similar way as it does at the top side of the blank surface. A crack (F) has been created here at an oblique angle (β) in relation to the direction of movement of the punch. This crack did not initiate concurrently over the circumference of the specimen. Because of this, on the inside cut surface area of the blank there is a thin stripe (its thickness varies over the circumference) for which the surface was generated by crack growth (E). This surface has a dull, matte, surface appearance, and the thickness of it varies irregularly over the circumference of the surface, sometimes this stripe is narrow, sometimes it is broader.

2.11. FE-modeling of the axisymmetric shearing operation

We built the new FE-model the same way as in an earlier study of shearing. For details other than those given below we therefore refer to that article [25]. One significant difference, however, was that now that we chose the flow stress of the workpiece material to be that given in the DEFORM material database for the Al-alloy AA3003, while in the earlier investigation we tried to soften this material when temperature increases as it does inside the shear zone. Modeling was done by means of Deform 2D, because this software has been used successfully by one of the authors in many other similar applications [51]. All dies were ,modeled as rigid and the specimen as rigid-plastic.

Fig.2.24 (a) shows the new simulation model where an imaginary wedge-shaped die mimics cracking. In the beginning of the stroke the wedge is kept in the same position as the lower shearing die, but at a stage corresponding to crack initiation in the experiment, the wedge is moved forward in the direction of crack growth (direction 1) to penetrate into the edge. His way a crack-like depression can be created on the edge as in the experiment, with full freedom of movement of the crack, both with regard to direction and velocity of movement. Later during shearing, when the crack halts, the forward movement of the wedge is stopped, and it is instead moved vertically downwards (direction 2) so that the crack length now starts to decrease.

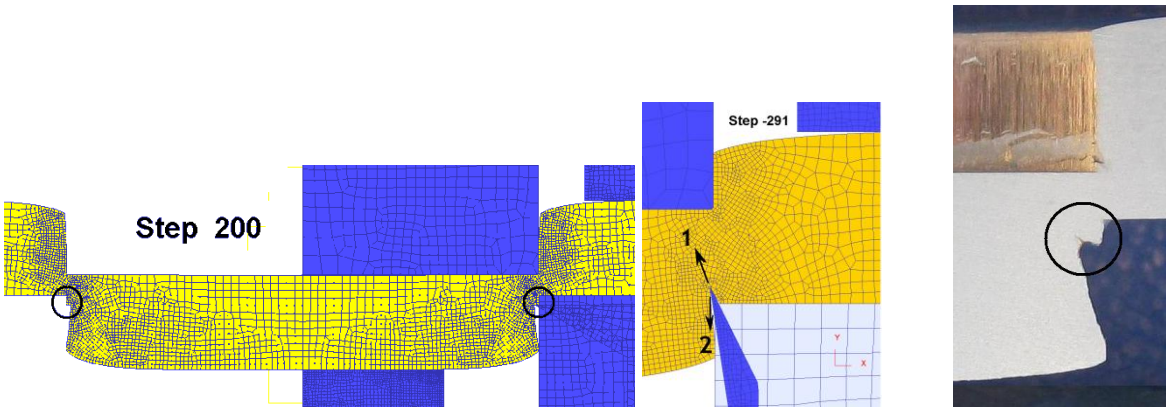

(a) (b) (c)

FIGURE 2.24. (a) Mirrored version of FE-model, (b) Close up view of simulated shearing zone with wedge-shaped die to create crack, and (c) Detail from experiment corresponding to that shown in (a).

In this simulation model the wedge was moved so that it agreed with the observation of the crack appearance in Fig.2.23 (a), concurrently taking into consideration the measured load-stroke curve shown in Fig.2.5.

A comparison between Fig.2.24 (a) and (c) shows that the final appearance of the crack (see circle) is very similar in the new simulation model and in the experiment. The full movement of the wedge throughout the whole simulation that we used is given in Fig.2.25 (a), and the resulting load-stroke curve obtained in this case is shown in Fig.2.25 (b). The experimental load-stroke-curve has a characteristic peak, then downwards curvature, followed by the flat plateau, finally droping rapidly down towards end of shearing. FE-simulations of axisymmetric and plane strain type give a straight declining curve behind the peak. The new FE-model with the presence of a crack-like depression in the cut surface of the blank that grows into the material, however, is able to reproduce the experimental curve with good accuracy, when "crack" growth is selected as in our model during the shearing operation. In Fig.2.25 (b) is shown the good agreement obtained between the experimental curve and that in our FE-model mimicking cracking.

To obtain this good agreement in load response the model had to be run in five separate stages, following after an initial stage characterized by plane-strain shearing without any crack. Then three stages followed in which the wedge was mimicking crack growth, with different growth velocity into the edge of the blank. After the third stage the wedge was

stopped and moved vertically downwards, first with high (stage 4) and then with low velocity (stage 5).

The velocity profile applied to the wedge during the different stages of simulation is shown in Fig.2.25 (a); After 1.5mm punch displacement the wedge starts to penetrate the edge with constant speed of 30mms^{-1} and an angle α=16°. After this there was a stage with high velocity of crack growth, i.e. 40mms^{-1}, before decreasing the velocity down to 5mms^{-1}. At a punch displacement of ~4.7mm crack growth was stopped as the wedge was moved vertically downwards, first with high velocity, and later on with less velocity.

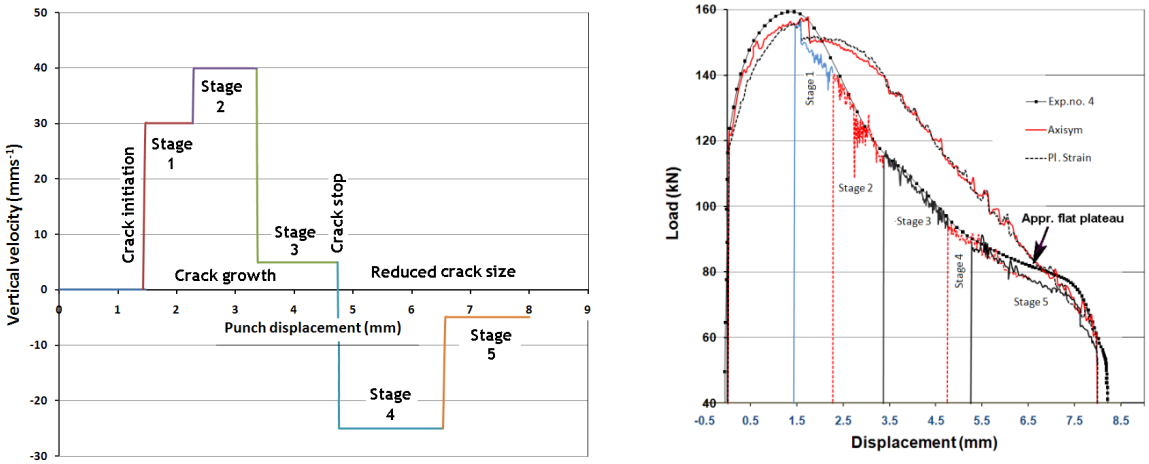

(a) (b)

FIGURE 2.25. (a) Velocity profile for the wedge forging a crack-like depression in the edge of the blank, (b) Load-stroke curve in new simulation model compared with experimental curve.

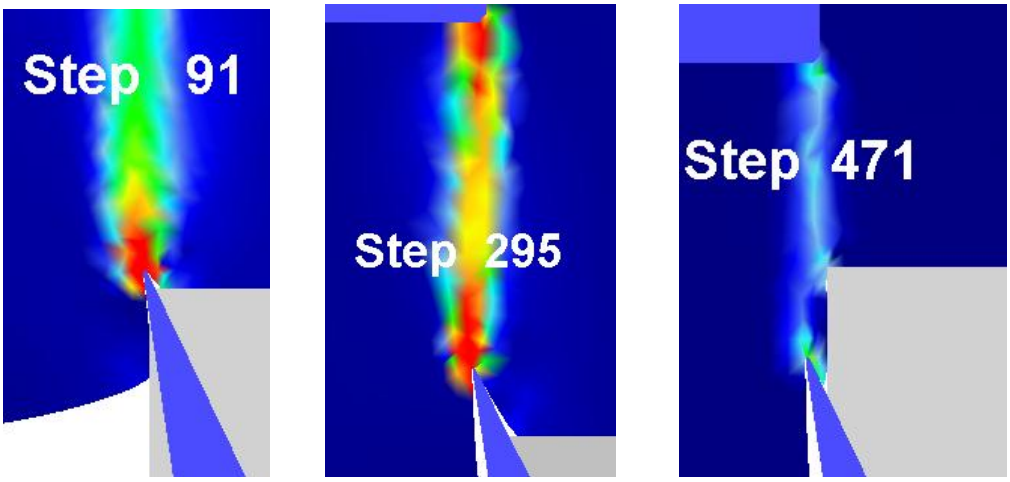

(a) (b) (c)

FIGURE 2.26. Different locations of wedge-shaped "cracking" tool: (a) After initiation of crack, (b) Growth to maximum crack size, and (c) Downwards tool movement; the crack becomes displaced out of the gap between the shearing edges.

In Fig.2.26 have been shown simulation pictures of the wedge at three different stages of the shearing process as it forms the crack-like depression. Fig.2.26 (a) is just after initiation of the crack; the shear band across the shear zone has not yet been significantly influenced by the presence of the crack, as the highest intensity of shearing appears along an approximately straight line extending between the two opposing shear edges. In Fig.2.26 (b), however, the crack has penetrated into the edge and has reduced the effective length of the shear zone by ~25% in comparison to a situation without a crack. Hence also the required punch force must have been reduced by a corresponding amount. Fig.2.25 (b) confirms that this is the case.

Fig. 2.26 (c) shows the situation after the wedge was stopped and moved downwards; the crack tip has been displaced downwards with the blank, so it remains no-longer in the shear zone between the edges. Instead a piece of workpiece material remains at the horizontal surface of the lower cutting edge, and shear takes place in a layer inside this material, without material sliding over the tip of the lower edge. These observations clearly depicts that the flat plateau towards the end of the load-stroke curve in shearing occurs because the crack becomes pressed downwards out of the shear zone between the two edges. As this takes place, the distance across the shear band remains approximately constant, or is only slightly reduced; hence the punch load remains approximately constant.

Fig.2.27 shows the FEM-predicted conditions near the lower edge where the crack appears in shearing, in terms of the Cockroft-Latham damage parameter, the largest principal stress and the effective strain. The figure depicts that the crack is created here because of the presence of a tensile stress zone [51] near this edge.

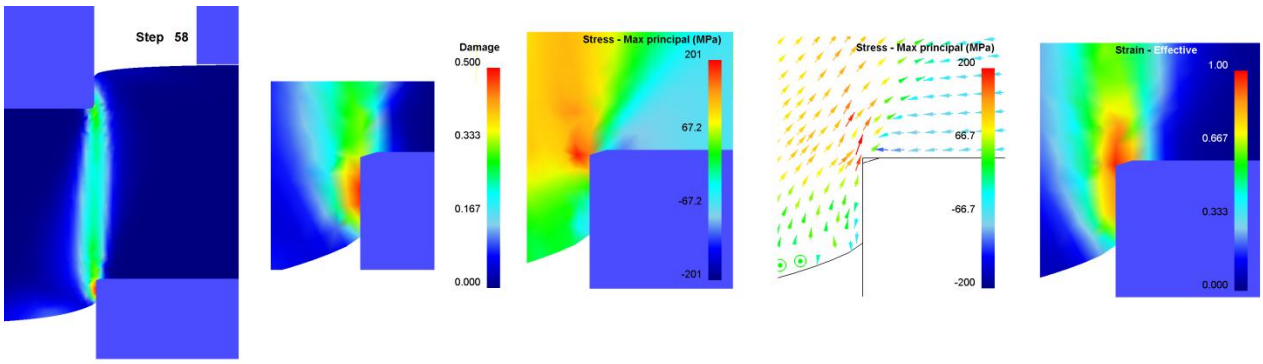

FIGURE 2.27. Conditions leading to crack formation in the sheared-off surface adjacent the lower edge: (a) Damage parameter, (b-c) Maximum principal stress and (d) Effective strain.

2.12. Discussion

It was tried to use an inverse FEA-approach to determine flow stress from an experimentally measured load-stroke curve. By adjustment of the flow stress it was arrived at a FEM-model that reproduced the experimental behavior well. However, to obtain good agreement, the flow stress of the material at temperatures just below 60°C had to be set unrealistically low. A possible explanation, why there was such bad agreement in the analysis between assumed and real flow stress of the material, may be that in the experiment the shear zone in reality moved laterally away from the plane where FEA predicted it to remain.

In spite of the problems encountered in our analysis, it shows that the deformation mechanics in shearing are so that our analysis approach can be viable if developed further. So to be able to acquire accurate flow stress data from load-stroke curves in shearing one must be able to model the shearing conditions as they are in the real test. In addition one must eliminate effects of friction by selecting appropriate shear edge geometry. Finally one must

use a sufficiently fine FEM-mesh and the FEM-model must be made accurate so that it mimics the real test.

An inverse modeling procedure was used in this work to derive flow stress data able to predict the same load-stroke response in FEM-simulation as in the experiment. When this approach is used it can be questioned if the resulting FEM-model will be able to describe the mechanics of the shear zone between the cutting edges correctly. This will not be the case unless the shear zone remains in the same location during experimental shearing as it does in the FEM model.

The modified flow stress data obtained by us had lower values toward end of shearing than if flow stress had been acquired in compression testing. So if the analysis is correct there must be more softening taking place in the shear zone during shearing than expected from normal flow stress data for the material. However, more work has to be done within this field to arrive at more secure conclusions on the flow stress and the mechanics of the shear zone in reality. In simulation it was not straightforward to reproduce the appearance of the experimental load stroke curve at high stroke values where it tends to flatten out. This rather flat level can however be explained if there at this stage is assumed an increase in friction between the workpiece and the tooling.

The work reported here shows that the use of internal grid patterns inside the material in shearing operations can provide useful information about the deformational conditions in the material that is being cut. By means of such grid patterns it is possible to identify the real deformations present in the shear zone. Our attempt to reproduce the behavior in the shear zone in the shearing gap between the approaching shearing edges shows that it is not obvious that a FE-model will be able to predict reality.

The advantage with the grid pattern technique used by us in this analysis on shearing is that we can use specimens that do not need to be split, and the pattern will be visible even though the deformations are heavy.

An important aspect when using the internal grid pattern we have used in this work, namely a pattern made by adding contrast material as stripes into the base material, is that the deformation properties of the material of the specimen must not be changed because of the insertion of the contrast material.

In this investigation we used a grid pattern composed of rather broad stripes, and there were many stripes laid across the specimen thickness. However, in order to check if there is localized shearing taking place over the section being cut, it will be sufficient to use thinner

contrast stripes. In addition one can reduce the number of stripes placed across the thickness of the specimen. With such use of a minimum amount of contrast material inside the specimen it will be less likely that the plastic flow behavior of the material of the workpiece will be influenced.

There are uncertainties about the accuracy of the material model used in the FEM-simulation in this work. In future work it is therefore recommended to collect more accurate flow stress data for the applied workpiece material, by for instance running cylinder compression experiments on the material.

When we earlier tried to model [25] the shearing process and the conditions in the shear zone we assumed reduced load behind the peak of the load-stroke curve to stem from thermal softening. When the flow stress at the raised temperatures (~50-60º C) predicted in the shear zone towards the end of the cut was lowered beyond what is realistic, we got the simulated load-stroke curve approximately equal that in the experiment, but we did not get a flat plateau near the end of the curve. Another explanation we excluded at that occasion was that the flat plateau was due to increased friction.

After these negative results [25] we started to look at the possibility that the characteristic shape of the load-stroke curve could be due to the growth of a crack into the workpiece material. Having previously studied crack modeling [51] using the FEM-code DEFORM, using the fracture mechanics tools provided with this program, we thought that modeling of the initiation and the growth of a crack this way would not be straightforward.

We therefore decided to try a new approach based on creating and propagating the crack in the material by a forging procedure, using a wedge-shaped tool, and forcing it to penetrate into the material to mimic cracking. When the model was built, we used a step-wise procedure for setting the movement of the wedge-shaped tool. Simulation was run shortly ahead, then it was checked if there was good agreement with the experimental load-stroke curve. When agreement had been obtained, a new velocity of the crack forming tool was decided at. In this way we arrived at the velocity profile depicted in Fig.2.25 (a) of the wedge-shaped tool. It is believed that real crack growth will agree well with that obtained by us, but in addition the velocity profile is expected to be somewhat smoothened out.

To validate the crack propagation rates we have obtained, additional experimental work is recommended. Shearing should then be performed to different shearing depths, and the actual crack depth obtained for each depth should be measured, to map real crack growth.

2.13. Conclusions

The mechanics of the shearing operation can be complex and hard to model by FEA. To be able to acquire accurate flow stress data from axisymmetric shearing experiments some conditions must be fulfilled. Friction between the shearing tool and the blank should preferably be eliminated. If the shear zone in reality moves laterally away from the plane extending between the shearing edges this must also be included in the FEA. Finally, the FEM-model must numerically be optimized to model the shearing process accurately.

Knowledge regarding the shear deformation in the internal shear zone in axisymmetric conventional shearing conducted on an Al-alloy can be obtained by FEM-analysis. In our analysis it was predicted that this zone remains rather thick, and without shear localization in the first $1/3^{rd}$ of the process. However, upon transition to the second stage the conditions changes as the shear zone starts to become thinner, concurrently as the shear intensity in it starts to increase. This trend continues throughout the last $2/3^{rds}$ of the process.

Use of an internal grid pattern inside the workpiece subjected to shearing can provide useful information regarding internal deformations in the material across the shearing gap. In this way it was shown by us that the deformations in the shear zone in the experiment deviated from those predicted in the FE-model. In the experiment localized deformation developed in the material adjacent to the sharp-edged counter-die ring, while in FEA deformations were predicted more even here.

Due to the localized deformations the experimental load-stroke curve showed a stronger gradual drop in load behind its peak value than in the corresponding simulation.

After localized shearing had progressed for a while, there was a transition to rapid fracture. A crack was formed and grew suddenly across the section of the bar. When this happened the shearing load dropped suddenly down, concurrently as the bar was cut into separate pieces.

In FE-modeling of shearing a sharp wedge-shaped tool can be used to mimic cracking in the material being cut. At the stage in the shearing experiment when the crack starts to appear in the material the wedge can be pressed into the cut-off surface of the slug to initiate the beginning crack; further movement of it can mimic crack growth.

Cracking in the workpiece material in sharp edged shearing occurs because of the presence of a tensile stress zone over the edge where cracking occurs.

The shape of the load-stroke curve in shearing depends strongly on crack formation and crack growth. A crack that grows into the material reduces the remaining thickness of the blank, hence required shearing load decreases in relation to shearing without crack presence. When the crack halts, it becomes gradually pressed out of the shear zone by the advancing cutting punch. In this stage the remaining material thickness across the shear zone will not change much, and because of this there appears a flat plateau in the load-stroke curve towards end of shearing.

3. ANALYSIS OF GAS POCKET FORMATION DURING EXTRUSION OF ALUMINUM PROFILES AND ESTABLISHING AN EXTRUSION SEAM WELD LIMIT DIAGRAM

3.1. Introduction

Recent development within the field of finite element analysis (FEA) has made it possible to simulate [48] on the computer the conditions as regards mechanical and thermal behavior of the extrusion metal of a billet when it is pressed through an extrusion die like in an industrial extrusion process. The accuracy of such an analysis, however, depends on how accurately the FE-model has been built, and on the input-data such as the flow stress and the boundary condition in the model; they must be accurate and descriptive for the alloy considered.

One important mechanical characteristic of the extrusion process is the metal flow inside the material of the billet during the course of the extrusion process. The fact that metal flow is of great importance for the result in extrusion was confirmed by classical experimental work conducted in the early years of extrusion [18, 4, 34, 38, 62, 2]. Then it was discovered that many of the common extrusion defects encountered in extrusion in fact are caused by metal flow phenomena, like for instance the formation of the defect commonly called pipe, towards the back end of the extruded rod.

Strong efforts were early [18, 21, 9, 14, 47, 37, 40] directed towards the development of visioplastic techniques that can show how the metal inside the billet flows forward towards the die, and through the primary deformation zone ahead of the dies used in industrial extrusion of Al-profiles. Thanks to this work advanced grid pattern techniques can now be used, such as for instance the technique where internal contrast material pins are inserted into holes drilled into a symmetry plane of an extrusion billet to create an internal pattern there. How such a grid pattern analysis is conducted, and the advantages of this kind of pattern, has been described in [48]. Moreover, methods have been developed making it possible to remove partially extruded billets from inside the extrusion container without damaging the outer surface skin of it by plastic deformation. When such removal techniques are used one can study accurately how the contact conditions between a billet and the tooling, (i.e., the die, the container wall and the ram head) have been during an extrusion experiment; the billet surface can either slide against the tool surfaces or there can be full sticking friction without sliding movement at all.

Hot or cold extrusion is the process by which a block of metal is forced through a die orifice under high pressure and is reduced in cross-section. Mostly, cylindrical bars or hollow tubes are produced this way but it is also possible to obtain complex shapes of products. However, products which can be produced by cold extrusion are relatively limited in size. If one considers axisymmetric forward extrusion, the main processing parameters which affect the resulting extrudate quality are; the press ratio, the die cone angle, the friction between the workpiece and the tooling, the mechanical properties of the material such as hardening and ductility characteristic, and the heating effects during forming. [41]

Friction affects not only the quality of the workpiece in metal forming but also the forming force. The force caused by friction depends on the lubrication conditions at the interface between workpiece and container. Thus, one should investigate different lubrications when studying the forming processes. In combined FEA and experiments were used to obtain friction coefficients for cold forging processes like forward bar extrusion, forward tube extrusion and backward cup extrusion. A new friction testing method has been investigated assuming that the friction coefficient can be estimated without necessity of knowing the forming load and the flow stress of the workpiece. Using a realistic friction model a rigid-plastic FE-code was used in this work to investigate the friction distribution in the metal forming process. In axisymmetrical forward extrusion was studied both using a classical plasticity model with isotropic hardening and a nonclassical constitutive model.

The required force for the extrusion process is commonly considered to be composed of four additive parts represented by the formula:

$$F = F_b + F_{dh} + F_{fd} + F_{ds} \tag{3.1.}$$

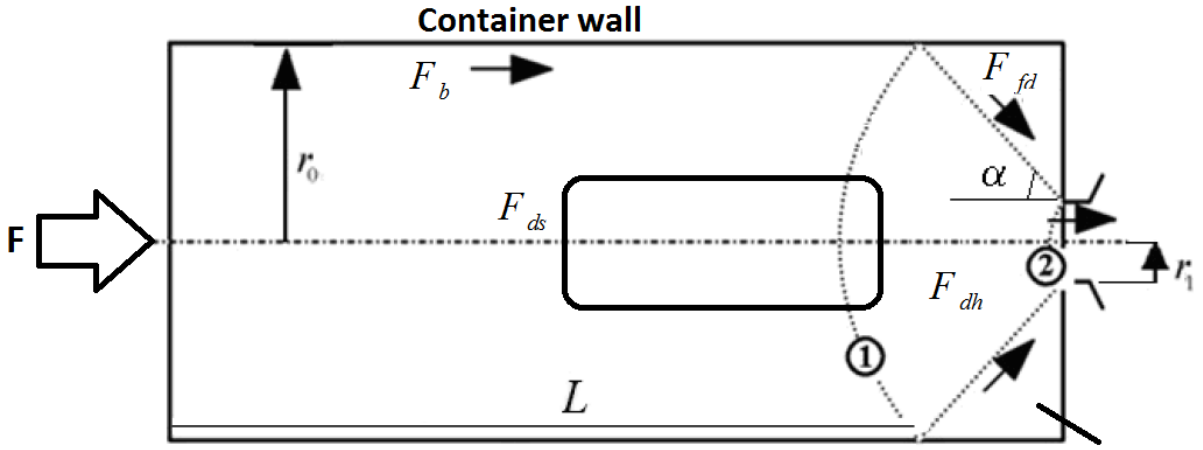

FIGURE 3.1. The total extrusion force is made up of four parts

These parts are shown in Fig.3.1; fc F is required to overcome the friction resistance against the container wall when the billet is pushed forward and starts to slide against the container wall, dh F is to overcome the deformational resistance to deform the metal homogeneously during flow through the conical primary deformation zone in front of the die, fd F is to overcome frictional resistance when the extrusion material in the primary deformation zone flows against the surrounding dead zone. Finally, ds F is the force to shear deform the material as it flows through the velocity discontinuities present at the entrance to and at the exit from the primary deformation zone.

In the literature it has been shown by theory how expressions can be deduced for each part of the force in eq.(3.1.), see for instance[3, 49, 36, 35, 39, 24, 43]. Then one arrives at the expression:

$$F = \overbrace{\tau \cdot 2\pi r_0 L}^{F_b} + \overbrace{\pi r_0^2 \bar{\sigma} ln \frac{r_0^2}{r_1^2}}^{F_{dh}} + \overbrace{\pi r_0^2 \frac{\tau_1}{sin\alpha\ cos\alpha} ln \frac{r_0^2}{r_1^2}}^{F_{fd}} + \overbrace{2\tau_2 \pi r_0^2 (\frac{\alpha}{sin^2 \alpha} - cot\alpha)}^{F_{ds}}, \quad (3.2)$$

where τ1 is the friction shear stress against the tooling, τ2 is the shear flow stress and σ the flow stress of the extrusion material. The other parameters used in the equation are shown in Fig.3.1. A similar equation for the extrusion force has also been developed by Avitzur [49] (based on an upper bound solution).

The hollow extrusion sections are produced by using porthole dies. The billet material is split by the die bridges into metal streams which pass through the portholes and around the mandrel. The re-joining of metal streams takes place in the welding chamber before the bearing zone of die. The quality of the welds in the extrusion profile has been subject to testing because the inferior weld might cause manufacturing problem which can reduce the productivity of the process, the mechanical integrity and the surface quality of the profile. On the other hand different testing procedures are adopted to check the welds that exist along the length of a profile. The testing methods are applicable only when the expensive extrusion dies are already built and corrected. [17]

One should be aware that the importance of the concept of maintaining adequate interfacial welding pressure between the metal streams making the seam weld has been known for a long time. Akeret [1] not only suggested a critical pressure of at least three times the flow stress of extruding material but also proposed certain geometries of welding chamber to attain proper welding of metal .

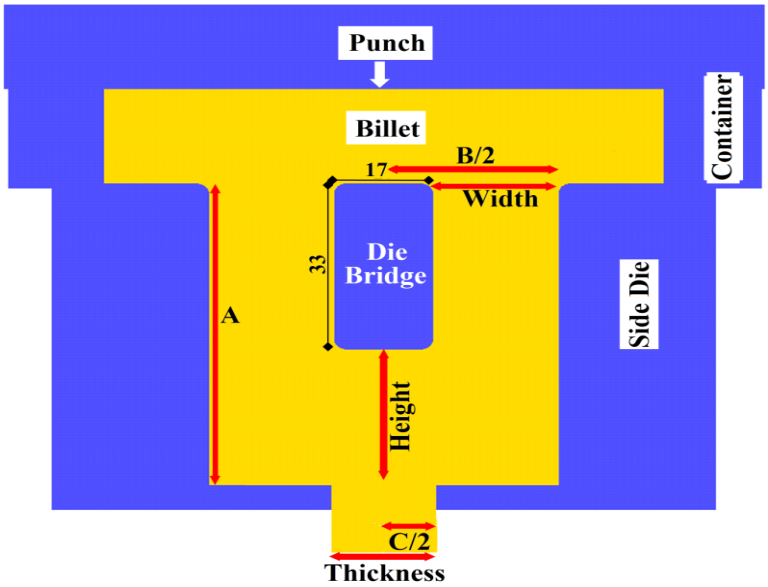

FIGURE 3.2. Geometrical condition in the 2D-extrusion models at start of simulation.

streams. For the case of pothole extrusion he also pointed out that it is important to attain adequate metal flow into the gaps between the cores of the mandrel. To obtain proper metal feed in this location various combinations of the welding geometries should be tested.

According to Akeret appropriate joining of the different material streams in the welding chamber require a sufficiently large welding chamber. When the welding chamber is too small the metal streams are not pressed completely into each other, and it is not possible to get a full profile section. When there is a wide welding chamber, one gets a dead zone

behind the bridge. Sometimes in the welding chamber behind the bridge, a gas pocket may be observed. If this gas pocket forms, there will be weak extrusion seam quality in the final extruded profile. In case of extrusion of hard alloys aiming at optimum die strength, a narrow welding chamber would be favorable. But, on the other hand the welding chamber should be wide in order to obtain complete filling of metal and optimum pressure conditions upon seam welding. Valberg [55] used a particular extrusion geometry which gives a gas pocket behind the bridge and low pressure seam welding conditions. A small welding chamber size close to the critical size was chosen intentionally to obtain a gas pocket behind the bridg to investigate the conditions of seam welding with little feed of metal into the weld chamber.

Though the billet preheating and speed affect the flow distribution and also changes the temperature within the die, design of the die has significant affect on the yield in extrusion production [16]. In order to get strong welds in hollow section profiles various weld criteria has been considered to obtain rules for proper die design. The height and width of the welding chamber in relation to the die exit has been considered critical and main factors to provide good extrusion seam welds.

Many rules and criteria for seam welds quality evaluation have been considered. The first study was by Akeret who expressed the maximum pressure at the interface between two material flows as the discriminating parameter for material welding. Another criterion was proposed by Piwnik and Plata, and it uses as discriminating parameter the integral over time of the contact pressure, rated to the actual effective stress acting on the contact surface. Another criterion was expressed by Donati and Tomesani [8], which considers the velocity as a correction factor, in order to reduce the influence of the dead zone below the web on the integral value.

However, with the availability of finite element codes, it is now possible [56] and easy to evaluate the plastic flow of material in the welding chamber in fine detail. In this study various simulations have been run where the geometrical parameters of the welding chamber have been varied to see how the nature of metal flow behind the bridge will change.

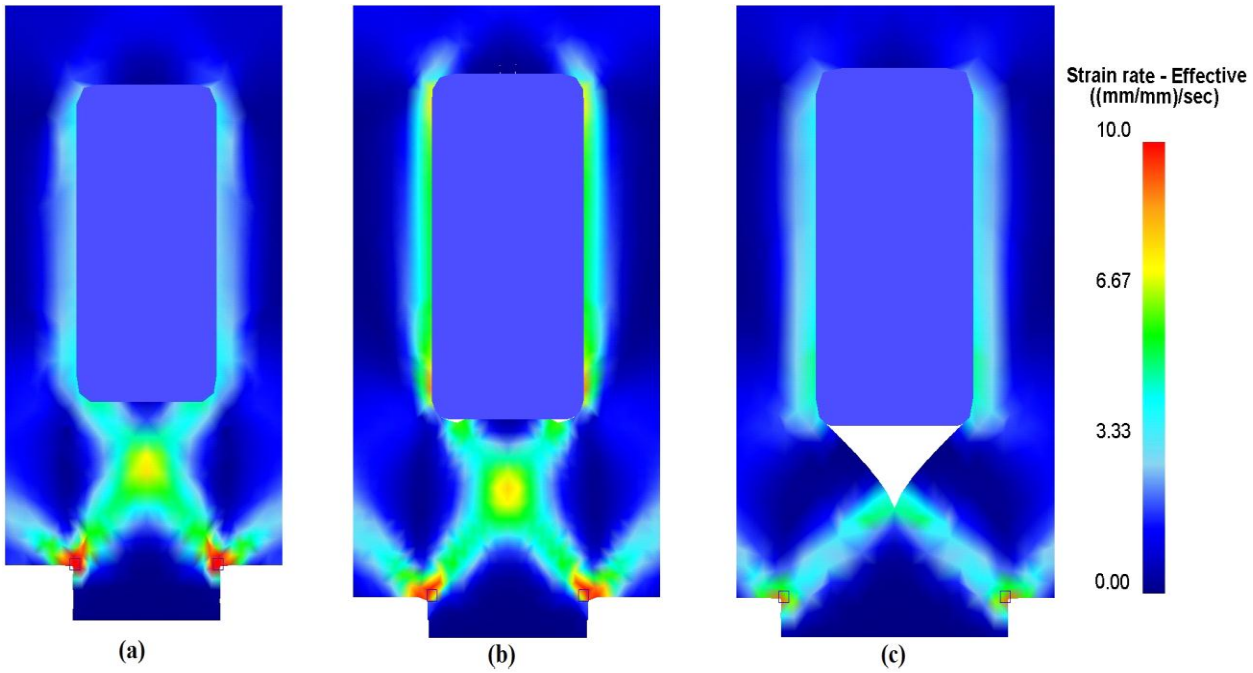

FIGURE 3.3. Reducing material feed into the space behind the rear end of a butt-ended bridge brings about a transfer from; (a) Complete filling → (b) Partial filling → (c) Presence of stable gas pocket behind the bridge.

3.2. Experimental work

Results from earlier laboratory extrusion experiments [54] performed before the turn of the last century will be used here for validation purpose (for experimental details see that work).

Industrial cast homogenized billets of 97mm diameter and 150 mm length were used in the experiments. They were turned down to 73 mm diameter before heating and extrusion using a 75 mm diameter container. The dies had holes of 9 mm diameter and the center-to-center-distances between the holes were 44.75 mm (LHD) and 14.9 mm (SHD) for the two different dies (at room temperature), respectively. The ram velocity was 5 mms^{-1}. Two alloys were investigated, i.e., AA6063 and AA7108. Grid patterns were made by inserting radial and axial indicator pins into holes drilled into the billets. The billet and the container had the same temperature, i.e., 480°C, at start of extrusion. Two partially deformed grid patterns obtained in the experimental investigation (after 14.3% partial extrusion) are shown at the top of Fig.3.6 for the purpose of comparison with corresponding patterns obtained in FEA.

3.3. Finite element model

The FE-code DEFORM 3D® was used to model the two-hole extrusion process. Models of axisymmetric extrusion were built for each hole distance (in one quarter because of the symmetry). Fig.3.4 shows the model for the LHD-case. Friction over the billet-die interface was modeled by the Tresca friction model or as complete sticking friction as explained in [48]. Accurate flow stress data of an AA6005 alloy had been acquired by us by cylinder compression. Because we have experienced that different 6000-series alloys show the same material flow we decided to use this accurate flow stress data in the model, even though the experimental grid patterns considered are for a different alloy (AA6082). The geometry of the tooling was equal to that of the laboratory extrusion press in which the experiments were performed. At beginning extrusion there was a slot between the billet and the container, i.e., the upsetting of the billet was included in the model. The dies were modeled as rigid and the workpiece material as ideally rigid-plastic. Extrusion speed was set equal that in the experiment. A Lagrangian incremental type of simulation was run and thermal exchange with the dies was included. Extrusion was simulated up to the same partial stage of extrusion as in the experiments, and a comparison with the experiments was made at this stage.

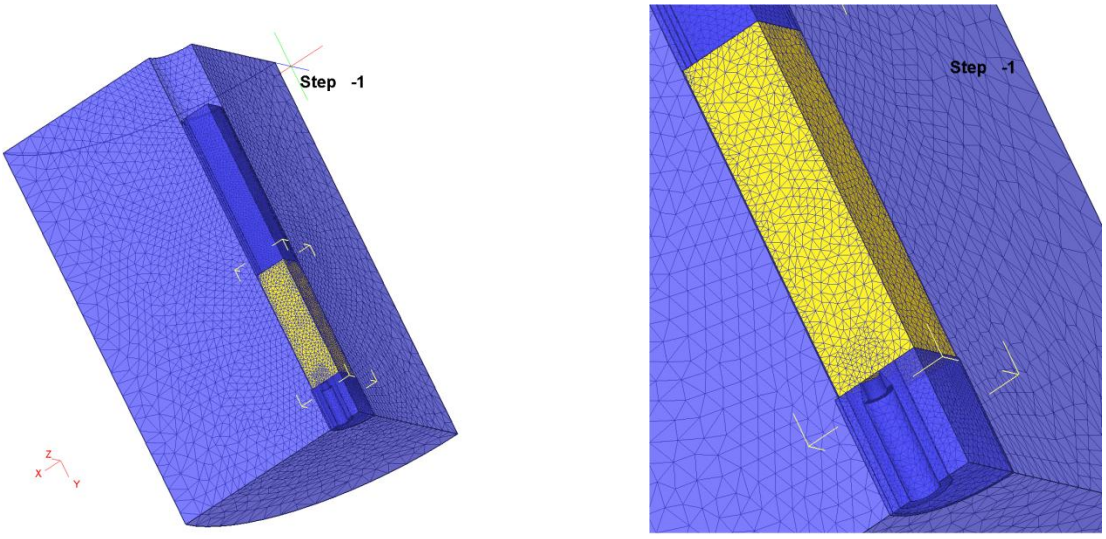

FIGURE.3.4. 3D FE-model to reproduce extrusion experiments.

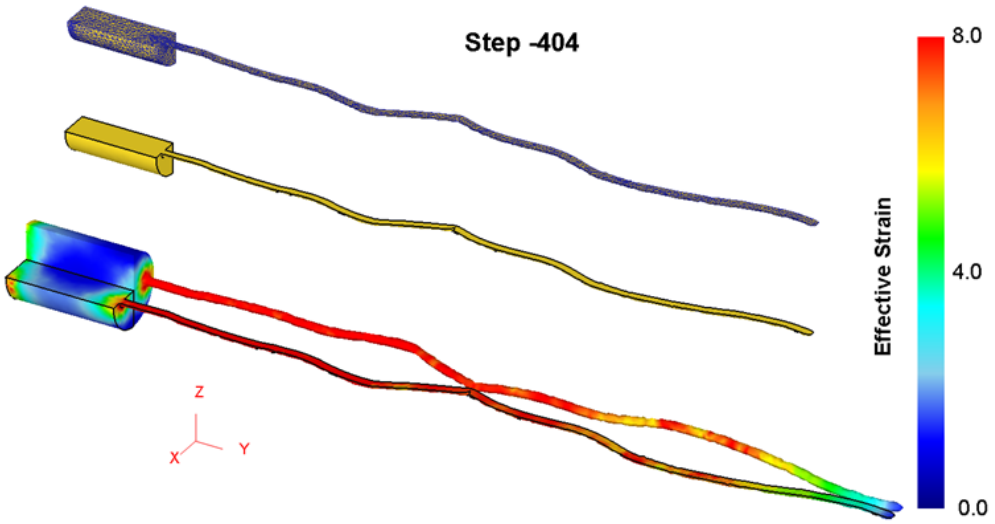

FIGURE.3.5. Partial extrusion step as shown by computer software.

3.4. Grid patterns in FEA vs. corresponding experimental patterns

The DEFORM-3D model of the billet and the extruded rods after partial two-hole extrusion is shown in Fig.3.5 for the case of LHD. Because the rod becomes very long it is not possible to show both the billet and the full rod without scaling the objects down. The FEM-mesh that was used (tetrahedral mesh with 16500 elements) is shown at the top, below is shown the contour of the model consisting of one quarter of the real process. Finally, at the bottom is shown the predicted deformation in terms of the distribution of the effective strain inside the rod and the partially extruded billet. Here the mirroring option in the simulation software has been used to visualize three quarters of the full process.

The grid pattern option in the postprocessor was used to make a pattern of radial stripes inside the initial billet as in the experiments; then the software computed the appearance of the pattern at the same partial step of extrusion as that used in the experiments. The obtained grid patterns are shown at the bottom of Fig.3.6 with the experimental pattern (AA6082) at the top. As this figure depicts there is very good agreement between the FEA-predicted and the experimental patterns, both for the long hole distance (LHD) and for the short hole distance (SHD) except for the details marked with arrows a and b in the figure.

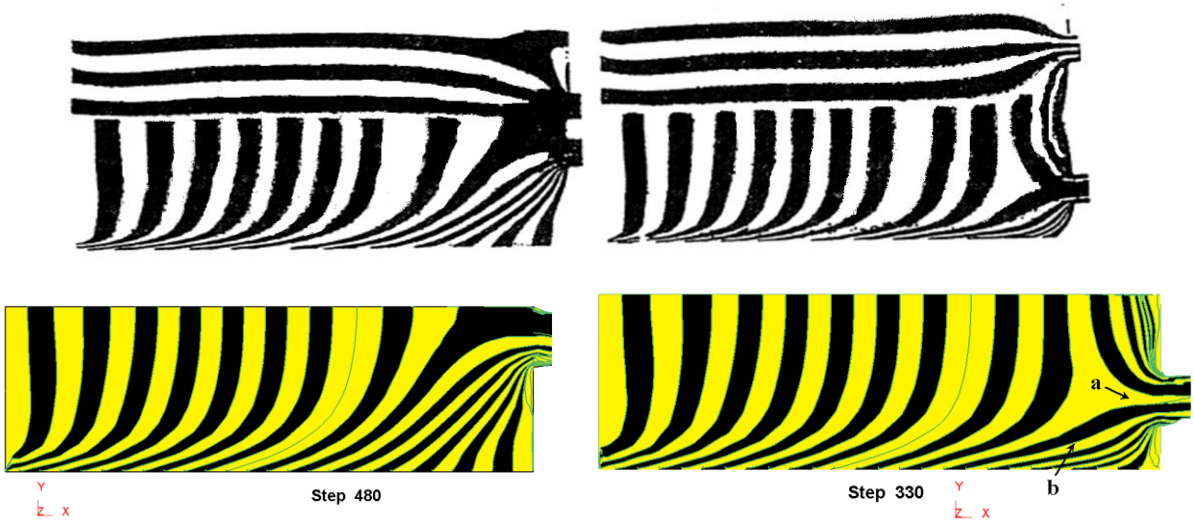

FIGURE.3.6. Grid patterns in the experiments (top) and in FEA (bottom) for the SHD and the LHD.

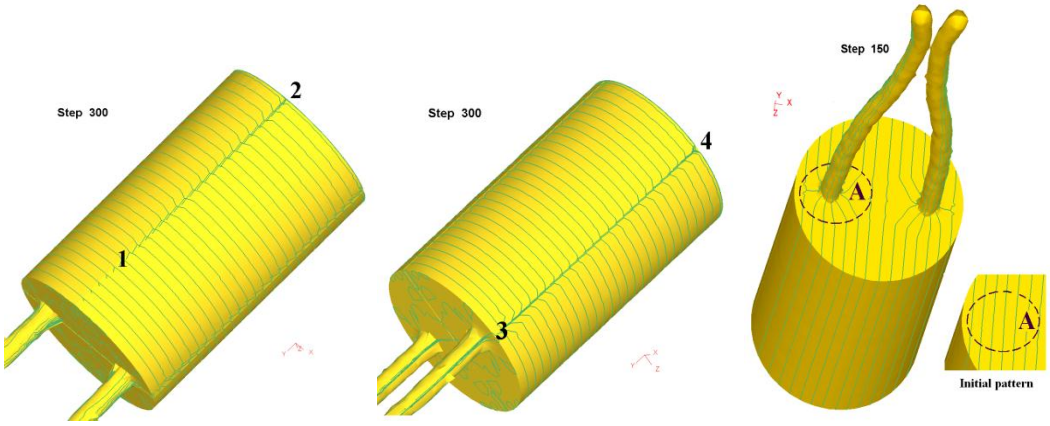

FIGURE.3.7. Predicted change of stripe pattern on the billet surface.

3.5. Other results

A pattern of transverse and longitudinal lines were created on the surface of the initial billet, and the FEA-predicted appearance of the same pattern at a specific partial step of extrusion is shown in Fig.3.7. As shown by this figure there is predicted sliding of billet material close to the die hole; in a ring-shaped area (A) over the interface between the front end face of the billet and the flat-faced die. This is not unexpectedly because there was specified Tresca friction with m=1 in this region in the model, and not full sticking. From the

appearance of the applied contrast pins it was confirmed sliding here also in the matching experiment.

As shown in Fig.3.7 there are predicted some disturbances in the appearance of the stripe pattern along the lines 1-2 and 3-4 on the peripheral surface of the billet. This surface remains in contact with the container wall under full sticking friction. But the simulation model predicts no sliding elsewhere on this periphery, so the sliding visualized locally along 1-2 and 3-4 is thought to be a numerical effect due to the presence of the symmetry planes in this location in the simulation model.

In Fig.3.8 is shown FEA-predictions of the strain rate distributions in the partially extruded billet at a specific stage of extrusion. As depicted in the figure there is a clear difference in appearance of the strain rate distributions in the two cases of SHD and LHD.

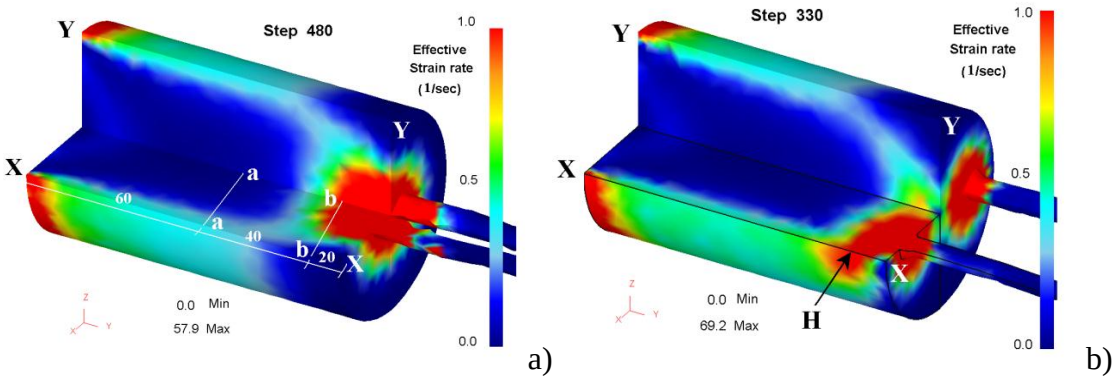

FIGURE 3.8. Predicted strain rate distributions on the surface of and in the interior of the partially extruded billets; a) SHD and b) LHD.

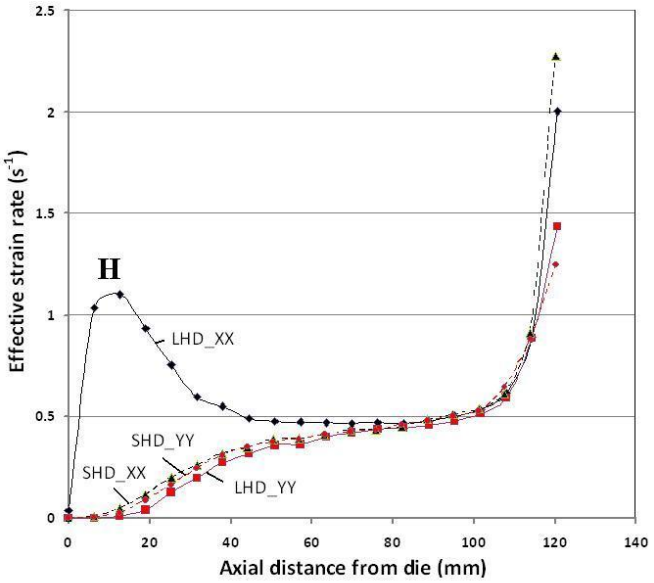

FIGURE 3.9. Strain rate distribution along lines X-X and Y-Y for different die hole distances.

While there is a high effective strain-rate zone in the region marked with H in the LHD-case, there is very low strain rates here for the SHD. To better quantify the differences the analysis option state-variable-along-a-line was used in DEFORM to find the distribution of strain rate along the lines X-X and Y-Y. The results were exported to a spreadsheet and the overlay-plot in Fig.3.9 was made. This figure shows that the X-X-distribution of effective strain-rate in the case of LHD represents an extreme with very high strain rates at location H on the boundary layer between the billet and the container wall.

To further investigate the conditions of flow the FEA-predicted axial velocity distribution across the shear zone adjacent to the container wall was recorded correspondingly as for the strain rate above, but now the recording was made across the shear layer of the billet, over the sections a-a and b-b inside the billet, see Fig.3.8. These velocity distributions are shown in Fig.3.10 for the simulations with different die hole distance.

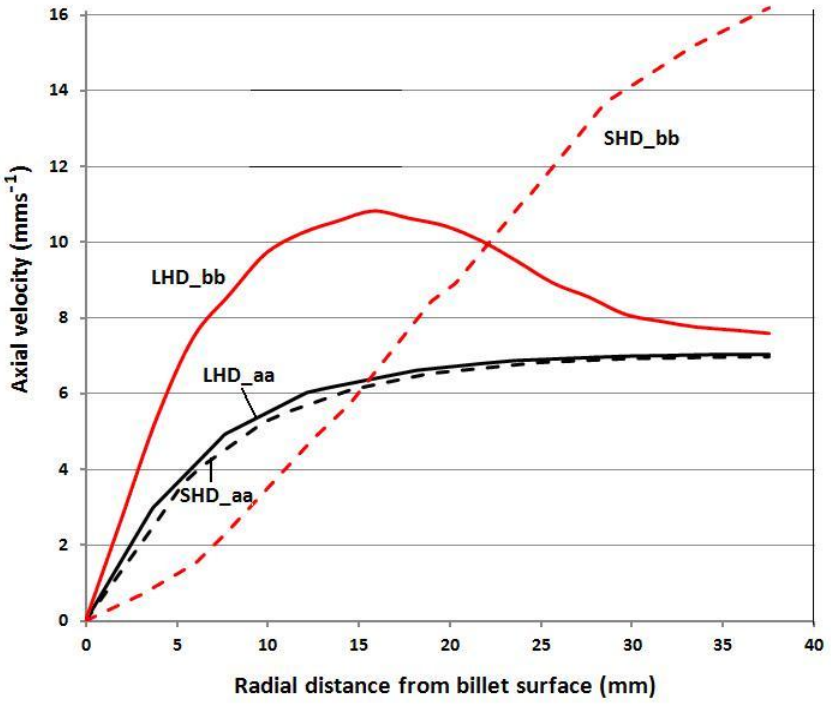

FIGURE 3.10. FEA-predicted axial velocity distribution along lines a-a and b-b for SHD and LHD.

As Fig.3.10 depicts the velocity gradient across the shear zone is not predicted much different for the section a-a (60 mm away from the die) for the LHD and the SHD. But there is great difference in the corresponding distribution over section b-b closer to the die (20 mm away from the die). At this position there is predicted a much steeper velocity gradient towards the container wall for LHD than correspondingly for SHD.

3.6. Extrusion Force and Pressure

The *average contact pressure* against the extrusion ram in extrusion can be determined from the measured *extrusion force F* by dividing it by the cross-sectional area of the ram head, *AS*. Thus the average ram pressure can be determined as

$$P = \frac{F}{As}, \tag{3.3}$$

Measured pressure data for a number of metals and alloys in forward rod extrusion have been published as graphs. They reveal that the extrusion pressure is approximately a linear function of the extrusion ratio R in each situation. Because the extrusion force is proportional to the extrusion pressure, the following relationship must exist between the extrusion force and the reduction ratio in extrusion:

$$F = a + b\ln R \tag{3.4}$$

The parameters a and b in this equation can be determined by curve fitting for each material. In addition the extrusion force generally depends on the applied extrusion speed; hence, the constants a and b also depend on the extrusion speed. In hot extrusion of common metals, it is observed that the extrusion force, and the extrusion pressure, will increase strongly as the extrusion speed is increased.

3.7. Theoretical Estimate of Extrusion Force and Pressure

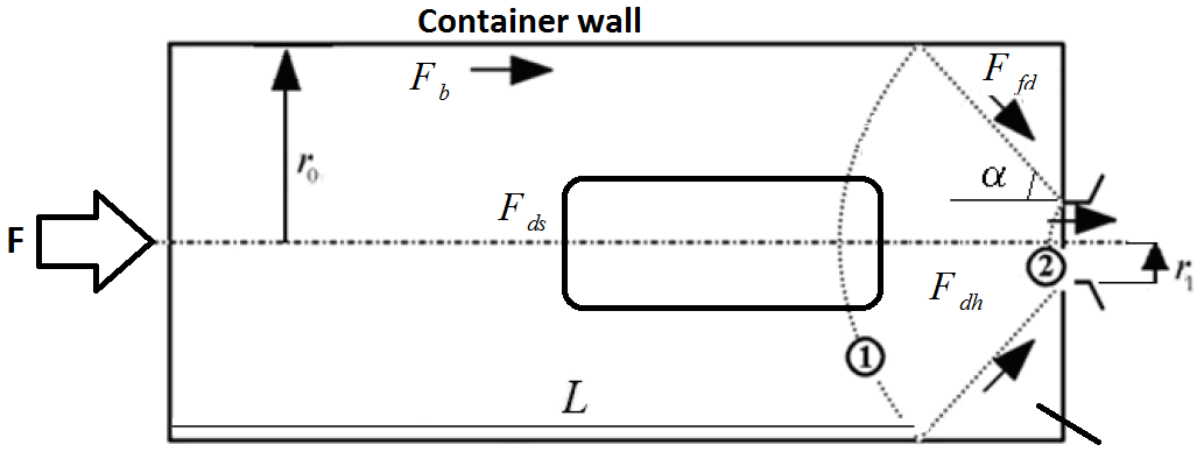

FIGURE 3.11 The total extrusion force is made up of four parts

The extrusion force and the extrusion pressure can be determined in theoretical analysis by use of (for instance) the slab method, or by an upper bound solution. In such a theoretical analysis, it is assumed that a number of different deformation phenomena in the extrusion process contribute separately to the total energy consumption in the process. The required energy input into the extrusion process and the required extrusion force are then divided into four separate *additive parts* (see Fig.3.11), as shown by the formula

$$F = Ff\,c + Fdh + Ff\,d + Fds \tag{3.5}$$

The first term, *Ff c*, is the force required to overcome the friction force against the container wall when the billet is pushed forward and starts to slide against this wall. The second term, *Fdh*, is the required force to overcome the deformational resistance to deform the metal homogeneously upon flow through the conical primary deformation zone in front of the die; see Fig. 3.11. If one considers a discshaped element of material flowing through this cone, the disc is compressed in the circumferential direction and it elongates in the axial direction.

The third term in eq. 3.5, *Ff d*, is the force required to overcome frictional resistance as the extrusion material in the primary deformation zone is sheared against the surrounding dead zone. If extrusion is conducted through a conical die instead, there is no dead zone ahead of the die, but the material will then slide against the die cone itself, and the term then will represent the force required to overcome friction against the die.

Finally, the last term, *Fds* , is the force required to shear-deform the material as it flows through the velocity discontinuities present at the entrance into the primary deformation zone and at the exit from this zone; see Fig. 3.11. Along these discontinuity lines the material will change its direction of movement. In the subsequent treatment, it will be shown how the four different load contributions just defined, which together make up the total extrusion force, can be determined by means of theory.

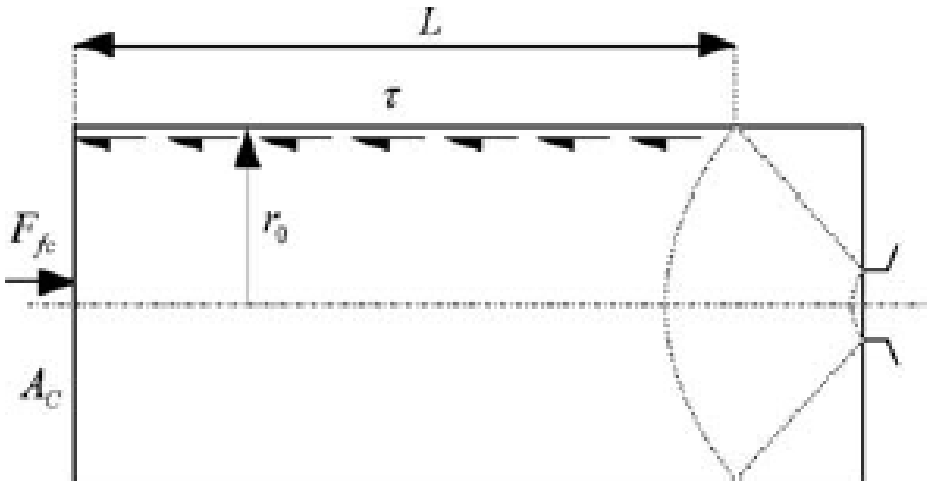

FIGURE 3.12. Force equilibrium for billet sliding against container wall.

3.8. Force Due to Friction against the Container Wall

An expression for the force contribution due to sliding friction against the container wall, *Ff c*, can be determined by considering force equilibrium for a billet of length *L* inside the container as expressed by eq. 3.6; see Fig. 3.12. The required force must counteract the shear stress τ directed against the sliding movement of the billet against the container wall:

$$Ff\,c = \tau \cdot AC = \tau \cdot 2\pi r0L \tag{3.6}$$

3.9. Force Due to Friction against the Dead Zone and Homogeneous Deformation Force in the Primary Deformation Zone

To obtain an equation for the two force components *Ff d* + *Fdh*, i.e., the component required to overcome friction against the die or the dead zone, and the component to homogeneously deform the material upon flow through the primary deformation zone, one can apply the theoretical slab method. When this is done, one usually assumes that the cone angle α of the primary deformation zone is small. Corresponding equations under the assumption of larger angle have been developed elsewhere.

Consider a material element in the form of a slab, sliding through the primary deformation zone ahead of the die, as depicted in Fig. 3.13. The shear stress τ and the normal stress component $p\alpha$ will act on the conical outer surface of the element; see Fig. 3.13 (a). These stresses on the slab element can be decomposed into two components acting in the horizontal and the radial direction, respectively, as done in Fig. 3.13. The decomposed components, when multiplied by the surface areas on which they act, yield the force components shown in Fig. 3.13 (b) and (c). By means of these components, a force balance for the whole slab element can be set up, for both the radial and the axial direction:

$$(\sigma_z + d\sigma_z)\pi(r + dr)^2 - \sigma_z\pi r^2 + F_z + F_z^r = 0 \tag{3.7}$$

$$\sigma_r 2\pi r dz + F_r - F_r^\tau = 0 \tag{3.8}$$

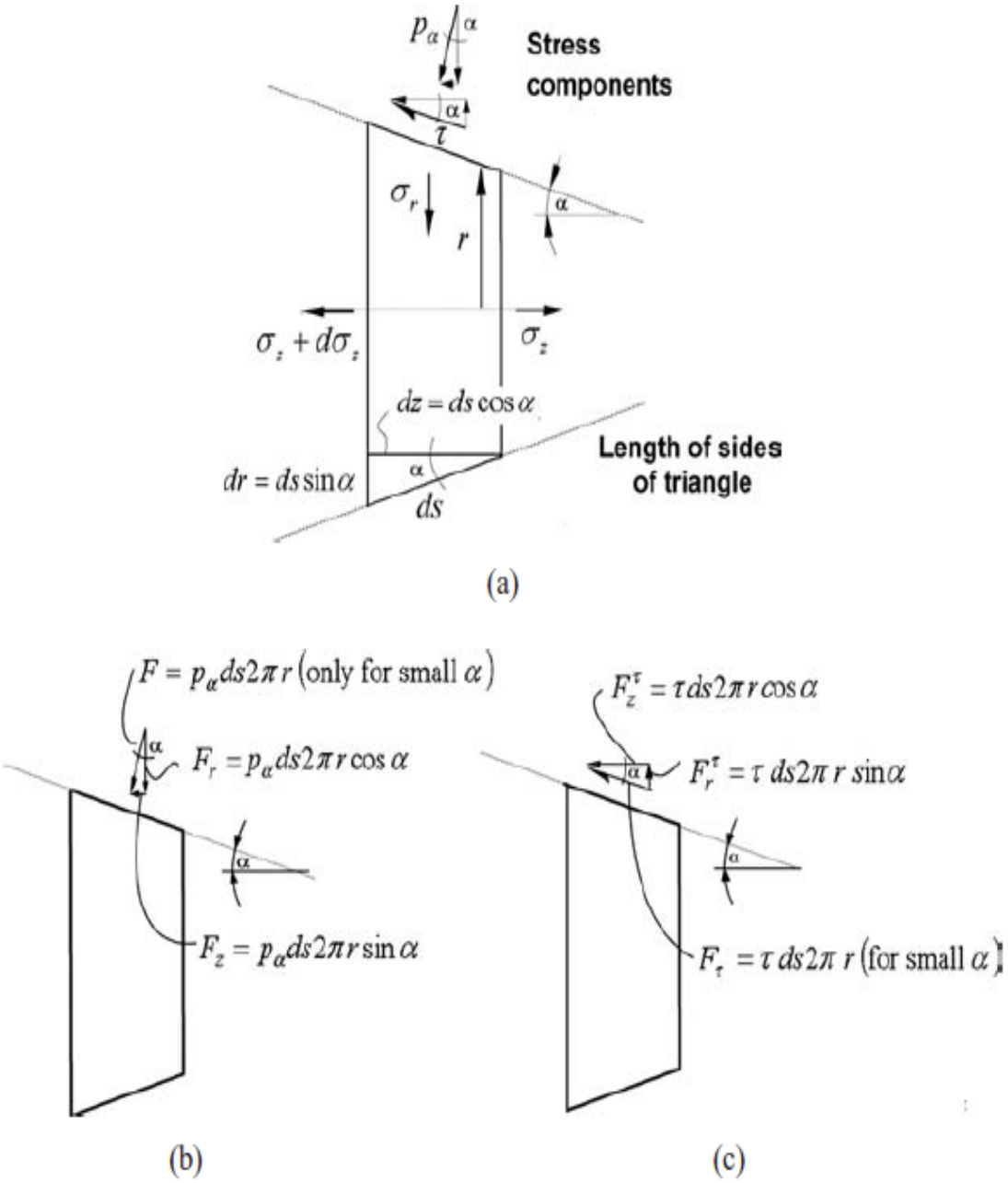

FIGURE 3.13. Force equilibrium for slab element sliding through conical converging channel. (a) Stress components. Force components on the channel wall due to (b) normal stress and (c) shear stress.

If the product of the stress and the area it acts on is introduced into these equations, see Fig. 3.13 (b,c), the following expressions are obtained:

$$(\sigma_z + d\sigma_z)\,\pi\,(r + dr)^2 - \sigma_z\,\pi r^2 + p_\alpha\,ds\,2\pi r \sin\alpha + \tau\,ds\,2\pi r\cos\alpha = 0 \quad (3.9)$$

$$\sigma_r\,2\pi r\,dz + p_\alpha\,ds\,2\pi r\cos\alpha - \tau ds\,2\pi r\sin\alpha = 0 \quad (3.10)$$

Equation yields the following result:

$$p_\alpha = \tau\tan\alpha - \sigma_r \quad (3.11)$$

The von Mises flow criterion coupled with the Levy–Mises flow rule for axisymmetric conditions yields the following relationship:

$$\sigma z - \sigma r = \bar{\sigma} \quad (3.12)$$

Now σ_r from eq. 3.12 can be inserted in eq. 3.11. Then p_α can be solved for and substituted in eq. 3.9 This yields the following differential equation:

$$r\,d\sigma_z + 2\left(\tau\tan\alpha + \bar{\sigma}\right)dr + 2\,dr\frac{\tau}{tan\alpha} = 0 \quad (3.13)$$

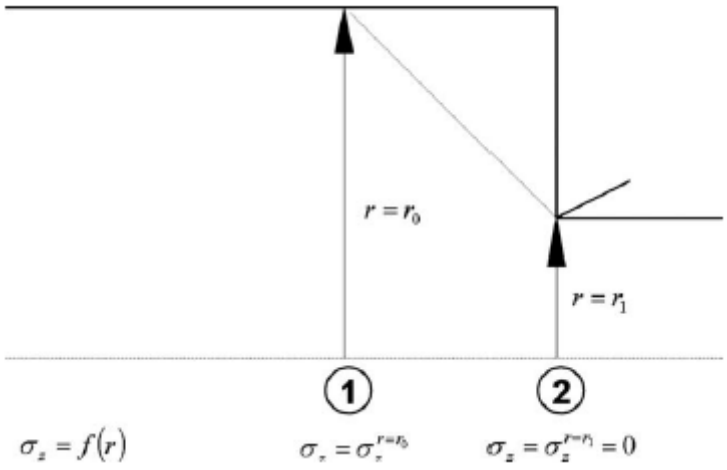

FIGURE 3.14. Boundary conditions at the inlet and the outlet from the conical deformation zone.

This equation has the following solution:

$$\sigma_z = -2\left(\tau\ tan\alpha + \bar{\sigma} + \frac{\tau}{tan\alpha}\right)\ln r + C \tag{3.14}$$

The boundary condition at the exit from the deformation cone, i.e., at the die orifice, see Fig.3.14, is

$$\sigma_z^{r=r_1} = 0 \tag{3.15}$$

This expression, introduced into eq. 3.14, gives the value of the integration constant:

$$C = 2(\tau\ tan\alpha + \bar{\sigma} + \frac{\tau}{tan\alpha}) \tag{3.16}$$

C can then be eliminated from eq. 3.15. The resulting equation expresses the general stress distribution in the *z*-direction in the primary deformation zone:

$$\sigma_z = \left(\tau\ tan\alpha + \bar{\sigma} + \frac{\tau}{tan\alpha}\right) ln\frac{r_1^2}{r^2} \tag{3.17}$$

By means of this expression, we now can determine the axial stress at the entrance into the deformation cone ,see Fig. 3.4

$$\sigma_z^{r=r_0} = \left(\tau\ tan\alpha + \bar{\sigma} + \frac{\tau}{\tan\alpha}\right) ln\frac{A_1}{A_0} \tag{3.18}$$

The expression can be rewritten as

$$\sigma_z^{r=r_0} = -(\overline{\sigma ln\frac{A_0}{A_1}} + \frac{\tau}{sin\alpha\ cos\alpha} ln\frac{A_0}{A_1}) \tag{3.19}$$

The force required to extrude the billet through the primary deformation zone can now be determined by multiplying the stress in eq. 3.19 by the cross-sectional area of the billet. In addition, it is reasonable to change the sign to make the extrusion force positive. The stress was initially defined so that the resulting extrusion force has come out negative. The final expression arrived at consists of two parts. The first part quantifies the required force to deform the material homogeneously during flow through the die; the second part is the force required to overcome friction against the die or the dead zone:

$$F_{dh} + F_{fd} = \pi r_0^2 \sigma_z^{r=r_0} = \pi r_0^2 \bar{\sigma} ln \frac{A_0}{A_1} + \pi r_0^2 \frac{\tau}{sin\alpha\, cos\alpha} ln \frac{A_0}{A_1} \qquad (3.20)$$

The shear stress τ against the die or the dead zone can be described in two fundamentally different ways. If one extrudes through a conical die, in the absence of dead zones, this stress is the friction stress transferred from the billet to the surface of the die cone, expressed as

$$\tau_i = \frac{m}{\sqrt{3}} \bar{\sigma} \qquad (3.21)$$

Here m is the Tresca friction factor and $\bar{\sigma}$ the effective flow stress of the extrusion metal. If extrusion is done through a flat-faced die instead, a dead zone of extrusion metal will appear in front of the die. The interior metal flow in the billet will occur against this dead zone. The shear stress then will equal the maximum shear stress of the billet metal, i.e., the shear stress specified in eq. 3.21, with m set equal to 1. In this case, eq. 3.20 can be expressed as

$$F_{dh} + F_{fd} = \pi r_0^2 \sigma_z^{r=r_0} = \pi r_0^2 \bar{\sigma} ln \frac{A_0}{A_1} + \pi r_0^2 \frac{\tau}{\sqrt{3} sin\alpha\, cos\alpha} ln \frac{A_0}{A_1} \qquad (3.22)$$

3.10. Force Due to Shear Deformation at the Velocity Discontinuities

During extrusion through a conical converging channel, there are two velocity discontinuities, one at the entrance to and one at the exit from the primary deformation zone; see the lines numbered 1 and 2 in Fig. 3.11. The force required to cause shear deformation along these lines, i.e., to maintain the velocity discontinuities, is denoted by the symbol *Fds* .

Let us assume the flow field through the primary deformation zone to be as defined in Fig. 3.15. Previously (see eq. 3.22) the power consumption during flow through a general velocity discontinuity was expressed as

$$\dot{W}S = k \Delta v \, dA \qquad (3.23)$$

Let us now consider a material particle that flows toward the first velocity discontinuity, $\Gamma 1$, so that after passage of the discontinuity it flows along a straight line oriented at an angle θ to the axis of the billet; see Fig. 3.15. The velocity change during passage of the line _1 then will be

$$\Delta v = v0 \sin \theta \tag{3.24}$$

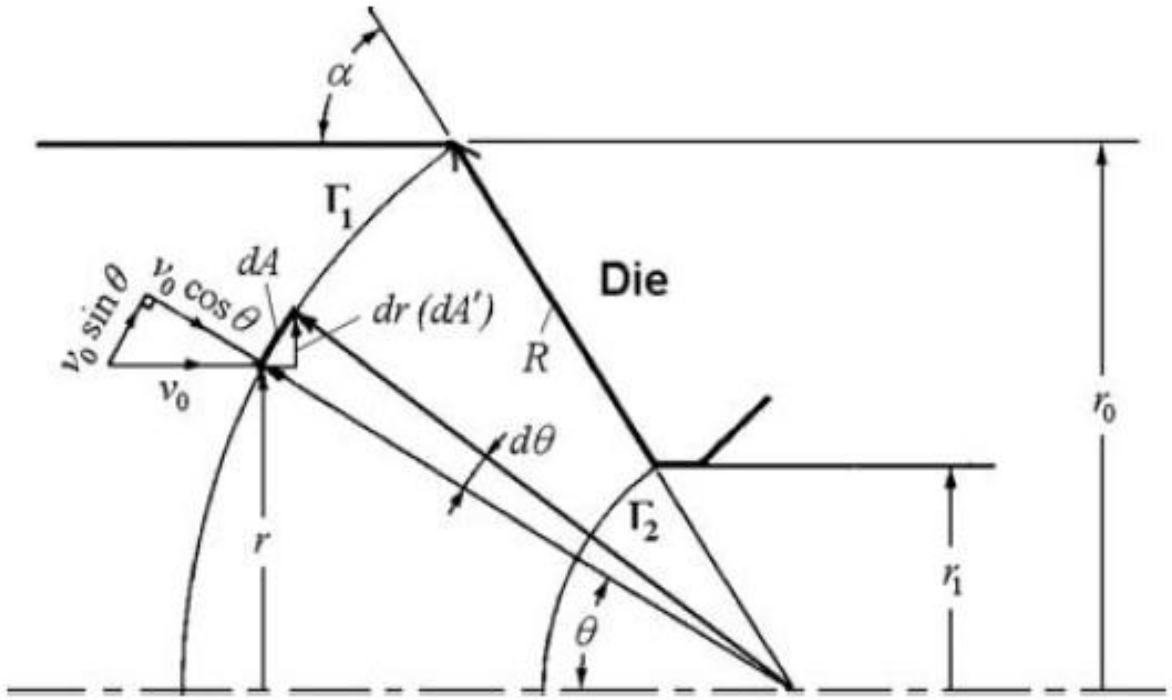

FIGURE 3.15. Assumed flow field through primary deformation zone.

Let us now first determine the differential dA. Because $R = r0/\sin \alpha$, one gets

$$r = R\sin \theta \Rightarrow \mathrm{d}r = R\cos \theta \, \mathrm{d}\theta \tag{3.25}$$

The area obtained upon rotation of dr (see Fig. 3.15) is dA' $\approx 2\pi r$ dr, so

$$\frac{dA'}{dA} = cos\theta \rightarrow dA = \frac{1}{cos\theta} \cdot 2\pi r \, dr \rightarrow dA = \frac{2\pi}{cos\theta} r \, dr$$

$$dA = \frac{2\pi}{cos\theta} R \, sin\theta \cdot Rd\theta \cdot cos\theta = 2\pi R^2 sin\theta d\theta \tag{3.26}$$

The power consumption upon passage of the material particle through the velocity discontinuity can now be expressed as

$$W_S = \int_A k\Delta v \, dA = \int_0^\alpha \frac{\bar{\sigma}}{\sqrt{3}} \cdot v_0 sin\theta \cdot 2\pi R^2 sin\theta d\theta$$

$$= \frac{\bar{\sigma}}{\sqrt{3}} v_0 \cdot 2\pi R^2 \int_0^\alpha sin^2 \theta d\theta$$

$$= \frac{\bar{\sigma}}{\sqrt{3}} v_0 \cdot 2\pi R^2 \left(-\frac{1}{2} sin\alpha\ cos\alpha + \frac{1}{2}\alpha\right)$$

$$= \frac{\bar{\sigma}}{\sqrt{3}} \pi v_0 \cdot r_0^2 \left(\frac{\alpha}{sin^2\alpha} - \frac{cos\alpha}{sin\alpha}\right)$$

$$= \frac{\bar{\sigma}}{\sqrt{3}} \pi v_0 \cdot r_0^2 \left(\frac{\alpha}{sin^2\alpha} - cot\alpha\right) \qquad (3.27)$$

If the energy dissipation upon passage through the second velocity discontinuity $\Gamma 2$ is also computed, one actually obtains the same result as for the first velocity discontinuity. Therefore (see Fig. 3.11), the following result is obtained:

$$\frac{1}{2} F_{ds} \cdot v_0 = \frac{\bar{\sigma}}{\sqrt{3}} \pi v_0 \cdot r_0^2 \left(\frac{\alpha}{sin^2\alpha} - cot\alpha\right)$$

$$\rightarrow F_{ds} = \frac{2\bar{\sigma}}{\sqrt{3}} \pi r_0^2 \left(\frac{\alpha}{sin^2\alpha} - cot\alpha\right) \qquad (3.28)$$

3.11. Result of the Theoretical Analysis

As shown in the preceding treatment, the extrusion force can be determined as the sum of four force components, determined by use of a force balance, the slab method, and an upper bound solution. The equations obtained this way, when summed, give the following expression for the extrusion force in axisymmetric forward extrusion:

$$F = F_{fd} + F_{fc} + F_{dh} + F_{ds}$$

$$= \tau \cdot 2\pi r_0 L + \pi r_0^2 \bar{\sigma} ln\frac{A_0}{A_1} + \pi r_0^2 \frac{\bar{\sigma}}{\sqrt{3} sin\alpha\ cos\alpha} ln\frac{A_0}{A_1} + \frac{2\bar{\sigma}}{\sqrt{3}} \pi r_0^2 \left(\frac{\alpha}{sin^2\alpha} - cot\alpha\right)$$

$$= \left(F_{fd} + F_{ds}\right) + A_0 \left(\bar{\sigma} + \frac{\bar{\sigma}}{\sqrt{3} sin\alpha\ cos\alpha}\right) lnR = a' + b' lnR \qquad (3.29)$$

As the equation depicts, the extrusion force obtained in the theoretical analysis depends on the same extrusion parameters as did the force described by the empirical formula given in eq. 3.4. Note that in eq. 3.29 the dependence of extrusion force upon extrusion velocity is included through the effective flow stress term $\bar{\sigma}$. The flow stress in warm and hot forming of metals commonly increases with increasing strain rate; hence, the flow stress must increase when the forming velocity is increased.

If one assumes the friction between billet and container wall to be expressed by Tresca friction, the symbol τ in eq. 3.29 can be replaced by the expression specified in eq. 3.21.

3.12. Case considered and extrusion loads from theory

The intention was to analyze hot extrusion of Al but for easier treatment the simpler case of cold extrusion of a material with constant flow stress was chosen instead. In addition, thermal effects were neglected to ease the analysis. Geometrical parameters in the process were as shown in Fig.3.11.

In the FE-model the workpiece material was defined rigid-plastic and all tools rigid. The flow stress describing the plastic behavior of the alloy was set constant (200 MPa). An Excel spreadsheet was used to calculate the load components *fc F* , *ds F* , *dh F* and *fd F* . The total force in rod extrusion was finally obtained by summing the parts. The analysis was conducted for a billet of 200 mm initial length, see Fig.3.11.

For the frictionless case and a die angle of α=45° the two parts *fc F* and *fd F* will be zero. For the high friction case (*m*=1) all four parts contribute to the total load. For a specific case of extrusion with a certain friction all parts are constant throughout the stroke with the exception of *fc F* .This part decreases as the contact length between the billet and the container wall decreases. The results of the spreadsheet computations are shown in Fig.3.16.

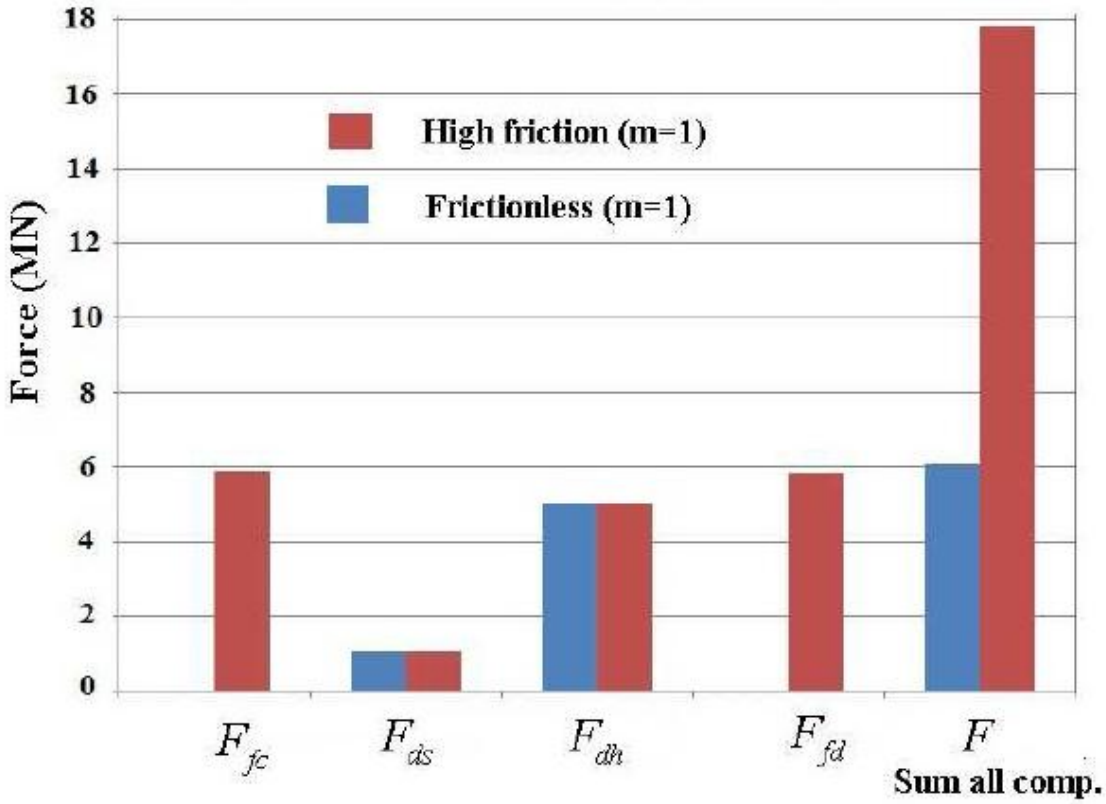

FIGURE 3.16. Theoretical load parts and total load

3.13. Finite Element Models

The finite element program DEFORM 2D® was used to simulate the pressure welding of metal in the extrusion process. A plane strain model was used in accordance with the extrusion models presented in applied metal forming [56]. The model was built in half because of the symmetry. The work piece material was defined rigid-plastic while the tooling and die were set rigid. The bridge was modeled rectangular with rounded corners and the rear end of the bridge had always butt-ended shape. The flow stress data describing the plastic behavior of the alloy AA6082 has been expressed by a Zener-Hollomon equation presented in [64].

The initial temperature of the workpiece was set to 480°C and 420°C for the tooling. A frictionless plate was used in the weld chamber behind the bridge to prevent the profile from moving sideways over the midline. Two kinds of friction conditions between the workpiece material and the tooling were used to establish the extrusion seam weld limit diagrams, i.e. either it was used frictionless conditions or a state of very high friction.

3.14. Material Flow in the Weld Chamber

The bridge divides the billet into two metal streams which join together behind the bridge in the weld chamber. The geometrical parameters of the welding chamber have significant effect on the material feed into the space behind the die, and how the extrusion material rejoins behind the bridge. There are three ways the material can join dependent on weld chamber geometry and amount of feed of metal into the space behind the bridge. This is visualized in Fig 3.3 by pictures taken from three different FE-simulations of extrusion welding.

Fig 3.3 (a) depicts the situation where the metal completely fills the weld chamber. By making the exit hole bigger it is possible to arrive at a situation where the feed of material into the space behind rear end of the bridge becomes insufficient to give complete filling, and a stable void would appear here throughout the course of an extrusion stroke, see Fig 3.3 (b). Finally, with even less feed into the region behind the bridge when using an even bigger die hole, the situation will be characterized by the formation of a stable gas pocket right behind the bridge, see Fig 3.3 (c).

The FEA-predicted distribution of effective strain rate in the material around the bridge and in the weld chamber varies as the material flow changes in the direction from complete filling behind the bridge, to the presence of a void here, and finally to the situation where a stable gas pocket appears. As Fig.3.3 depicts the strain rate distribution in case of complete filling behind the bridge is characterized by a distinct deformation cross in the weld chamber. As the feed of material into the space behind the bridge is reduced the X is gradually replaced by a strain rate distribution characterized by the shape of a V turned upside down.

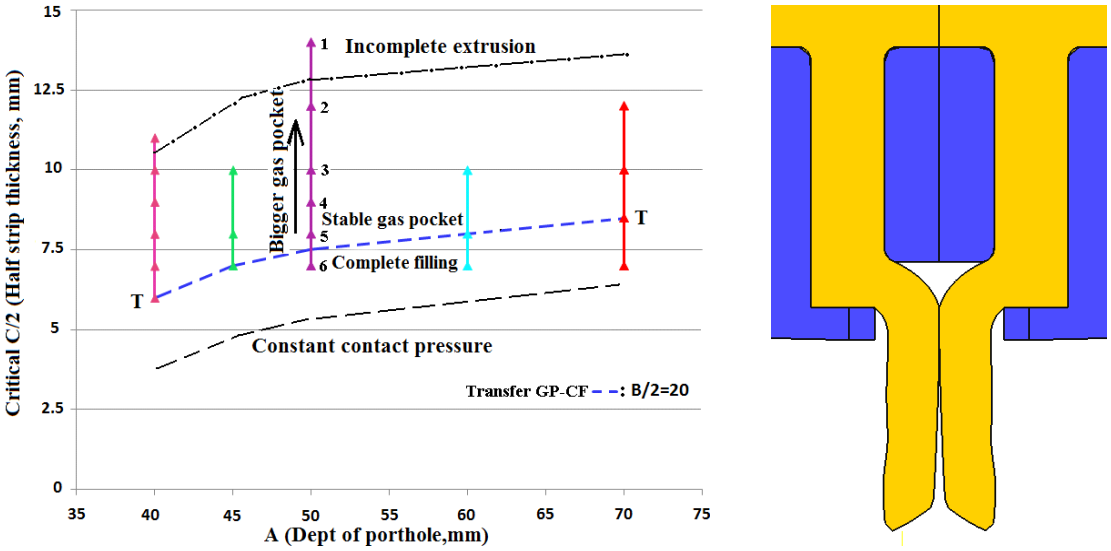

(a) (b)

FIGURE 3.17. a) Identification of an ESWL-line for 2D extrusion seam welding and b) Situation where an incomplete extrusion is obtained.

3.15. Extrusion Seam Weld Limit Diagram

To study how the extrusion conditions affect the material feed around and behind the bridge, in simple case of idealized frictionless plane strain 2D extrusion welding, a large number of simulations were run in which the extrusion weld chamber was changed systematically. This brings about the transfer described in connection with Fig. 3.3, i.e. from complete filling behind the bridge to presence of a stable gas pocket here throughout the course of the extrusion stroke. For each simulation the nature of the metal flow was checked after the situation in the weld chamber had become stable. Concurrently a diagram was made to identify when transfer between different states of flow takes place in the weld chamber. This diagram is shown in Fig. 3.17 (a). Here each bar represents a series of simulations of extrusion with all extrusion parameters kept constant with the exception of the width of the die opening which is being reduced downwards along each bar.

Simulation of the extrusion process for the case B/2=20mm and C/2=14mm with the die hole set equal to 14mm is represented in Fig. 3.17 (a) by the point denoted 1. With this extrusion geometry the appearance of metal flow was as shown in Fig. 3.17 (b), i.e. an incomplete extrusion was obtained. Knowing this fact a new simulation was run but this time with the die hole made a bit smaller, i.e. the parameter C/2 was set equal to 12mm. The new

simulation is represented by the point denoted 2 in Fig. 3.17 (a). With this new extrusion geometry, more feed of material into the space behind the bridge was predicted and complete extrusion was obtained. However, there was still not sufficient feed behind the bridge to avoid the formation of a stable gas pocket here. Three additional simulations represented by the points 3, 4 and 5 in Fig. 3.17 (a) were then run in which the die hole was reduced further in stepwise manner from 10, to 9 and then to 8mm. In all three cases a stable gas pocket was predicted appearing behind the bridge, but the size of the pocket became smaller as the C/2 value was decreased.

Then a final simulation was run for the same extrusion geometry with C/2 reduced down to 6mm. The simulation showed that there was sufficient feed of metal into the weld chamber behind the die bridge to fill up the whole space here, and a situation of complete filling of the weld chamber had been obtained. Thus, by running of altogether six simulations we had confirmed that the nature of metal flow in this idealized 2D-extrusion welding die can be of three different categories. With a big die opening the metal flows through the weld chamber without being able to produce a complete cross section in the "extrusion". Then, if the die opening is made smaller there is more feed into the weld chamber and a transition occurs to a state where a complete extrusion is formed, but a gas pocket will reside behind the bridge during the extrusion stroke. Finally, as the die hole is reduced further a new transition takes place and the weld chamber fills up completely with extrusion metal.

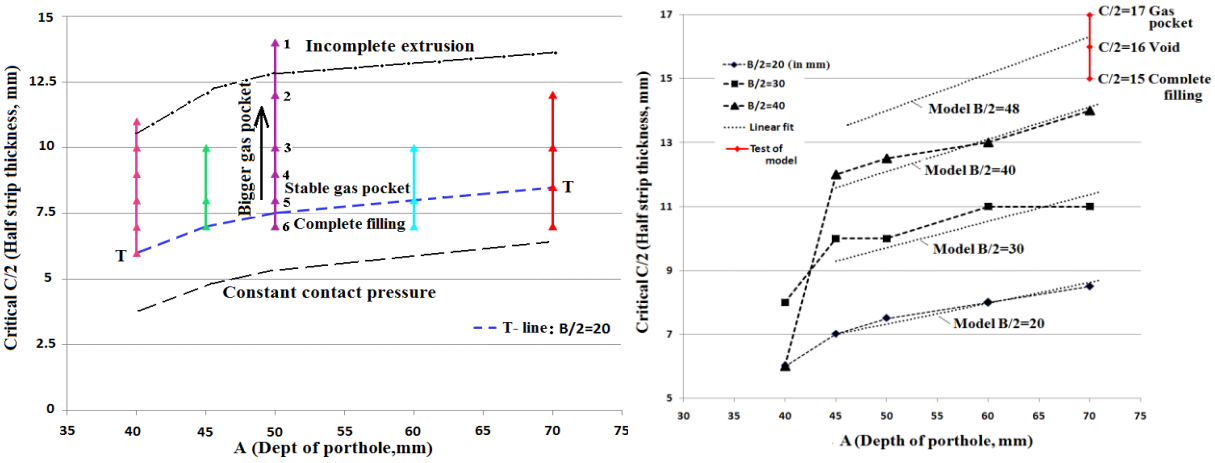

(a) (b)

FIGURE 3.18.(a) Extrusion seam weld limit diagram (ESWLD) obtained by FEA of 2D extrusion welding. (b) ESWLD from FEA and predictions of our model.

Additional simulations were then run for different values of the porthole depth (A). Thus the transition point between extrusion causing complete filling of the die and a stable gas pocket was identified, see Fig. 3.17 (a), for multiple A-values. Now a line was drawn that connected all points by which there was this transition. Assuming that it is unfavorable to run extrusion seam welding with presence of a gas pocket behind the bridge, we have arrived at an extrusion seam weld limit

(ESWL) line for frictionless extrusion with B/2=20, and different values of the porthole height (A), represented by the line denoted T-T in Fig. 3.17 (a). It should be mentioned here that friction will shift this line upwards in Fig. 3.17 (a) so the results can be elaborate for the case of having friction between the workpiece and the tooling.

The same analysis, as that above for B/2=20mm, was now repeated for B/2=30mm and then for B/2=40mm to obtain two additional ESWL-lines. In Fig.3.18 all three lines obtained for the case of B/2=20, 30 and 40mm are plotted into what we will denote an extrusion seam weld limit diagram (ESWLD).

We chose to exclude the points for A=40mm which represents a weld chamber of very small height, and then fitted each of the obtained ESWL-lines to the linear equation ($C/2=aA+b$), as shown in Fig. 3.18. A diagram was then made in which the constants a and b of the linear equations were plotted as a function of the B-value. From the graphs a linear fit was made for the constants; b=0.1486B/2+1.0989, a=0.0018B/2+0.029.

This way we arrived at an equation for the critical dimension of the die hole, i.e. the parameter C/2, by which there is a transfer (as C is decreased), from a gas pocket being present behind the bridge to complete filling in this location:

As Fig.3.19 shows there is acceptable agreement between the model we have obtained this way and the transition lines determined by FEA. The prediction of the model for the case of a die where the porthole extends as far away from the midline of the process as the container does, i.e. an extrusion geometry where there is no ledge between the wall of the container and the die, is also shown in this figure. A series of simulation were now run for this situation and the depth of the porthole set equal to A=70mm and B/2 equal to 48 mm. For this geometry the model predicted C/2 to be equal to 15, 16 and 17mm. When the simulation was run we found that it represented a situation where the gas pocket behind the bridge disappeared as the die opening was reduced further. These test simulations have also been shown in Fig.3.18 (b) where they appear at the top of and at right hand side of diagram.

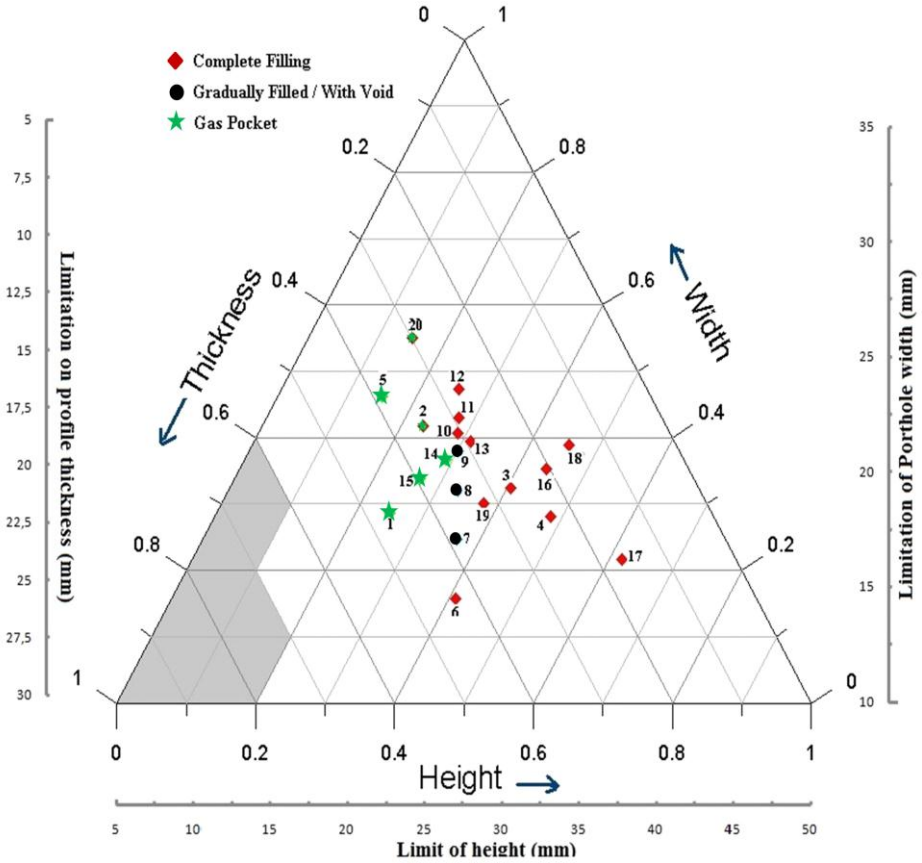

FIGURE 3.19.Ternary extrusion seam weld limit diagram summarizing the behavior of metal flow behind the bridge.

3.16. Ternary extrusion seam weld limiting diagram

In order to cover the variation in the behavior of material flow due to the geometrical changes in the welding chamber, a ternary plot of FE-simulated data is shown in Fig. 3.19. The three geometrical parameters of the die used to make the triangle plot are the ***width*** of the porthole channel, the ***height*** of the weld chamber and the ***thickness*** of the extrusion as shown in Fig. 3.2. Twenty four simulations, each based on different geometric measures, were run to study the characteristics of material flow through the welding chamber and particularly joining behind the bridge. It should be noted here that these simulations only deviated from those used to make the ESWL-diagram presented in the previous section with respect to friction conditions between tooling and extrusion metal. The ternary diagram is based on simulations in which a high-friction state was applied the ESWL-diagram was made for the frictionless case.

Each of the three parameters of welding chamber geometry influences the behavior of metal flow. The minor changes in one of the parameters have significant impact on the way material flows; but it has always some contribution from the remaining parameters. All results obtained from the models have been plotted in the ternary graph. The ternary extrusion seam weld limiting diagram here shows the contribution of each geometrical parameter with respect to the nature of the metal deformations within the welding chamber. The graph is a Barycentri plot on the three variables; height, width and thickness which sum up to a constant (1 in this case). The diagram graphically depicts the proportions of the height, width and thickness for one particular extrusion geometry as dots in the triangle. The dots have been distinguished according to the nature of material flow behind the bridge, whether there is a gas pocket or there is complete filling there. The position of the dots along with their separation according to these metal flow phenomena leads us to the regions within the diagram where behavior of metal flow can be predicted as the geometry of welding chamber changes.

Each simulation has been given a number and represented by a dot in the limiting diagram. All those simulation models, in which the region behind the bridge was completely filled by the material, have been marked with red color (♦). The black circular dots (●) present the simulation models where there is formation of a void behind the bridge or material slowly fills up the region during the course of extrusion. The green dots (*) show the presence of a gas pocket which remains till the end of extrusion stroke. It is important to notice that for the green points (*) the transition from one form of metal flow to the other is gradual.

It is important to notice that simulation models were made within limitations of geometrical measures, e.g. the width of the porthole cannot exceed the radius of the billet. Similarly there have been limitations on the maximum and minimum values of the profile thickness. The maximum height value has been taken as 14mm. While remaining within certain limiting values the results have been combined into the form of ternary extrusion seam welding limit diagram. The shaded areas of the diagram predict those regions of extreme geometrical combinations of weld chamber height, porthole width and profile thickness where the extrusion process or the product does not remain appropriate.

The trend of points with the green color (*) is towards the left side of the diagram marking a region of gas pocket formation. While most of the areas in the right bottom corner of diagram show complete filling behind the bridge.

3.17. Discussions

As depicted in Fig.3.6 there is very good agreement in the appearance of the experimental and the simulated grid pattern in the case of SHD. But for the case of LHD there is a clear difference as regards the pattern in the locations marked a and b in the figure. In the experiment a particular radial grid stripe has been caught in the middle of the die hole when extrusion was stopped. But in simulation the same grid stripe has flown through the hole. This seems to be due to the fact that in simulation the shear zone in position b is predicted less localized than in the experiment. When there is less flow in the shear zone, there must be more flow in the mid-stream in front of the die hole, and the material particles here, defined by this stripe, will flow faster forward toward the hole as they did in the simulation.

As Figs.3.9 and 3.10 depict the simulation model reveals that even though the shear zone adjacent the container wall at a short distance 20 mm above the hole (b-b) is much more intense in case of LHD than SHD, this has no effect on shearing further behind along the container wall, 60 mm above the die hole (a-a). The velocity gradient from the surface towards the billet centre in this location is almost the same for both the LHD and the SHD.

The analysis thus shows that if the holes first are kept close each other, and then are moved far from each other, this change will alter the metal flow ahead of the die significantly, even though the change will not be sensed in the back-end part of the billet, at the early stage of extrusion analyzed here, namely 14.3% partial extrusion.

An initiative has been taken to establish an extrusion seam weld limit diagram (ESWLD) with the help of finite element code of DEFORM 2D. The adoption of the FEM method has allowed the running of simulations with various geometries of the porthole and the welding chamber in combination with the die outlet. The plastic flow of the deforming material behind the die bridge has been covered in a quite accurate way for each design of welding chamber.

This work alternatively could have been done by experiments but at more labor and very much higher costs. We chose to use FEA for this analysis because it has been shown previously that real metal flow [64] and gas pocket formation [56] behind a die bridge in laboratory extrusion are well described by appropriately built FE-models.

In the ESWL-diagram a transition, or a boundary line, is identified that establishes the regions where there is enough material feed behind the bridge to get complete filling instead of gas pocket formation, and vice versa. The diagram also depicts what extrusion parameters

expand the filled region so that gas pocket formation better can be avoided. Two conditions that were found to contribute to improved material filling behind the bridge was change of die design by increasing the width of the portholes, or increasing the height of the weld chamber.

The concept of limiting lines can of course be brought further, by instance by identification of corresponding boundary lines located further down in the diagram (at lower C/2-value) that provides a specific constant pressure right behind the bridge, where the re-joining of the metal streams occur. In Fig.3.18 (a) such a thought line providing a particular pressure level at the back end of the bridge has been drawn into the diagram. The more exact shape and location of this line must be determined in future analysis of extrusion seam welding.

The ESWL-diagram presented in Fig.3.18 is considering extrusion with frictionless conditions between the tooling and the extrusion material. Presence of friction, and especially high friction, or even sticking friction, as usually encountered in unlubricated Al-extrusion, is thought to ease filling of metal into the space behind the bridge, and would in that case shift the limiting lines of the ESWLD upwards towards higher C/2. Additional investigations where the influence of friction is included in the ESWLD are welcomed.

The ESWL-diagram constructed here is only valid for the specific idealized case of extrusion welding with a fixed die bridge geometry considered here. But in spite of this it is thought that similar diagrams can be made for any other bridge geometry, and other porthole dies, simple or more complex. One advantage of the diagram is that it allows the increased tendency of metal filling into the space behind the bridge to nbe quantified through the reduction in the critical C/2 parameter.

Ternary ESWLD is presenting the contribution by all three geometrical variables towards the flow of material into the welding chamber. The diagram has been made by running simulations within certain assumed limitations according to size of bridge and billet. Further statistical data input can increase the predictability of material flow and refine the shaded regions. Another method would be to choose regions of potentially same color points and use Monte Carlo's method on each region, to determine the probability of any new point being of the same color. For example, looking at Fig. 3.19 a circular region inclosing mostly green color points (*) can be chosen. We may need to run more simulations to have good probabilistic result. Of course, greater the number of points better the result and easier to choose regions.

The ESWLD's established here predict three situations of material flow. The conditions of incomplete filling (gas pocket formation) where the material joins together but the weld formed is not considered of sufficient ductility. When the material completely fills the space behind the bridge the seam weld formed can be considered of sound quality. The third intermediate situation is when the material flows with the formation of a small void at the corner of the square ended bridge. The gradual transition from the complete filling to the void formation has been successfully tracked in the diagrams. The void formation shows the critical situation where material feed behind the bridge is not plentiful. Insufficient material feed at this geometrical set up may influence the shape of the mid-section of the profile. This is because the material behind the bridge is being pulled by the relatively fast moving material away from the rear end of bridge.

3.18. Conclusions

Because of the availability of grid pattern experiments for two-hole extrusion it has been possible to confirm that metal flow predicted in our FEA-model is very close to real flow. This is especially true for the die with short distance between the holes. For the die with holes placed further apart from each other, there was more discrepancy between simulation and experiment. The peripheral shear zone in front of the die (and adjacent to the container wall) then appeared more localized in the experiment than in FEA.

The FEA reveals that the metal flow in front of the die changes strongly when the two holes in the die are moved sufficiently far apart from each other. With short die hole distance the main metal flow will be in the middle of the billet. With long distance between the die holes, however, the holes will appear close to the container wall, and the main metal flow ahead of the die will then be directed laterally away from the centre of the billet toward the container wall.

The analysis shows that the tested formula eq.(3.2) tends to overestimate calculated extrusion load highly because the formula for the load component due to friction on the conical dead zone ahead of the die is predicted much too high.

FEA applied on a case of idealized 2D porthole extrusion welding has helped to establish an ***extrusion seam weld limit diagram*** (ESWLD) to characterize the metal flow phenomena present behind the rear end of a die bridge, and to identify when there is a transfer from gas pocket formation here to a situation of complete filling.

The two types of diagrams, including the rather complicated ternary diagram, show when there can be expected a change in the nature of material flow and how the geometry of the extrusion die affects the occurring flow phenomena.

It is proposed to extend the concept to include prediction of seam weld pressure right behind the die bridge, so it can also be shown how the joining pressure are affected by the varying geometry of the portholes, the welding chamber and the profile thickness.

4. DETERMINING THE WELD QUALITY IN EXTRUSION WELDING

4.1. Introduction

Extrusion welding is a solid state welding process used to produce hollow extruded profiles of light metal alloys. There are two kind of solid state welds formed in such extrusion; one is commonly denoted the transverse weld (or the charge weld) and the other the longitudinal weld (or the seam weld).

The transverse weld is formed because of the non-continuous nature of the extrusion process where one billet is extruded on top of remnants of the previous billet which cannot easily be removed from a hollow extrusion die. The longitudinal weld, on the other hand, is formed because of the splitting of the billet material into two separate streams by each web of the die. The streams then flow past the webs (through the portholes located between the webs) and meet again at the rear end of the web in a cavity inside the die commonly called the welding chamber. Here the metal streams join together before they flow through the die orifice as the hollow extruded profile. Thus a hollow extruded profile will in addition to the charge weld contain as many seam welds as there are webs in the applied extrusion die.

If the extrusion conditions are not set properly in hollow profile extrusion the obtained profile may have unacceptable weld quality over part of its length, eventually over the full length, due to presence of weld defects, either occurring in the transverse or in the longitudinal weld.

To study what really happens in extrusion welding a large number of investigations have been performed throughout the years. A review paper was published in 2002 that summarizes [53] the knowledge on extrusion welding at the beginning of the 20ieth century. Early work was mainly of experimental nature but was able to give good understanding of what are the basic mechanisms of welding when extrusion welds are formed. One can say that the current status within this field is that it is known well what are safe extrusion welding conditions so bad extrusion weld quality is actually a problem in the industry.

In the 20ieth century additional work on extrusion welding has been performed. With strong and fast computers, and powerful FEA-programs, it has become possible [6, 65] to FEM-simulate the metal flow in the applied extrusion dies. The main trend is therefore currently investigation of extrusion welding by FEA to predict actual state variables in the extrusion weld chamber. In addition extensive experimental investigations [15] have been

reported, in which the aim was to find what mechanical properties can be obtained in an extrusion weld when the local process conditions in the weld chamber are varied.

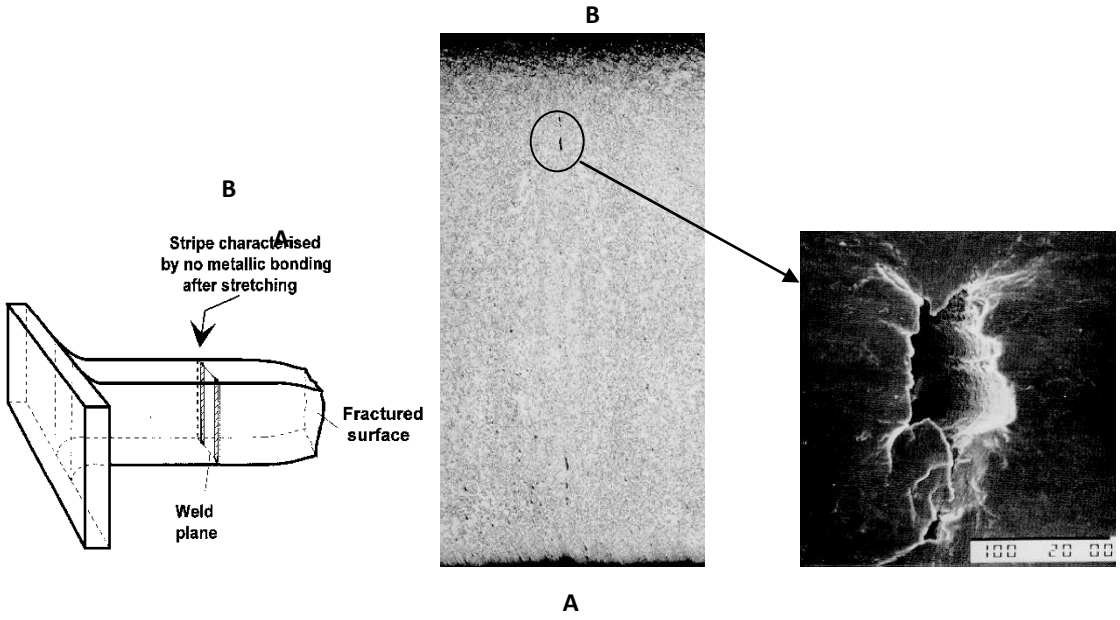

(a) (b) (c)

FIGURE 4.1. Tensile test specimen that fractured outside the seam weld; (a) One "half" of the fractured specimen, (b) Defect in the microstructure in inferior extrusion weld and (d) Extrusion defect in stretched specimen as viewed in SEM.

4.2. Mechanical testing of extrusion welds

The most commonly used test method for assessing the quality of extrusion welds in a profile in research work is probably the tensile test. Test specimens oriented in the direction orthogonal to the weld are prepared, and then stretched to fracture. If failure occurs in the weld, the strength of the weld is evaluated from the yield stress or the tensile strength of the material as measured in the test, while ductility is evaluated from either elongation, or contraction of area of the test specimen at fracture. It is generally agreed upon that the ductility of the weld is a better measure of quality than strength, as welds with quite serious defects might have good strength. Defective welds therefore can be sorted out and scrapped based on ductility values if the specimen fractures in the weld.

If the failure occurs outside the weld the quality of the weld is often supposed to be better than that of the parent metal. But is this really the case? An example will now be

presented that depicts that this is not necessarily true; in Fig.4.1 is shown a sketch of one part of a fractured tensile test specimen taken from a special profile with an extrusion seam weld in its middle. But the profile contained two serious extrusion weld defects as there were two unwelded stripes with no metallic bond that extended along the length of the profile. The figure shows that this specimen necked down and fractured away from the mid-section of the specimen which contained the weld defect, in spite of it having this serious internal weld defect. The example clearly demonstrates that a specimen with an extrusion weld may perform well in an ordinary tensile test even though the weld quality can be inferior.

This behavior is easily explained if the material away from the weld where the neck appears is softer than that in the weld zone itself. Upon stretching necking would then start in the softer region instead of in the hard weld zone. The degree of plasticization in the section of the specimen containing the defects would therefore not become so high that it would demonstrate the material weakness in reality present in this location. On continued stretching deformation would therefore be localized and would only take place in the neck, in spite of the presence of a serious material defect in the cross-section nearby.

Other static test methods than tensile testing has been used to determine weld quality in extrusion welding. Such methods are the bending test, the flattening test and various fracture mechanical tests. The quality of industrial extrusion welds is also commonly tested by expansion tests; a mandrel is then pressed into the open end of a hollow profile, or the profile is expanded hydraulically. If the profile expands sufficiently before it fractures, this ensures acceptable ductility in the material and confirms that the profile does not contain serious defects. Expansion tests can be difficult to apply in some non-circular hollows, and in these cases flattening, or etching tests may be used instead.

For critical applications of light metals profiles with extrusion welds one can use fracture mechanics tests on samples taken from the profiles. In such tests a pre-crack is forced to propagate along the weld plane. Extrusion welds that behave satisfactorily in a tensile test may in a fracture mechanics test have reduced toughness compared to that of the parent metal away from the weld. In this case the welds usually have higher content of inclusions in the extrusion weld than outside it. The weld will thus represent a favorable plane for crack propagation compared to the locations away from the weld.

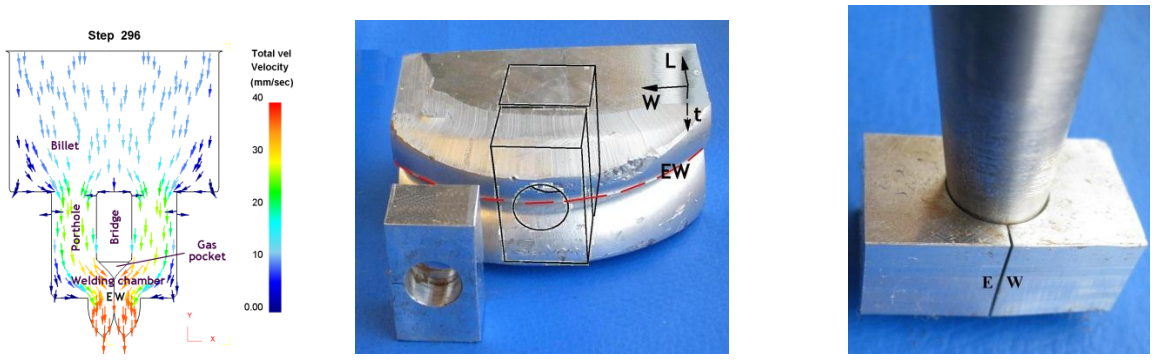

(a) (b) (c)

FIGURE 4.2. (a) Idealized 2D-extrusion with stable gas pocket behind bridge. Test technique; (b) Location of sample in profile with extrusion weld. (c) Mandrel expansion to specimen fractures.

Under dynamic loading the fatigue strength for various reasons will be considerably lower in fusions weld than in the parent metal outside the weld. In extrusion welding, however, the situation may be opposite, as the fatigue properties of a sound extrusion weld may be equal to, or better than that of the parent material.

4.3. New innovative concept for testing of extrusion welds

The new test concept for determining the quality of extrusion welds is best explained by referring to Fig.4.2. In Fig.4.2(a) a picture from a FEA-analysis of a simplified 2D extrusion process are shown in which two metal streams are joined by extrusion welding behind a bridge. In this case the conditions in the welding chamber were chosen so that the weld chamber behind the bridge did not fill completely up with metal, instead a stable gas pocket remained behind the bridge during the course of the extrusion process. Fig.4.2 (b) shows the obtained extrudate in such an experiment where a strip profile was extruded with an internal seam weld (EW) in the midplane of the strip (hatched lines), in which the weld extended over the full width (W) and length (L) of the profile.

In order to test one extrusion weld at a time by mandrel expansion a test specimen with a special geometry was designed, see the drawing shown in Fig.4.3 (a). The specimen was made as a small rectangular block with a round hole in the middle, and the hole was machined into the specimen at the location where the weld is present. Thus in mandrel

expansion of the specimen it will fracture across the plane containing the weld. The actual strip profile that was tested in this case had dimensions W=59mm and t=24mm, see Fig.4.2(b).

Finally, Fig.4.2(c) shows the situation after end of the mandrel expansion test performed on this specimen. The mandrel has been forced into the hole of the specimen, to a depth so that a crack has propagated across the thin section at one side of the specimen. As this plane was coincident with the seam weld of the extrusion, crack initiation and growth must have occurred along the weld plane in the specimen.

In Fig.4.3 (b) is shown how a number of specimens were prepared from the AA6082 strip profile (which wasin a rather hard condition since it after extrusion had been stored for some years. The specimens were on purpose taken from a location near the front end and additional locations further backwards along the profile. The part of the profile that was tested represents the start up region of the extrusion process, during which conditions are non-stationary inside the die, before the metal flow becomes of steady-state nature. Because of this it was thought that there might be variation in weld quality over this part of the extrusion. Specimens were taken from altogether three rows inside the profile, one row at one side (S1), one in the middle (M) and finally one row at the other side (S2) of the strip. With the exception of three specimens they were all expanded by a mandrel to fracture. This was done in a tensile test machine; the mandrel was gripped and held by one of the crossheads, while a plate was put on top of the other crosshead. A nut was laid on top of the plate as counter-die so that the tip of the mandrel coming out of hole of the specimen could move freely downwards into the hole of the nut.

During the test the load-displacement curve of the upper crosshead of the test machine was measured and recorded. When the specimen fractured at one side, see Fig.4.2 (c), the measured load dropped immediately down to zero. It was thus straightforward from this recording to determine the mandrel displacement length at the instant of specimen fracture. This parameter quantifies the ductility of the specimen tested in the expansion test.

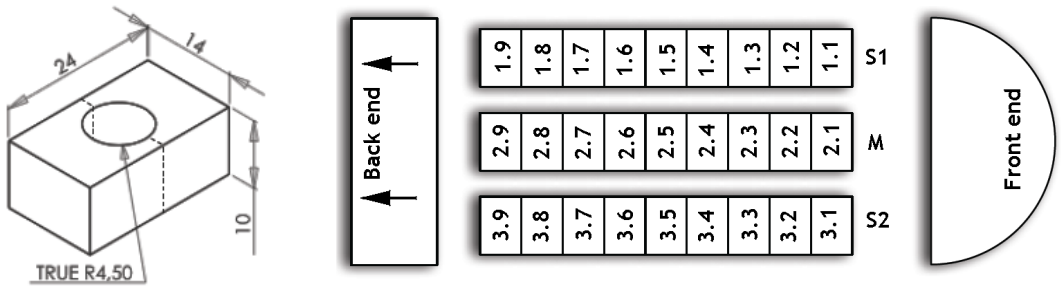

(a) (b)

FIGURE 4.3. (a) Geometry of the new test specimen. (b) Location and numbering of specimens taken from the front end portion of the strip profile with an interior extrusion seam weld.

4.4. Results of weld testing

Load-stroke curves recorded in the expansion test specimens from the row S1 in the profile are shown in Fig. 4.4 (a). As the figure shows the load rose up very high in Exp.1.1 as no lubrication was applied between the mandrel and the specimen in this test. Since there was metal transfer from the specimen to the mandrel when the test was run under dry friction conditions, it was decided in continuation to perform the test in lubricated condition. In the next tests a lubricant was applied to the mandrel and inside the hole of the specimens. The required penetration load of the mandrel was now significantly reduced (by ~ a factor of 2) and the variation in load from one specimen to another one was rather small. All in all two types of load-stroke curves occurred; some with a smooth increasing trend, others with distinctive fluctuations in load. The first type of curves occur in cases where the lubrication is good so that sliding of the mandrel inside the specimen hole is smooth with even friction. The second type is most likely caused by lubricant breakdown so that contact is characterized by stick-slip fluctuations. The two types of behavior were observed to occur although the same lubricant was used, namely a commercial Cu-paste.

As shown in Fig.4.4 (a) a rapid drop in load was observed when the specimen fractured in the weld at one side of the hole, machined into the rectangular block. Hence, from the load-stroke curve it is straightforward and fast to find the mandrel penetration depth into the hole at the instant of fracture. This parameter has been plotted in Fig.4.4 (b) for all specimens subjected to testing. In addition four reference specimens were made in which

there were sound material without presence of any weld in the cross-section of the specimen where the hole is placed, and where fracture occurred.

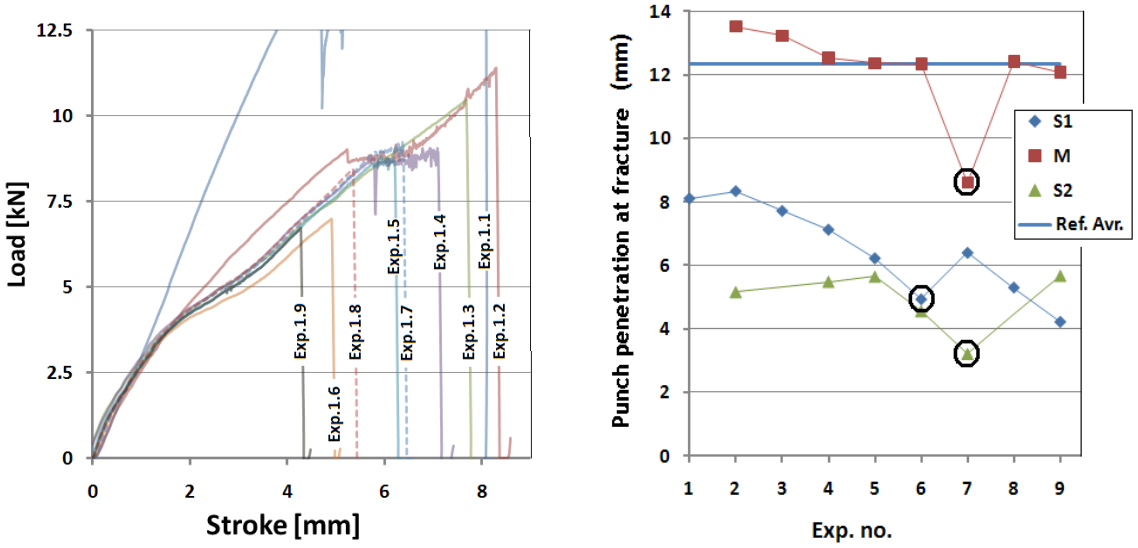

(a) (b)

FIGURE 4.4. (a) Load-stroke curves recorded in mandrel testing of specimens from row S1. (b) Ductility data in terms of penetration depths for all tested specimens.

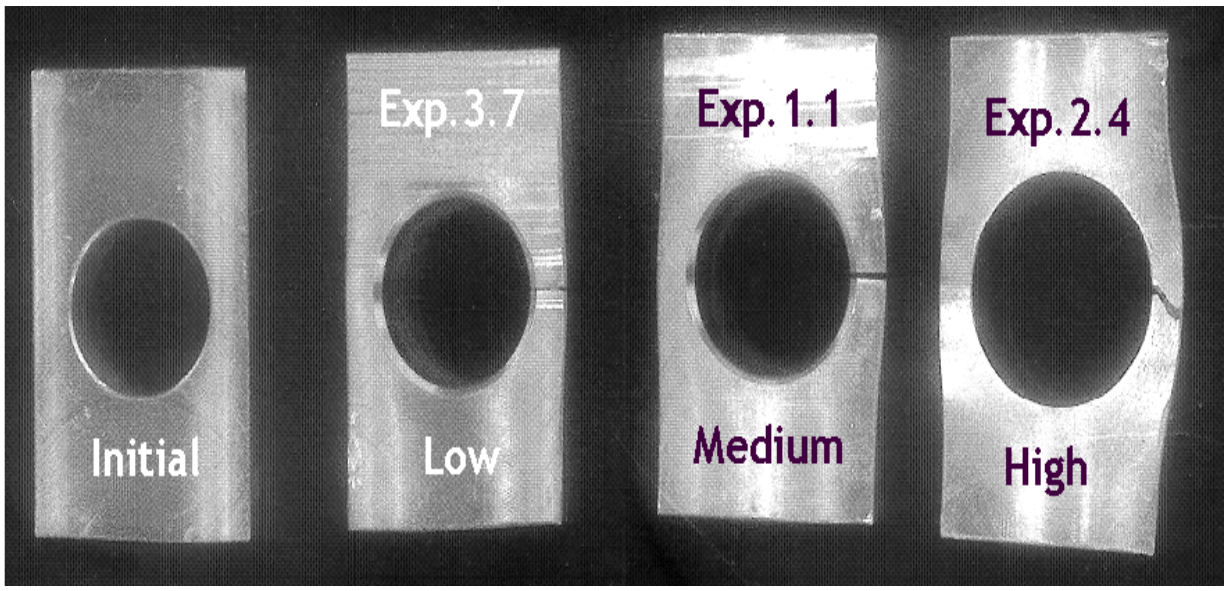

FIGURE 4.5. Initial specimen and specimens with different degrees of ductility.

As Fig. 4.4 (b) depicts there was a significant variance in the measured ductility between the different tested specimens. The punch penetration depth (PPD, in mm) at the instant of fracture of the weld can be divided in three classes for the different specimens. There was one class with low ductility (PPD=3-6), one with medium ductility (PPD=7-9) and one with high ductility (PPD=11-14). High ductility was experienced in the reference specimens without weld, and in all specimens from the row in the middle of the strip (M in Fig.4.3 (b)), with one exception, i.e. specimen 3.7 which had medium ductility. Medium ductility was also found in the specimens near the front end of the profile in row S1 at the side of the strip, while further behind in this row the specimens had low ductility. Finally, the ductility of all specimens taken from side row S2 was in the low regime.

As noted from Fig.4.4 (b) in all rows of specimens taken from the profile there was a decrease in ductility from the front end and backwards along the profile. In addition there was an even reduction in ductility along each row of specimens, with the exception of one measurement point at each row which had less ductility, so the even trend was broken, namely those measurements marked with circles in the Fig.4.4 (b). First thought was that this might be because of spread in behavior for the specimens, but since the low ductility value is observed to occur at approximately the same distance from the front end of the profile, it might be that this is a significant trend, and that the profile actually has less ductility at the location from which specimens numbered 1.6, 2.7 and 3.7 are taken.

4.5. The mechanics of the expansion test

To investigate the mechanical behavior of the test specimen upon mandrel expansion a FEM-model of the expansion test was build using the FEM-program DEFORM 3D.

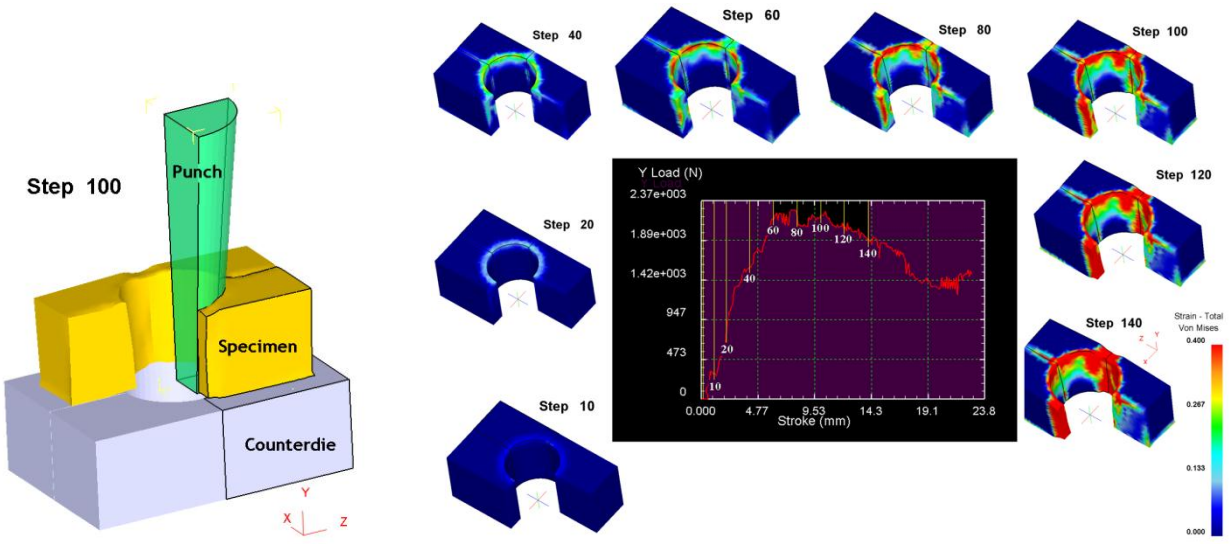

(a) (b)

FIGURE 4.6. (a) FEM-model of mandrel expansion test, (b) Load-stroke curve plus deformation distribution (von Mises strain) in the test specimen from FEA at different stages of the expansion process.

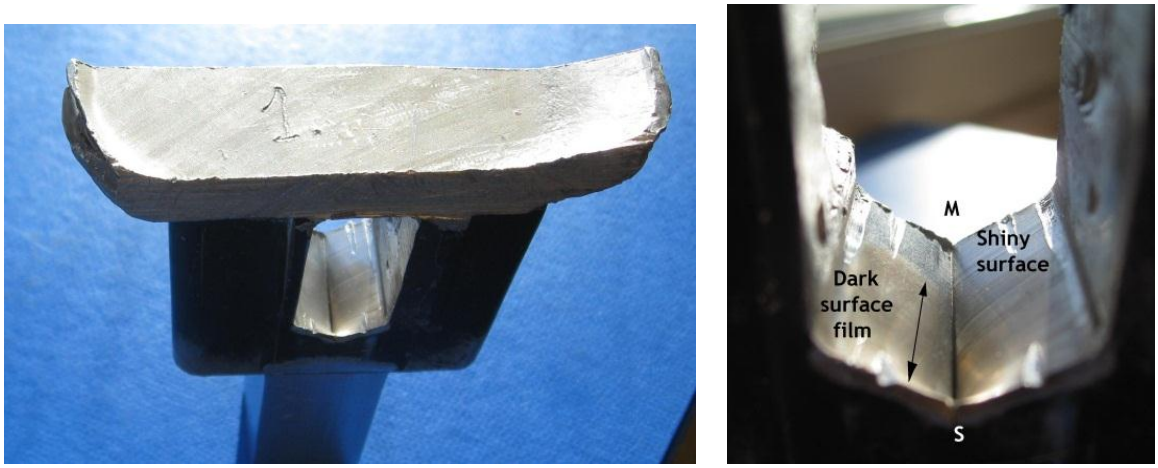

(a) (b)

FIGURE 4.7. (a) Photograph of half of the extrusion material rest showing location where metal streams encounter at tail end of gas pocket, and: (b) Detail showing presence of dark film at the surface of the metal flowing into the seam weld.

One quarter of the process was modeled and a view of the model is shown in Fig.4.6 (a). In the simulation friction was described by a Tresca friction model in which the friction factior was set equal to m=0.8. The model was used to study how the test specimen is expected to deform plastically as the mandrel penetrates down into the hole of the specimen. It was also used to determine expected shape of the load-stroke curve in the test.

The predictions of the model is seen in Fig.4.6 (b) where the load-stroke curve is shown in the middle. The predicted deformations in the specimen at different stages of penetration of the mandrel are also shown by simulation pictures of the specimen placed around the curve. As this figure shows the load-stroke curve will increase until necking starts in the thin part of the specimen near the hole. Due to the necking phenomenon the load will reach a maximum value, and then will start to decrease. A thick specimen will deform by expansion caused by the mandrel, but in addition bending will be superimposed on the specimen in the location where it necks down. Because of this there is larger strain at the top side of the specimen than at the bottom.

4.6. Discussion and conclusions

While in the commonly used mandrel test a piece of the profile is expanded by forcing a mandrel into the hollow of the extruded profile, the new test is based on cutting a rectangular piece out from the profile wall so that the extrusion seam weld extends across the short mid-axis of the rectangle. A hole is then machined from the side into the middle of the rectangle, and the specimen obtained this way, is expanded by forcing a mandrel into the whole. This test specimen design secures highest strains in the thin part of the specimen which concurrently contains the seam weld. Reduced weld quality will therefore cause early fracture in the weld.

Specimen preparation in this test is easy and cheap, and it is also cheap to conduct the test. The test has been applied on a special profile with an extrusion seam weld. The test revealed that part of the weld was of bad quality because of a black contaminant film, probably lubrication, seeping into the weld during the extrusion process. In the mid-region of the welded profile where shiny Al-surfaces were joined together, however, the weld quality was good. Here the weld performed as good as the parent profile material outside the weld. Since the first try-out of the test gave so promising results, further application and try-out of the test is looked forward to.

CONCLUSIONS AND APPLICATION

1. In the course of the thesis it was concluded that:

1.1. There can be cases, when, performing a tensile test of the extruded profile, a break will originate outside the extrusion welding area and the extruded seams in the extrusion process will not be tested, although there are some micro cracks observed in the seam;

1.2. There can be cases, when, under the influence of precipitation hardening of metal, the quality of the extruded seams with defects (micro cracks) is better than the quality of metal outside the seams area;`

1.3. Degree of deformation in the joint is a better quality indicator than the tensile test (coherence between the force applied to the specimen and volume of the deformation) for identification of defects in the extrusion welding;

1.4. Performing shearing experiments with an aluminum specimen:

1.4.1. the shear zone becomes narrower and the material starts to become deformed, breaking, after transition to the second phase (~1/5 of thickness of the material used for the test);

1.4.2. after ~3/5 of the process, the effect of the Plateau (a repeated increase of the load) is observed in the deformation curve, which originates when the billet material concentrates in the lower section of the shear course, thus creating tramps;

1.5. Geometrical parameters of the extrusion die have an impact on the quality of extrusion welds;

1.6. Some low-grade welded joints in the extrusion process can originate not only under the influence of speed and temperature, as it was considered up to now, but also depending on the geometry of extrusion dies;

1.7. The new quality inspection method of the extruded aluminum welded seams permit much more accurate quality inspection measurements of the extruded seams if the measurements are performed to the welded joints instead of the whole profile.

2. Application:

2.1. The geometrical limit diagram of extrusion die provides recommendations to manufacturers in selection of the geometry of extrusion die;

2.2. The new quality inspection method of the extruded aluminum welded seams provides recommendations for improvement of the extrusion welding technology;

2.3. The new quality inspection method of the extruded aluminum welded joints is universal – it can be also used to perform the quality inspection measurements of other metals.

3. There is a patent application submitted to the Norwegian Patent Office (see Appendix 1).

APPENDIX

Appendix 1.

Application of patent submitted

NTNU Discovery forprosjekt

*Prosjektbeskrivelsen som følger søknad om **NTNU Discovery forprosjekt** skal være på maksimalt 5 sider inkludert forside og vedlegg. Bruk font Arial min. 11 pkt. Bruk gjerne nedenstående mal for prosjektbeskrivelse. Dersom dere benytter eget oppsett, sørg for at alle relevante elementer er beskrevet.*

Prosjekttittel (5-10 ord)
Gi søknaden en kortfattet og beskrivende tittel: **KLIPPING MED NULL KLARING**

Oppsummering (maks 200 ord)
Gi et kort sammendrag av prosjektet med vekt på formålet , de mest sentrale utfordringene, anvendelsespotensial for resultatene og omsøkt beløp
Formål: Bygge en prototyp klippemaskin for klipping av langstrakte emner av metall, plast, kompositter eller lignende med null klaring mellom klippestempel og motstående klippevertøy. Utfordringer som en vil møte i arbeidet regnes som greitt overkommelig siden utstyret er enkelt. Det er dessuten testet og funnet å gi et meget godt klipperesultat i NTNU's laboratorium. I første omgang skal bedriften ASVO Måløy bruke utstyret for å resirkulere nylontrosser med stålkjærne som kasseres fra den norske fiskeflåten. Klippeutrustningen skal så markedsføres for å finne annen norsk industri som trenger denne løsningen.

Prosjektleder (person som er ansvarlig for gjennomføringen av prosjektet og rapportering)

Navn	Henry Valberg
Tittel/ stilling	Professor
Institutt	Institutt for produktutvikling og materialer
Telefonnummer(-e)	93822/91897604
E-postadresse	Henry.valberg@ntnu.no

Andre prosjektdeltakere (forsker, oppfinner, studenter, eksterne, etc)

Navn:	Tilhørighet/ Institutt/ Selskap	Rolle
Janis Kandis	NTNU/Riga University	Forsker
Arnfinn Willa Hansen	NTNU	Overing.

[x] Jeg har vært i kontakt med NTNU Technology Transfer AS om denne ideen.

Hovedmål

Formuler et konkret og etterprøvbart hovedmål som gir en beskrivelse av resultater som planlegges oppnådd i løpet av prosjektperioden.
Hvilke spørsmål skal prosjektet gi svar på?
Hva er planen videre dersom prosjektet gir positive resultater?

Klippeinnretningen som er laget skal bygges inn i en kommersiell vedklyver for å teste ut funksjonalitet ved klipping av trosser ved ASVO i Måløy.

Prosjektet skal gi svar på hvordan utstyret fungerer ved industriproduksjon.

Innretningen skal markedsføres i Teknisk Ukeblad.

Man skal forsøke å få til lokal produksjon av utstyret ved en verkstedbedrift i Norge.

Oppfinnelse/ idé

Beskrivelse av ideen, hva som er unikt, om det finnes liknende produkter eller tjenester. Hva er gjort av arbeid til nå (teknisk, kommersielt, markedsmessig)? Hvilket problem skal oppfinnelsen løse?

Klippeinnretningen som er laget er vist i figuren nedenunder. Den består av to.deler; et klippestempel (a) forsynt med en spalt. Stemplet har en ytre diameter slik at det akkurat går inn i motstående ringformede klippeverktøy (b). I (c) i figuren er de to delene vist montert sammen med en bjelke av aluminium lagt inn i spalten for avklipping i begge ender.

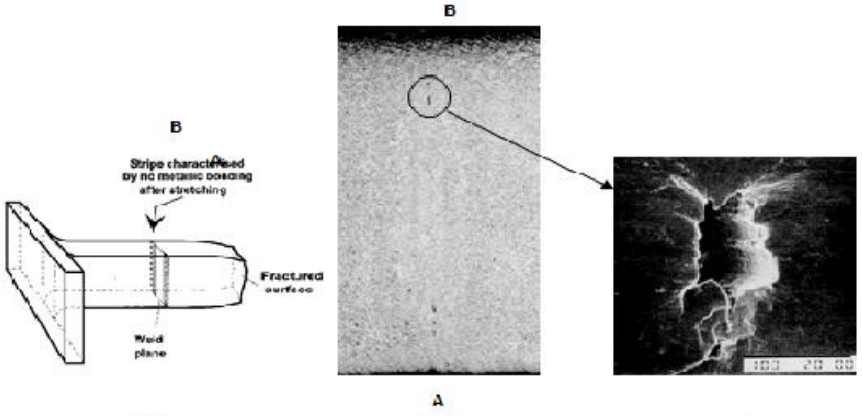

FIGUR 1. Klippeprosess: (a) Klippestempel med spalt for innføring av emne som skal klippes, (b) Al-bjelke brukt som emne (Al) og nedre klippeverktøy i form av en stålring, (c) Konfigurasjon av klippeinnretning ved begynnende klipping.

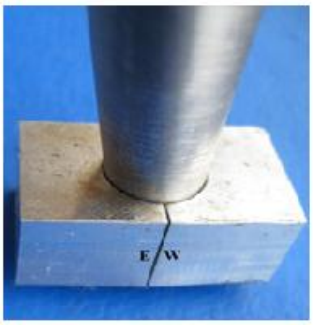

FIGUR 2. Bjelke før, etter delvis klipping, og etter full avklipping.

Klippeverktøyene er testet ut i NTNU's laboratorium på små bjelker av Al og ved klipping av en kassert trosse fra fiskeflåten i Norge.

Potensielt marked og kunder

Hvem er kunde og sluttbruker, hvilke behov har de og hvem er de mest betalingsvillige kundene? Gi indikasjon på kommersielt potensial, markedsstørrelse, prising. Hvilke kommersielle aktører er behovet diskutert med og hva er tilbakemeldingene?

Bedriften ASVO Måløy skal bruke prototypen for resirkulering av trosser. Andre kunder kan være andre norske bedrifter som vil dele opp stenger, tau, kabler, etc.

Konkurrerende løsninger

Beskriv sammenlignbare og/eller konkurrerende løsninger i markedet i dag. Fordeler og ulemper mellom eksisterende løsninger og den nye løsningen.

Bedriften ASVO Måløy har undersøkt hva som finnes av egnet eutstyr for klipping av kasserte trosser fra fiskeflåten, men har ikke kommet over tilfredsstillende utstyr.
Klippeprosessen er uttestet i NTNU/IPM's laboratorium på en trosse oversendt fra ASVO Måløy. Testingen viste at man med denne innretningen lettkunne klippe av trossen, se bilde:

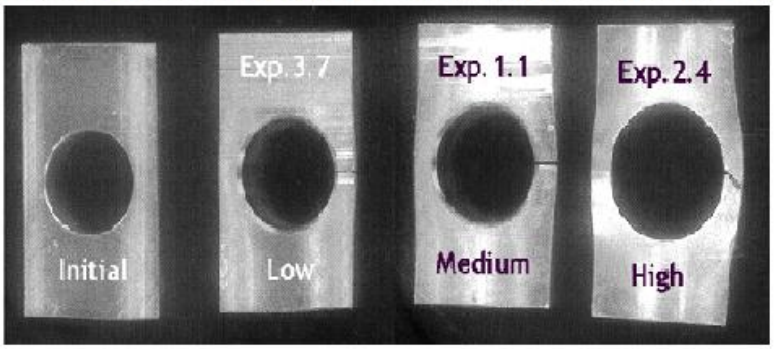

Tentativ forretningsmodell

En tentativ forretningsmodell/kommersialiseringsstrategi for løsningen (selskapsetablering, lisens, hvor i verdikjeden?)

Intellektuelle rettigheter

Hva er forskningsbakgrunn/ bakgrunn for ideen og hvem har bidratt til utvikling fram til nå? (finansiering, personell, bruk av fasiliteter, materialer eller andre ressurser)
Avklaring av eierskapet til teknologien/ konseptet/ løsningen
Finnes det patenter eller annen dokumentasjon som ligger i nærheten av oppfinnelsen?

Klippeprosessen er fremkommet med utgangspunkt i grunnleggende forskning utført av søker for på teoretisk basis å studere deformasjonsforhold i intense skjærsoner.

Det er laget en publikasjon på dette arbeidet og den vil bli publisert på konferansen ESAFORM som arrangeres i Belfast i april i år.

Det er ikke gjennomført mer dyptgående undersøkelser vedrørende patentering idet en regner med at prinsippet er kjent.

Aktiviteter/ tidsplan og milepæler

Hva skal leveres når? Beskrivelse av hva prosjektet skal ha oppnådd på et visst tidspunkt og hvilke aktiviteter som må gjennomføres for å nå milepæl.

Bygging av prototyp, 20. mai 2011

Testing av prototyp ved industribedrift (ASVO Måløy), 30. juli 2011

Kostnadsplan

Kostnadsplanen for prosjektet sammenfattes i de fire angitte kostnadsartene nedenfor. Planen skal vise hvordan kostnadene fordeler seg over prosjektperioden og skal vise totalkostnadene for gjennomføringen av prosjektet, ikke bare det som søkes dekket av NTNU Discovery. Alle beløp oppgis i 1000 kr.

Kostnadspost	*Kostnad (kNOK)*
Personal- og indirekte kostnader	70
Eksterne konsulenttjenester	
Utstyr og materialer	30
Leie av laboratorium	
Andre driftskostnader	30
SUM	130

Kommentarer (andre driftskostnader *skal* spesifiseres):

Finansieringsplan

Finansieringsplanen skal vise hvordan prosjektet skal finansieres. Den omfatter både bidrag i form av penger og indirekte bidrag som egeninnsats, forskningsinfrastruktur osv. Alle beløp skal være i 1000 kr.

Finansieringskilde	*Finansiering (kNOK)*
Indirekte bidrag (egeninnsats, forskningsinfrastruktur, etc.)	
NTNU Discovery	100
Eksterne midler (offentlig finansiering)	
Eksterne midler (privat finansiering)	30
Annen finansiering	
SUM	130

Kommentarer (andre finansieringskilder enn NTNU Discovery *skal* spesifiseres):

Eksterne midler er kontantbidrag fra ASVO Måløy,

Appendix 2.

Acknowledgement of receipt of the New test method for use in industry 1

NTNU

Faculty of Engineering Science and Technology
Department of Engineering Design and Materials

Our date | Our reference

Your Date | Your reference

To the members of the P-16 Promotion Council

This is to state that Janis Kandis, who stayed at the Department of Materials and Engineering Science where the undersigned is working as a professor, during part of his PhD-study at Riga Technical University, has the permission to use figures and other information from publications worked out by the undersigned.

Moreover, Mr. Kandis has contributed in the development of a new ring expansion test at my department, which can be used successfully for the testing of the quality of extrusion welds. The test has been used on test specimen from industrial profiles with differing weld quality, collected in the Norwegian Al-industry, represented by the companies Hydro Aluminium and Benteler

Finally, it is to be stated that the above mentioned ring expansion technique will be considered patented.

Trondheim 19.11.2012

Henry Valberg

(Prof.)

Address
NO-7491 Trondheim

Org.no. 974 767 880
E-mail:
ipm-info@ivt.ntnu.no
http://www.ivt.ntnu.no/ipm/

Location
Richard Birkelandsvei 2b
Gløshaugen

Phone
+ 47 73 59 37 68
Fax
+ 47 73 59 41 29

Phone: + 47

Appendix 3.

Acknowledgement of receipt of the New test method for use in industry 2

Størst i Nordfjord
Fjordenes Tidende
Nr. 79 • 102. årgang • Måløy, mandag 11. juli 2011 Løssalg kr. 20,-

Madcon satte standarden da de danset med de lokale barna under **Vanylvsråkk 2011 som gikk av stabelen denne helgen.** Side 8 og 9

Eid-trener Michael Sjöquist og hans mannskap tar sommerferie som beste lokale lag selv om **Eid tapte for Arna-Bjørnar lørdag** Sporten

Håpet svinner

(Foto: Sindre Blåvik Kvalheim)

Helse Førde har nå utnevnt et nedbemanningsutvalg som skal tilrettelegge for all nedbemanning og omplassering som en følge av avviklingen av den ortopediske avdelingen ved Nordfjord sjukehus.

Seksjonsleder i ortopedi ved Nordfjord sjukehus Oddrun Rye (bildet) er en av de som er utnevnt til å sitte i utvalget. Hun mener at stemningen blant de ansatte nå er mer oppgitt enn noensinne. Side 4 og 5

Maskin løyser avfallsproblem

Selstad AS har i lang tid hatt eit problem med avfall etter produksjon av trosser med stålkjerner. ASVO Måløy AS har samarbeida med professor Henry Valberg ved NTNU i Trondheim om ei ny maskin som kutter trossene, slik at restmaterialet kan resirkulerast. Side 6 og 7

Sentralbord: 57 84 90 00 Tipstelefon: 57 84 90 99 E-post: fjt@fjt.no www.fjt.no

Politisk ukorrekt bilavgift

Det er for dyrt å omregistrere bil i Norge, og det hindrer at landets bilpark blir sikrere og mer miljøvennlig, mener NAF.

– Den upopulære omregistreringsavgiften bør erstattes av et fast gebyr som kun dekker statens kostnader ved omregistrering, sier Christina Bu, miljørådgiver i NAF.

Skal man kjøpe en vanlig familiebil som er fire år gammel i dag, må man regne inn nær 10 000 kroner for omregistrering. Avgiften blir høyere jo nyere og tyngre bilen er, og kan komme opp i over 22.000 kroner. At avgiften blir høyere for nyere biler, gjør at den virker i motsatt retning av myndighetenes mål om en sikrere og mer miljøvennlig bilpark. Omregistreringsavgiften bør ikke ha innvirkning på valget av bruktbil, og i hvert fall ikke i negativ retning.

En spørreundersøkelse NAF har gjort viser at omregistreringsavgiften påvirker valget av bil. Fire av ti spurte mener at en lavere omregistreringsavgift vil føre til at de skifter bil oftere.

– De med eldre biler var mest enig i dette, i tillegg til de som har familiebiler. Familier er nok mest opptatt av å skaffe seg en sikker og praktisk bil som ikke er for gammel, sier Bu.

– Derfor bør det komme en flat eierskifteavgift som kun dekker kostnaden ved omregistrering. I Sverige er registreringsavgiften 50 kroner og i tillegg må man betale 80 kroner for skiltene. Norge bør ligge i nærheten av svensk nivå, mener Christina Bu.

Fire av fem biler som omsettes i Norge er bruktbiler, så hva slags bil bruktkjøperne velger har avgjørende betydning for bilparkens alder. Den norske personbilparken har en gjennomsnittsalder på 10,4 år, over to år eldre en gjennomsnittet i Europa. Nyere biler er sikrere og har lavere utslipp enn eldre. Derfor er fjerning av omregistreringsavgiften et enkelt grep for at flere skal kunne reise sikkert og miljøvennlig.

Har kutta taupr

ASVO Måløy AS har samarbeida med NTNU for å få ei maskin som kan kutte trosser, og løyser svaret på eit 50 tonn stort avfallsproblem for Selstad AS.

Janne Wiltrien Listhaug
jannewiltrien.listhaug@fjt.no
57 84 90 00

– Dette er ein vinn-vinn situasjon, ASVO får no levert inn plast og stål hver for seg, seier Arve Selstad ved Selstad AS om nyvinninga som skal resirkulere avkapp og feil frå trosseproduksjon ved bedrifta.

Fredag fekk ASVO teste ut maskina med besøk frå oppfinnarane frå NTNU og ein representant frå Selstad AS.

Avfall

– Utfordringa starta med at Selstad hadde eit avfallsproblem, seier Betty Hessevik ved ASVO.

Selstad AS er ein leiande leverandør av produkt til fiskeri- og oppdrettsbransjen, og noko av produksjonen deira er mellom anna trosser med stålkjerne i ulike dimensjonar.

Avkapp og feilproduksjon av dette materialet har vore eit problemavfall for Selstad i mange år.

Ifølgje Arve Selstad ved Selstad AS ligg avkapp og feilproduksjon på rundt 50 tonn i året.

Kvitt eit problem

– Dette betyr at vi forhåpentlegvis blir kvitt eit avfallsproblem. Det vi hiver no blir køyrt på deponi. Det er ikkje eit miljøproblem, men det fyller opp i naturen, seier Selstad om avfallet.

Han fortel vidare at dei har opplegg på levering av rein plast, men at dei har prøvd mykje forskjellig for å bli kvitt avfallet etter trossene, mellom anna forbrenning.

– Det er betre å gjenbruke det enn å grave det ned, seier professor Henry Valberg frå NTNU.

– I forhold til å vaske plastposar slik eg gjer heime, er dette mykje betre. Eg kan ha godt samvit resten av livet, smiler Valberg.

– Eit steg vidare

– Vi skal starte produksjonen i løpet av hausten, seier Hessevik.

ASVO har prøvd å finne ulike løysingar på problemet med å kutte trossene, og har mellom anna investert i skjæreutstyr utan å lykkast med å få ein sikker og god produksjon.

–Brannvesenet som har store klipparar kom og prøvde, men dei klarte ikkje å klippe den av, fortel Hessevik.

– Vi prøvde også med kappskjever. Det var ei dødfødd løysing, med mykje røyk, brenning, støy og lyd, forsett ho.

Løysing

I januar starta kontakten mellom ASVO og NTNU. ASVO tok kontakt for å sjekke om det fanst kreative verktøy for å løyse utfordringa med trossene, og svaret kom frå professor Henry Valberg i form av «trosseklipparen».

– Eg trur det kjem til å fungere kjempebra. Det er viktig at alle som jobbar her kan vere med å bruke den, den må vere enkel å bruke og sikkerheit er viktig, seier assisterande produksjonsleiar Laila Johansen.

ASVO hålpar å klare å ta unna det Selstad har til overs etter trosseproduksjonen. Og i periodar når det nødvendigvis ikkje er mykje anna arbeid er det flott å ha denne biten, ifølgje Hessevik.

– Neste ledd

Produksjonsleiar Selma Strand Larsen ser på løysinga med «trosseklipparen» som neste ledd i arbeidet med miljøgevinstar. ASVO resirkulerer mellom anna notliner frå garnflåten som kanskje tidlegare har blitt brent eller hamna på havets botn.

– Og med trossene, går alt til gjenvinning i staden for deponi, seier Larsen.

– Det betyr også alternative arbeidsoppgåver, fortset ho.

ASVO Måløy AS er eit samarbeidsvirke som arbeider på oppdrag frå NAV i Vågsøy, Selje og Stryn for å gi dei som har ei kortvarig eller langvarig avgrensing i sine valmulegheiter sjansen til å leve eit aktivt og fullverdig liv.

Gjenvinning: Etter at trossene er kappa, vrir ein dei for hand og separerar stålet og plasten. Betty Hessevik (f.v.) og Selma Strand Larsen.

Søkjer kandidatar til Frivillighetsprisen

I lokalsamfunn over heile landet vert det kvart år lagt ned frivillig innsats tilsvarande 113.500 årsverk, og no er det tid for å nominere kandidatar til den nasjonale Frivillighetsprisen 2011. Kjenner du nokon som har utmerkt seg med frivillig innsats, engasjement og pågangsmot til beste for den enkelte og samfunnet?

I så fall kan du nominere vedkomande som kandidat til Frivillighetsprisen 2011.

Det er organisasjonen Frivillighet Norge som deler ut prisen. Nominasjonen er organisert fylkesvis, og hovudutvalet for kultur avgjer kven av forslaga frå Sogn og Fjordane som skal vere fylket sin endelege kandidat til prisen. Den siste Sogn og Fjordane-vinnaren av prisen er Malakoff Rockfestival, som fekk prisen i 2009.

oblem

«Traussklipparar»: ASVO Måløy AS har fått NTNU til å lage ei løysing på problemet med å kutte opp avkapp og feilproduksjon av trausar ved Sebdal AS. F.v.: Selma Strand Larsen, Arve Sebdal frå Sebdal AS, Bjørn Sundal, Betty Hessevik, Laila Johansen, Janis Kandis og professor Henry Valberg frå NTNU. (Begge foto: Janne Weltzien Lødeng)

– I prinsippet ei stor saks

– Det er ein vedklyver produsert i Kina, der vi har kopla ut klyveren og sett inn eit klippeverktøy, slik at ein kan klippe trosene, seier professor i metallforming Henry Valberg.

Han jobbar ved Institutt for produktutvikling og materialar ved NTNU i Trondheim.

– Vi jobbar konkret med klippeprosjekt, og kan hende dukkar det opp nokon som trung løysingane, seier professoren.

– Om ein er smart får ein mykje ut av ein vedklyver, smiler Valberg.

Saman med seg hadde Valberg Janis Kandis frå Latvia, som studerer og jobbar med doktorgraden sin ved NTNU.

Han jobbar med klippeprosessar og har fire publikasjonar på det aktuelle området.

Ei helg med skjemt og alvor

Inviterer: Marita Aarvik (t.v.) og May Sissel Årvik Ligia håper på stor oppslutning om «Tilbake til røtene» på ytre Stadlandet i helga. (Privatfoto: Hildegunn Lekven Halten)

Til helga lokkes folk «Tilbake til røtene» på Stadlandet, med Ervik-preike og nyskrevet revy om livet i Bolkevikja.

Kari Midtgård Riisberg

kari.riisberg@fjt.no
958 94 333

«Tilbake til røtene» har blitt arrangert to gonger før, i 2004 og i 2008. Det har vore så vellykka at arrangørane satsar igjen, og frå fredag til sundag denne uka er det klart for ei nytt treff på ytre Stadlandet.

Bygdelaget er arrangør, og ei gruppe på fem–seks personar, blant andre May Sissel Årvik Ligia og Marita Aarvik, står bak det heile. Det store målet er at folk skal kome møtast og prate med både gamle kjende og nye folk.

Lokalrevy

– Vi har mange som kjenner til mye lokalhistorie og slekt, og vi har elles mye fra området som vi ønsker å vise fram. For andre gang er det også laga en lokal revy med mange ord, uttrykk og sagn fra området, sier Marita Aarvik.

– Det er dei same folka som er arrangørar og skriver teksten til *Bolkevikja – fram og tilbake*, og vi er også med og spiller i teaterstykket, fortel May Sissel Årvik Ligia.

Hun nemner revykvelden på fredag kveld som ei av høgdepunkta for helga.

– Forrige gang var det både skjemt og alvor i stykket om Bolkevikja. Denne gangen er det mest skjemt, og vi har lagt så tilrette har trilla på svingane, men det er også litt alvor mellom linjene, sier hun.

Alle er velkomne

Sist det var «Tilbake til røtene» var ei par hundre menneske innom arrangementet.

– Vi håper det skal komme en del folk. Dette er et arrangement som alle er velkomne til å være med på, både de som har røtter på ytre Stadlandet og andre, sier Årvik Ligia.

Hun anslår at de fire grendalaga Honningsvåg, Ervik, Årvik og Morkadalen til sammen har rundt 250 innbyggere. Da er det jo ekstra kjekt om de klarer å samle et par hundre besøkende i løpet av de fire dagene med «Tilbake til røtene». Overnatting skal ikke være noe problem:

– Her er jo campingplass, og elles har det vist seg at de fleste som kommer har familie eller venner de bor hos, eller har sommarhus i området. Og om noen trenger det, er vi behjelpelige med å skaffe overnatting, sier hun.

Nytt revystykke: Fredag vises en ny Bolkevikja-revy. Bildet er frå den førrige. (Foto: privat)

Base i grendaskolen

Grendaskolen på ytre Stadlandet er base for arrangementet. Den åpner torsdag med kafé og salgsutstilling av maleri og rosemaling. Kjerringa Husflidlag har også ei utstilling som varer heile helga.

Fredag er det tre alternative fotturer, til Bolkevikja, Hovden og Kyrnosa, eller en kan være med på yoga. Om kvelden er det salg av fiskemat, teaterforestillinga *Bolkevikja – fram og tilbake*, og dans til musikk fra Heidi og Kjell.

I fiskekonkurransen lørdag er det premier for største fisk, største fangst totalt og minste fisk. Her blir det fiska i sjøen, med stang og snøre fra land. Midt på dagen serverer kokker fra Stadfisk fiskemiddag på skolen. Seinere blir det grilling, karaoke ved Per Sindre og premieutdeling for fiskekonkurransen.

Ervikpreika

– Ervikpreika søndag formiddag er også et høydepunkt. Den er på kirkegården i Ervik hvor vandt er noenlunde bra. Dette er ei preike med tradisjoner fra gammelt av, sier May Sissel.

Søndag er det Stad Gardsmat som er kokker, og de serverer stormsuppe på grendaskolen før arrangementet avsluttes om ettermiddagen.

REFERENCES

1. *Akeret R., "Extrusion Welds-quality aspects are now center stage". 5th Int. Al Extrusion Technology Seminar, Vol 1, 1992, pp.319-336.*
2. *Akeret, R.: "Untersuchungen uber das Strangpressen unter besonderer Beruck-sichtigung der thermischen Vorgange, Aluminium," Vol. 44, 1968, pp. 412-415.*
3. *Altan T., S.-I., Oh and H. L. Gegel "Metal forming, fundamentals and applications", ASM Int.,1983, pp.189-229*
4. *Altan, T., Oh, S.-I., and Gegel, H. L.: "Metal Forming, Fundamentals and Applications," ASM Int., 1983, pp. 189-229.*
5. *Ambrogio G. et al.:"Numerical analysis of the fracture surface in thick sheets blanking", ESAFORM , 759-760, (2004).*
6. *Ceretti E., Giardini L. and C., Int. Conf. on Sustainable Manufacturing, Canada, 125-132 (2008).*
7. *Ceretti E., L. and C. Kopsavilkumiardini, Int. Conf. on Sustainable Manufacturing, Canada, 2008. pp. 125.-132.*
8. *Ceretti E., Mazzoni L., Giardini C., "Simulation of metal flow and welding prediction in porthole die extrusion: the influence of the geometrical parameters". Int. J. Material Forming, 2009, Vol. 2 Suppl 1:101-104 DOI 10.1007/s12289-009-0494-9 © Springer/ESAFORM 2009.*
9. *Chakrabarty, J.: "Theory of Plasticity," Elsevier, 2006.*
10. *Chang T. M. and Swift H. W., J. of Inst. of Metals, 78, 119-146 (1950-51).*
11. *Chang T. M. and Swift H. W., J. of Inst. of Metals, 78, 119-146 (1950-51).*
12. *Chang, T. M. :"Shearing of metal blanks", J. of Inst. of Metals, Vol. 78, 1950-51, pp.393-414.*
13. *Chang, T. M. and Swift, H. W.:"Shearing of metal bars", J. of Inst. of Metals, Vol. 78, 1950-51, pp.119-146.*
14. *Coffin, L. F., and Rogers, H. C.: Trans. Am. Soc. Metallurgists, Vol. 60, 1967, p. 681.*
15. *Donati L., L. Tomesani and G. Minak, J. of Materials Proc. Technology, 191, 127-131 (2007).*
16. *Donati L., Tomesani L., "The effect of die design on the production and seam weld quality of extruded aluminum profiles", J. of Materials Processing Technology ,*

164-165, 2005, pp.1025-1031.

17. *Donati L., Tomesani L., "The prediction of seam welds quality in aluminum extrusion". Journal of Materials Processing Technology 153-154, 2004, pp.366-373.*
18. *Dürrschnabel W., "Der Materialfluss beim Strangpressen von NE-Metallen" (in German), Metall, Vol.22, 1968, I: pp. 426-437, II: pp. 995-998 and III: pp. 1215-1219.*
19. *Ganesan, S. M., Khan, Y- A., Valberg, H., Moe, P. T. and Hansen, A. W.:"Shearing applied as test method for acqusition of flow stress data at high strain and strain rates", Int. J. Material Forming, 2008, Vol.1, pp.519-522.*
20. *Ganesan, S. M., Khan, Y. A., Valberg, H., Moe, P. T. and Hansen, A. W.:"Shearing applied as test method for acquisition of flow stress data at high strain and strain rates", Int. J. Material Forming, 2008, Vol.1, pp.519-522.*
21. *Hosford, W. F., and Caddell, R. M.: "Metal Forming, Mechanics and Metallurgy," Cambridge Univ. Press, 2007.*
22. *ISO 2740:2009, Sintered metal materials, excluding hardmetals -- Tensile test pieces*
23. *ISO 6892-1:2010, Metallic materials -- Tensile testing: Method of test at room temperature*
24. *Johnson, R. W., and Rowe, G. W.: "Redundant work in drawing cylindrical stock," J. Inst. Metals, 1968, Vol. 96, p. 105.*
25. *Kandis J., Valberg H. and Wu W., Advances in Materials and Processing Technologies, October 24th to 27th, Paris (2010).*
26. *Kandis J., Wu W. and Valberg H., "The mechanics of the shearing process studied by FEM-analysis with experiments", Advances in Materials and Processing Technologies, October 24th to 27th, Paris (2010).*
27. *Kandis, J., Valberg, H. and Wu, W.:"Use of axisymmetric shearing as technological test method to gather flow stress and ductility data for metals", ibid.*
28. *Kandis, J., Wu, W. and Valberg, H.:"The mechanics of the shearing process studied by FEM-analysis with experiments", Advances in Materials and Processing Technologies, Paris, Oct. 24th -27th, 2010.*
29. *Karthik, V.:"Tensile-shear correlations obtained from shear punch test technique using a modified experimental approach, J. of Nucl. Mat., Vol.393, 2008, pp.452-*

432.

30. *Khan, Y. A., Ganesan, S. M., Valberg, H., Moe, P. T. and Hansen, A. W.:"Deformation conditions in conventional shearing dependent on geometrical parameters of tooling", Int. J. Material Forming, 2008, Vol.1, pp.535-538.*
31. *Krämer W., Ber. Inst. Umformtechnik, University of Stuttgart, in German, 1969, pp. 125-131*
32. *Krämer W., Ber. Inst. Umformtechnik, University of Stuttgart, in German, 1969, pp. 134-136*
33. *Krämer, W.:"Untersuchung über das Genauschneiden von Stahl und Nichteisenmetallen", Ber. Inst. Umformtechnik, University of Stuttgart, 1969 (in German).*
34. *Laue, K., and Stenger, H.: "Strangpressen; Verfahren - Maschinen - Werkzeuge," Aluminium-Verlag, D¨usseldorf, 1976.*
35. *Laue, K.: "M¨oglichkeiten werkstoffgerechter Gestaltung von Leichtmetallprofilen," Z. f. Metallkunde, Vol. 54, 1963, pp. 667-671.*
36. *Lefstad, M., Reiso, O., and Johnsen, V.: "Flow of the billet surface in aluminium extrusion," Proc. 5th Int. Aluminum Extrusion Technology Sem., Chicago, 1992. Vol. 2, pp. 503-517.*
37. *Mises, R.: "Mechanik der fasten K¨orper im plastisch deformablen Zustand," G¨ottingen Nachrichten, Math. Phys. Kl., 1913, p. 582.*
38. *Pearson, E. C., and Parkins, R. N.: "The Extrusion of Metals," 2nd ed., Chapman and Hall, London, 1960.*
39. *Pugh, H. L. D., and Watkins, M. T.: "Experimental Investigation of the Extrusions of Metals," The Inst. of Prod. Engg., Brighton, England, 1960.*
40. *Rees, D. W. A.: "Basic Engineering Plasticity", Elsevier, 2006.*
41. *Saanouni K., Mariage J.F., Cherouat A., Lestriez P. "Numerical prediction of discontinuous central bursting in axisymmetric forward extrusion by continuum damage mechanics" Computers and structures, 82, 2004, pp.2309-2332*
42. *Støren S., Andersen L.: Private communication Hydro Aluminium and Bentelers.*
43. *Støren S., Valberg H.: Private communication NTNU.*
44. *Timmerbeil C., C., Werkstattstechnik und Maschinenbau, 47, 231-239 and 350-356 (1957), in German.*
45. *Timmerbeil C., C., Werkstattstechnik und Maschinenbau, 47, 231-239 and 350-356*

(1957), in German.

46. *Timmerbeil, C. :"Untersuchung des Schneidvorgangs beim Blech", Werkstattstechnik und Maschinenbau, Vol.47, 1957, pp.231-239 and pp.350-356 (in German).*
47. *Tresca, H.: "On the flow of solid bodies subjected to high pressures," C. R. Acad. Sci. Paris, Vol. 59, 1864, p. 754.*
48. *Valberg H. S., "Applied metal forming; including FEM analysis", 1st Ed., Cambridge University Press, New York, USA, 2010, pp.256-259*
49. *Valberg H. S., "Applied metal forming; including FEM analysis". 1st Ed, Cambridge University Press, NY, USA, 2010, pp.337-343*
50. *Valberg H. S., Applied metal forming; Including FEM-analysis, Cambridge University Press, 2010, pp. 123-138*
51. *Valberg H. S., Applied metal forming; Including FEM-analysis, Cambridge University Press 2010, pp.325-327*
52. *Valberg H., Int. J. of Materials & Product Technology, 17, 2002, pp. 497.- 556.*
53. *Valberg H., Int. J. of Materials & Product Technology, 17, 2002, pp. 483-492.*
54. *Valberg H., Coenen F. P. and Kopp R., "Metal Flow in Two-Hole Extrusion", 6th Int. Al Extr. Technol. Sem., Chicago, Illinois, May 14 - 17, 1996, Vol.1, pp. 113-124.*
55. *Valberg H., Loeken T., Hval M., Nyhus B., Thaulow C., "The extrusion of hollow profiles with a gas pocket behind the bridge". Int. J. of Materials and Product Technology, Vol. 10, Nos 3-6, 1995, pp. 222-267*
56. *Valberg H.S., "Applied metal forming; including FEM analysis". 1st Ed, Cambridge University Press, NY, USA, 2010, pp.285-288*
57. *Valberg, H. S.:"Applied Metal Forming; Including FEM-analysis", Cambridge University Press, 2010, pp.257-265.*
58. *Valberg, H., and Misiolek, W. Z.: "Plastic deformations in indirect hot extrusion of an aluminium alloy characterised by FEM-analysis with experiment," Proc. 9th Esaform Conf., Glasgow, 2006, pp. 487-490.*
59. *Valberg, H., and Pohl, C.: "Boundary conditions and metal flow in forward extrusion of aluminium alloys," Conf. Proc. Euromech 435, Valencienne, 2002, pp. 33-45.*
60. *Valberg, H., and Sandbakk, Ø.: "Direct non-lubricated Al-extrusion partitioned into*

the sub-processes shearing, scratching, radial compression and extrusion," Proc. 6th Int. Conf. on Material Forming, Salerno, Italy, 2003, pp. 307-310.

61. *Valberg, H., and Uyyuru, R. K.: "New accurate experimental techniques to quantify metal flow inside workpiece - and along boundary interface of workpiece - in metal forming," Proc. 2nd Int. Conf. on Tribology in Manufacturing Processes, Nyborg, Denmark, 2004, Vol. 2, pp. 453-474.*
62. *Valberg, H.: "A modified classification system for metal flow adapted to unlubricated hot extrusion of Al and Al-alloys," Proc. 6th Int. Aluminum Extrusion Technology Sem., 1996, Chicago, Vol. 2, pp. 95-100.*
63. *Valberg, H.: "Experimental techniques to characterize large plastic deformations in unlubricated hot aluminium extrusion," Key Engineering Materials, Vol. 367, 2008, pp. 17-24.*
64. *Welo T., Smaabrekke A., Valberg H., "Two-dimensional simulation of porthole extrusion". Aluminium, Vol.71, No.1, 1995, pp. 90-94.*
65. *Xianghong W. et al., Materials Science and Engineering A 435-436, 266-274 (2006).*
66. *Xianghong W. et al., Materials Science and Engineering, 2006, pp. 435.-436 and pp. 266.-274.*